General Disclaimer

One or more of the Following Statements may affect this Document

- This document has been reproduced from the best copy furnished by the organizational source. It is being released in the interest of making available as much information as possible.

- This document may contain data, which exceeds the sheet parameters. It was furnished in this condition by the organizational source and is the best copy available.

- This document may contain tone-on-tone or color graphs, charts and/or pictures, which have been reproduced in black and white.

- This document is paginated as submitted by the original source.

- Portions of this document are not fully legible due to the historical nature of some of the material. However, it is the best reproduction available from the original submission.

MFC FORM 422 (VERTICAL) (AUGUST 1960)

APPLICATION		PART No.	MF	REVISIONS			
NEXT ASSY	USED ON			SYM	DESCRIPTION	DATE	APPROVAL

SUMMARY TEST REPORT ON NICKEL-CADMIUM BATTERIES FOR APOLLO TELESCOPE MOUNT

UNLESS OTHERWISE SPECIFIED DIMENSIONS ARE IN INCHES TOLERANCES ON: FRACTIONS DECIMALS ANGLES	ORIGINAL DATE OF DRAWING 6/22/70 DRAFTSMAN / CHECKER TRACER / CHECKER ENGINEER / ENGINEER	SUMMARY TEST REPORT FOR NICKEL-CADMIUM BATTERIES FOR APOLLO TELESCOPE MOUNT	GEORGE C. MARSHALL SPACE FLIGHT CENTER NATIONAL AERONAUTICS AND SPACE ADMINISTRATION HUNTSVILLE, ALABAMA
MATERIAL	SUBMITTED L. E. Paschal		
HEAT TREATMENT	L. E. Paschal		
FINAL PROTECTIVE FINISH	APPROVED	SCALE / UNIT WT	DWG SIZE A — 40M22411 — SHEET 1 OF 84

SUMMARY TEST REPORT ON NICKEL-CADMIUM BATTERIES FOR APOLLO TELESCOPE MOUNT

by

W. W. Kirsch
A. E. Shikoh

Prepared under Contract No. NAS8-20055 by

SPERRY RAND
SPACE SUPPORT DIVISION
Space Power Sources Section
Huntsville, Alabama

For

Power Branch
Electrical Division
Astrionics Laboratory

NASA-GEORGE C. MARSHALL SPACE FLIGHT CENTER

ABSTRACT

This summary report presents the operational testing and evaluation program conducted on 20-ampere-hour nickel-cadmium (Ni-Cd) batteries for use on the Apollo Telescope Mount (ATM). The test program was initiated in 1967 to determine if the batteries could meet ATM mission requirements and to determine operating characteristics and methods. The ATM system power and charging power for the Ni-Cd secondary batteries is provided by a solar array during the 58-minute daylight portion of the orbit; during the 36-minute night portion of the orbit, the Ni-Cd secondary batteries will supply ATM system power.

The test results reflect battery operating characteristics and parameters relative to simulated ATM orbital test conditions. Maximum voltage, charge requirements, capacity, temperature, and cyclic characteristics are presented.

TABLE OF CONTENTS

40M 22411

TABLE OF CONTENTS (Continued)

LIST OF ILLUSTRATIONS

LIST OF ILLUSTRATIONS (Continued)

LIST OF ILLUSTRATIONS (Continued)

LIST OF ILLUSTRATIONS (Continued)

LIST OF TABLES

SUMMARY TEST REPORT ON NICKEL-CADMIUM BATTERIES FOR APOLLO TELESCOPE MOUNT

SUMMARY

An operational and evaluation test program was conducted by the George C. Marshall Space Flight Center (MSFC) on nickel-cadmium (Ni-Cd) batteries for use on the Apollo Telescope Mount (ATM). Each ATM 20-ampere-hour battery is composed of 24 series-connected sealed Ni-Cd cells manufactured by the General Electric Company. Testing was conducted under simulated ATM orbital conditions consisting of a 58-minute charge time and a 36-minute discharge time within a temperature range of minus 20 degrees Celsius (°C) to 40°C. A 4000 cycle operational life is required for ATM. Research and development testing was directed toward determining Ni-Cd battery characteristics, such as, maximum voltage, charge requirements, capacity, temperature, and cyclic characteristics. Of all the recommended charging regimes and techniques, a combination constant current/constant voltage technique was most applicable for ATM. The important cell and battery control parameters, based on the charge regime, were as follows: typical cell voltage levels were limited to 1.47 to 1.55 volts during charge to prevent hydrogen evolution; charge current was limited by hydrogen evolution possibilities on the high side and by inefficient charge acceptance on the low side; recommended charge termination control was via a third electrode signal but no specific load values or control limits were available.

Initial maximum voltage tests were conducted using a 10-ampere constant current charge until the total battery voltage reached a preset level determined by the maximum allowable individual cell voltage of 1.47 volts at 25°C. Then, the charge was limited to a constant voltage charge. Cell voltage divergence occurred during initial tests and was caused by a difference in capacity of the individual cells or as a result of a memory phenomena. Memory is an unexplained loss of usable capacity and is a function of temperature and cyclic history. Two methods were used to reduce the cell divergence: one method was by reducing the constant voltage charge by at least 0.6 volts below the maximum battery voltage; the other method was to match all cells on an ampere-hour in-and-out basis. Tests of matched and unmatched batteries using the modified charge regime resulted in a higher total capacity for the matched battery which was attributed to the higher voltage to which the battery is charged. An increase in battery operating voltage was attributed to the 24 matched cells. The charge regime was subsequently refined with the maximum individual cell voltage established at 1.5 volts and the constant voltage charge reduced 0.8 volt below the maximum allowable battery voltage. The maximum cell voltage or battery voltage is also temperature dependent. Typical maximum voltage values are 36.8 volts at minus 10°C, 36 volts at 10°C, and 34.6 volts at 30°C. The use of the maximum voltage level as a battery charging limit appears to delay the onset of memory.

40M 22411

Charge acceptance efficiency has been determined to be a function of current rate and temperature. High charge rates are detrimental to the battery when the battery is at low temperature with hazards of possible hydrogen evolution. A 15-ampere charge rate was chosen for compatibility throughout the ATM temperature range. Charge rates of 15 ampere-hours at minus 20°C were performed and found to be acceptable.

The cyclic operation of a Ni-Cd battery requires that more electrical energy be replace during charge than is removed during discharge. The ratio of ampere-hours-in to ampere-hours-out is defined as recharge fraction. The recharge requirements for 20-ampere-hour cells have been empirically determined for loads ranging from 100 to 300 watts and for temperatures from minus 10°C to 30° C. These recharge values are an improvement in the state-of-the-art. At 20°C with a 200-watt electrical load, the battery recharge fraction was reduced from 120 to 107 percent while battery efficiency was increased from 75 to 85 percent. Under these conditions the heat generated per cycle has been decreased from 28 watts to 17 watts.

The third electrode signal characteristics tests resulted in the determination of internal third electrode resistance and signal temperature response, and depicted the nonuniformity of cell response when the cells were subjected to identical cyclic operations. Maximum internal resistance occurs when the external load is between 150 and 300 ohms. At maximum internal resistance the third electrode signal approaches a constant current source. The constant current characteristic can be used to facilitate the selection of three control cells with nearly identical third electrode signal characteristics to provide charge termination in a flight battery.

Useful battery capacity was determined as a function of temperature, cyclic history, and charge/discharge control parameters. Available battery capacity was found to decrease after extended cycling and this capacity degradation rate increased with increasing temperatures. This capacity degradation, considered as a memory phenomena, may be reduced by operation under varying cycling conditions. A significant capacity recovery may be obtained by discharging the battery and shorting out each cell for a minimum of 72 hours. Also a partial restoration of capacity can be achieved by subjecting the battery to several cycles at 0°C.

From these results, the ATM flight battery operating limits and operating specifications were established. The flight battery will be charged at a rate which is limited by (1) a maximum charge of 15 amperes, (2) available solar array output, and (3) maximum allowable battery voltage. The charge regime will be a constant current charge until the total battery voltage reaches a preset level, determined by the maximum allowable individual cell voltage, then the charge is limited to a constant voltage charge that is maintained 0.8 volt below the maximum allowable battery voltage. All cells of each 24-cell battery will be matched on an ampere-hour in-out basis with a match criterion of ±1 percent of rated capacity. Charge termination will be controlled

by the highest voltage of three redundant third electrode signals. Redundant signals will be accomplished by proper choice of third electrode load resistors affixed to cells of nearly identical third electrode signal characteristics. The operating techniques and specifications established for the ATM batteries should provide safe operation and maximum useful battery capacity for the duration of the ATM mission.

1. INTRODUCTION

This report summarizes the operational testing and evaluation program conducted on Ni-Cd batteries for use in the ATM power system. The test program was conducted to determine if Ni-Cd batteries could meet the ATM mission requirements, and to determine battery operating characteristics and efficient methods of operation. The test program was limited to evaluation of the controllable battery characteristics including voltage, charge current, overcharge, depth of discharge, temperature, and cell matching.

The ATM, as an earth orbiting satellite, has power requirements of 0 to 4000 watts. Each orbit of the ATM will be approximately 94 minutes in duration. A solar array will provide ATM system power and charging power for the secondary batteries during the 58-minute daylight portion of the ATM orbit. During the 36-minute night portion of the orbit, the secondary batteries will supply ATM system power. The proposed ATM power system requires eighteen 24-cell, 20-ampere-hour batteries. The power requirements for each battery, as presently specified, will be between 50 and 300 watts with a nominal load of 200 watts.

In addition to the power requirements, the secondary power system has two additional restrictions: all the heat generated must be dissipated by passive cooling, and an 8-month (4000 cycle) operational life is required.

Ni-Cd batteries were selected for the ATM mission because of their reliability, cycling capabilities, and known life capabilities. In addition, standard aerospace 20-ampere-hour Ni-Cd cells were available for immediate testing and evaluation, thus a research and development program was not required. A Ni-Cd cell and battery investigation was started in March 1967 to determine whether these batteries could meet the ATM mission requirements.

An initial literature search was conducted to provide a starting base for the test program and provide a background in existing battery specifications, characteristics, and operating techniques. The primary sources of information were references 1 and 2. Pertinent information derived from the literature research is presented in paragraph 2, which reflects the Ni-Cd battery information and recommended operating parameters at the beginning of the test program.

40M22411

2. NICKEL-CADMIUM BATTERY RESEARCH DATA

2.1 Nickel-Cadmium Cell Characteristics. The sintered-plate, sealed Ni-Cd cell, manufactured by General Electric Company, was chosen for the ATM mission. The plates of these cells are constructed of a perforated, nickel-plated, mild-steel base strip upon which a porous nickel structure has been sintered. The positive plates are impregnated with nickel hydrate and the negative plates are impregnated with cadmium hydrate. The cell case is stainless steel. The positive and negative terminals are isolated from the cell case by a ceramic-to-metal seal. The hermetic seal for each cell is achieved by welding the cover assembly to the case and by the ceramic-to-metal seals. The electrolyte is a 34 percent aqueous solution of potassium hydroxide (KOH).

Sealed Ni-Cd batteries have electrical properties that are difficult to predict. To a great extent the problems involved are inherent in the nature of the chemical system whose properties vary with the history of the cell and in the cycles of operation immediately preceding the measurement being taken. This variable is real and is in part based upon the properties of the electrodes.

The negative electrode functions during discharge by dissolving the cadmium metal and reprecipitating cadmium hydroxide as fine crystallites in the pores of the electrode plaque. Similarly, during charge, cadmium hydroxide dissolves and is redeposited at the electrode surface as cadmium metal. The size of the deposited crystallites depends upon the conditions of deposition: high currents and low temperatures give a finely divided deposit; low currents and high temperatures give a coarser deposit of larger crystals. The discharge characteristics of the negative electrode depend upon the microscopic surface area of the electrode-active materials. As the charging current and temperature change, the characteristics of the subsequent discharge voltage curves vary, even though the state of charge and the discharge conditions are the same. Thus a battery charged at high temperature, when cooled and discharged, delivers a lower output voltage discharge wave than the same battery charged at low temperature and discharged under the same conditions. Similarly, a cell discharged under conditions conducive to formation of low surface area deposits (low current and high temperature), charges at a higher potential than the same cell discharged in another way.

The positive electrode is also unpredictable in behavior, depending upon the temperature and the current at which it is charged. Unlike most battery electrodes, the nickel hydroxide electrode undergoes oxidation and reduction in the solid state; the reaction occurs preferentially at the surface and diffuses inward. Therefore, the surface composition, which determines the electrode potential, differs from the interior composition. The degree of difference is controlled by the rates of oxidation which is a function of temperature. As a result, the capacity, or state of charge, of the electrode is not a single-valued function of electrode potential. Variations in electrode potential greater than those experienced at end of charge can occur because of the above phenomena.

The capacity balance of the electrode pack (positive and negative electrodes) is critical to cell operation. It is almost impossible to exactly match the capacity of the positive and negative electrodes in a cell, hence, cells are deliberately built to have either an excess of negative or positive plate capacity. Negative limiting cells have an excess of positive capacity. Cells of this type show a marked voltage rise at the end of charge. These cells have not been built in sealed versions since the overcharging of the negative electrode gives hydrogen which is difficult to recombine at useful rates.

Positive limiting cells have excess negative capacity with the positive electrode becoming charged and discharged before the negative. On overcharge, the positive electrode gasses oxygen which can be recombined at the negative electrode at useful rates. Because any oxygen generated during overcharge can recombine, the cell can be sealed, hence, all spacecraft batteries are made with this type cell. Although it is necessary to use positive limiting cells for sealed operation in order to assure evolution of oxygen only on overcharge, the use of excess negative capacity is required for additional reasons. These reasons include provision for negative capacity to accommodate the oxygen stored in the gas phase during charging of the cell and to allow for the increase in positive capacity normally found when cells are used for prolonged periods of time.

Because of the multiple and often simultaneous chemical reactions occurring within the Ni-Cd cell, the variables influencing the cell's electrical characteristics have been inseparable. Ignoring the effects of age and cycle life, the discharge curve of a cell depends upon temperature, charge mode, efficiency, discharge current, capacity, and state of charge at the beginning and the end of discharge. Consequently, the individual limiting properties of the cells may be discussed separately but an understanding of the interdependency of the various factors is essential to the prediction of cell performance.

2.1.1 Charge-discharge reactions. The generally accepted Ni-Cd chemical reactions are as follows:

At the negative electrode:

$$Cd + 2OH^- \rightarrow Cd(OH)_2 + 2e^-$$

$$E_{rev} = -0.809 - 0.059 \log a\,(OH^-)$$

At the positive electrode: The positive electrode reactions are in some doubt, however, the following reaction has been suggested:

$$2\,NiOOH + 2H_2O + 2e^- \rightarrow 2Ni(OH)_2 + 2OH^-$$

$$E_{rev} = 0.480 + 0.059 \log \frac{a(H_2O)}{a\,(OH^-)}$$

This suggested reaction shows a deviation of the measured electromotive force (emf) from the theoretical as a function of alkaline concentration which was interpreted from the formation of solid solutions of NiOOH and $Ni(OH)_2$. The emf may be expressed as a function of the H_2O activity in the electrolyte. The combined form of the reaction is then:

$$2NiOOH + Cd + 2H_2O \rightarrow 2Ni(OH)_2 + Cd(OH)_2$$

$$E_{rev} = E^\circ - 0.059 \log a(H_2O)$$

In a cell operating in a starved condition, the water consumption is large in comparison with the amount available in the electrolyte solution and changes occur in the activity and the emf of a nickel electrode.

2.1.2 Gas evolution and recombination. Several electrode reactions involving gas evolution can occur in a Ni-Cd cell. At the nickel electrode, an overcharge reaction occurs in cells which are positive limited, i.e., the capacity of the cadmium electrode is greater than that of the nickel electrode:

$$4OH^- \rightarrow O_2 + 2H_2O + 4e^-$$

After the termination of charge, oxygen evolution is continued by decomposition of the active material, and increases in rate as an elevation in temperature occurs. This process occurs until total discharge. At the cadmium electrode or auxiliary electrodes in a charging cell:

$$4e^- + O_2 + 2H_2O \rightarrow 4OH^-$$

Upon termination of charge, the following recombination occurs:

$$2\,Cd + 2H_2O + O_2 \rightarrow 2Cd(OH)_2$$

Nitrogenous impurities which may be introduced into the electrolyte from the electrode impregnation process can set up an oxidation-reduction cycle that can rapidly discharge a sealed cell.

At the cadmium electrode, the following reaction occurs:

$$NO_3^- + H_2O + Cd \rightarrow NO_2^- + Cd(OH)_2$$

$$NO^- + 3Cd + 5H_2O \rightarrow NH_3 + 3Cd(OH)_2 + OH^-$$

At the nickel electrode, ammonia is then reoxidized back to nitrite:

$$NH_3 + 6NiOOH + H_2O + OH^- \rightarrow 6\,Ni(OH)_2 + NO_2^-$$

The cycle can continue until the cell is discharged, the rate being dependent on concentration and temperature. A concentration of a few parts per million of impurities can give very high self-discharge rates. Eventually, the impurities are converted to free nitrogen to the extent of 1 percent each cycle leaving a permanent nitrogen pressure within the cell:

$$2NH_3 + 6NiOOH \rightarrow N_2 + 6Ni(OH)_2$$

If the cell becomes negative limiting, hydrogen can evolve at the negative electrode during overcharge:

$$2H_2O + 2e^- \rightarrow H_2 + 2OH^-$$

Without catalytic recombination devices, this reaction is almost irreversible and results in long-lasting internal pressure. Even those cells which are manufactured with an excess negative capacity become negative limited after extensive cycling and long periods of inactivity.

When the cell is completely discharged and current is forced through the cell in the discharge direction, the potential of the cell will reverse and the cell is overdischarged.

At the nickel electrode:

$$2H_2O + 2e^- \rightarrow H_2 + 2OH^-$$

At the cadmium electrode:

$$4OH^- \rightarrow O_2 + 2H_2O + 4e^-$$

Oxygen will recombine in charging processes, but hydrogen will not significantly recombine without the presence of a catalyst.

These gas evolution reactions can significantly affect cell performance. The rate of oxygen evolution at the positive electrode during charge is controlled by the current associated with the oxygen evolution reaction. Little or no oxygen is released during the early stages of charge. As the cell nears maximum charge, its potential rises and the rate of oxygen evolution increases exponentially with rising potential.

2.1.3 Expressions for electrode potentials. The half-cell electrode potentials may be written in terms of concentrations:

$$E_{rev} = E^\circ - \frac{RT}{nF} \ln \frac{\text{(oxidized state)}}{\text{(reduced state)}} = E^\circ - \frac{RT}{nF} \ln \frac{a_{ox}}{a_{red}}$$

where:

a_{ox} = activity of oxidized state

a_{red} = activity of reduced state

E° = electrode potential when all substances involved are in their standard states of unit activity

R = 8.314 joules/°K-mole

F = 96,500 coulombs

n = valence (= 1 for monovalent ions, 2 for divalent ions)

T = Kelvin temperature.

At 25°C,

$$E_{rev} = E^\circ - \frac{(2.303)(8.314)(298.15)}{(96,500)(1)} \log \frac{\text{(oxidized state)}}{\text{(reduced state)}}$$

$$E_{rev} = E^\circ - 0.0590 \log \frac{a_{ox}}{a_{red}}$$

Considering the reaction:

$$Cd + 2OH^- \rightarrow Cd(OH)_2 + 2e^-$$

$$E_{rev} = E^\circ - 0.0590 \log \frac{a(OH)}{a(Cd)}$$

Since a(Cd) = 1

$$E_{rev} = -8.09 - 0.0590 \log a(OH^-)$$

Considering the reaction:

$$2NiOOH + 2H_2O + 2e^- \rightarrow 2Ni(OH)_2 + 2OH^-$$

then it follows that:

$$E_{rev} = 0.480 + 0.059 \log \frac{a(H_2O)}{a(OH^-)}$$

40M 22411

and for the total reaction:

$$2NiOOH + 2H_2O + Cd \rightarrow 2Ni(OH)_2 + Cd(OH)_2$$

$$E_{rev(T)} = \text{sum of half-cell potentials}$$

$$E_{rev(T)} = E^\circ - 0.059 \log a(H_2O)$$

2.2 Typical Operating Parameters. Of all the recommended charging regimes and techniques, a constant current/constant voltage technique was most applicable for ATM. The important cell or battery control parameters, based on the preceding charge regime, are discussed in the following paragraphs.

2.2.1 Charge current. Charge acceptance is the term designating the ampere-hour efficiency of charging a cell. All of the current passing through a cell results in some type of electrochemical reaction, but only a portion is utilized to build charge on the electrodes. In Ni-Cd cells, the charging reactions, $2Ni(OH)_2 + 2OH^- \rightarrow 2NiOOH + 2H_2O + 2e^-$ and $Cd(OH) + 2e^- \rightarrow Cd + 2OH^-$, are accompanied by other reactions that consume current but do not charge the electrode. These reactions are chiefly the decomposition of electrolyte to form free hydrogen and oxygen:

At the nickel electrode:

$$4OH^- \rightarrow O_2 + 2H_2O + 4e^-$$

At the cadmium electrode:

$$4H_2O + 4e^- \rightarrow 2H_2 + 4OH^-$$

Nickel-cadmium cell charge acceptance approaches 100 percent as a function of charging current as shown in figure 1. Charge acceptance is a complex function of the electrode's history, the charge rate, the temperature, the electrolyte concentration, the impurities present in electrodes and electrolyte, and the state of charge of the electrode. The charge acceptance of sintered-plate cadmium electrodes approaches 100 percent over a wide range of charge rate, temperature, and electrolyte variables.

Although the negative plate charge acceptance is close to 100 percent, there are three limitations imposed for proper plate performance. Each of these limitations concerns the evolution of hydrogen which occurs when the plate is overcharged, when the charge rate is in excess of the charge level, or when the cell is subjected to a high charge rate at low temperatures. The low temperature charge rate is a function of temperature and decreases as temperature decreases. Hydrogen in Ni-Cd cells, with the exception of cells containing a fuel cell auxiliary electrode,

40M 22411

cannot be recombined. Therefore, when the cell is operated under conditions in which hydrogen is evolved it will eventually fail. Cell rupture as a result of excessive pressure will occur at 300 pounds-per-square-inch-gauge (psig) in a restrained cell, or at approximately 50 psig in an unrestrained cell. An additional phenomena is the masking of the auxiliary electrode signal whenever hydrogen is evolved.

The charge acceptance of a nickel-hydroxide electrode is relatively low, about 70 percent at room temperature for charging at the 10-hour rate (C/10), where C is the rated capacity of the battery. This is an average figure for the charging part of the cycle, with most of the loss occurring in the last 5 to 10 percent of the electrode capacity. The charge acceptance has been measured by comparing the plate capacity at various temperatures to the capacity at 25°C with all charging parameters remaining constant. As shown in figure 2, the capacity at 40°C was 0.5, the capacity at 0°C was 1.3, and the capacity at minus 40°C was 1.4.

Charge acceptance of the nickel-hydroxide electrode effectively limits the upper operating temperature to 40°C or less. The lower temperature limit is determined by the hydrogen evolution at given charge rates.

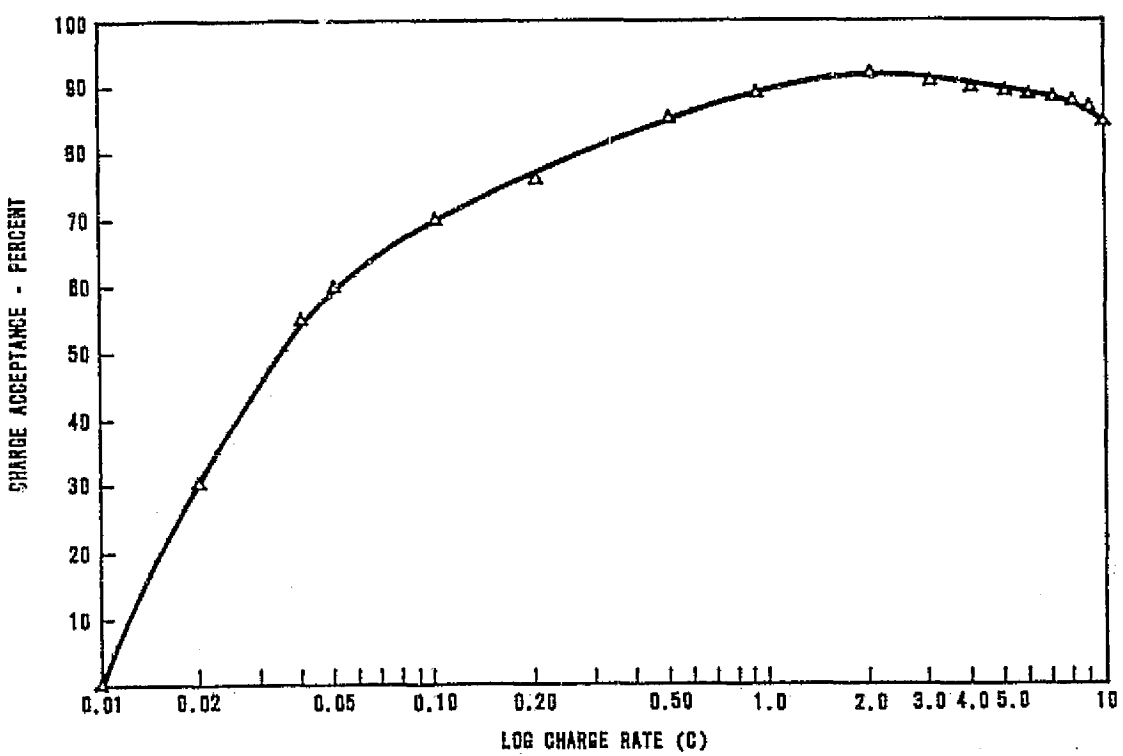

FIGURE 1. NICKEL-CADMIUM CELL CHARGE ACCEPTANCE

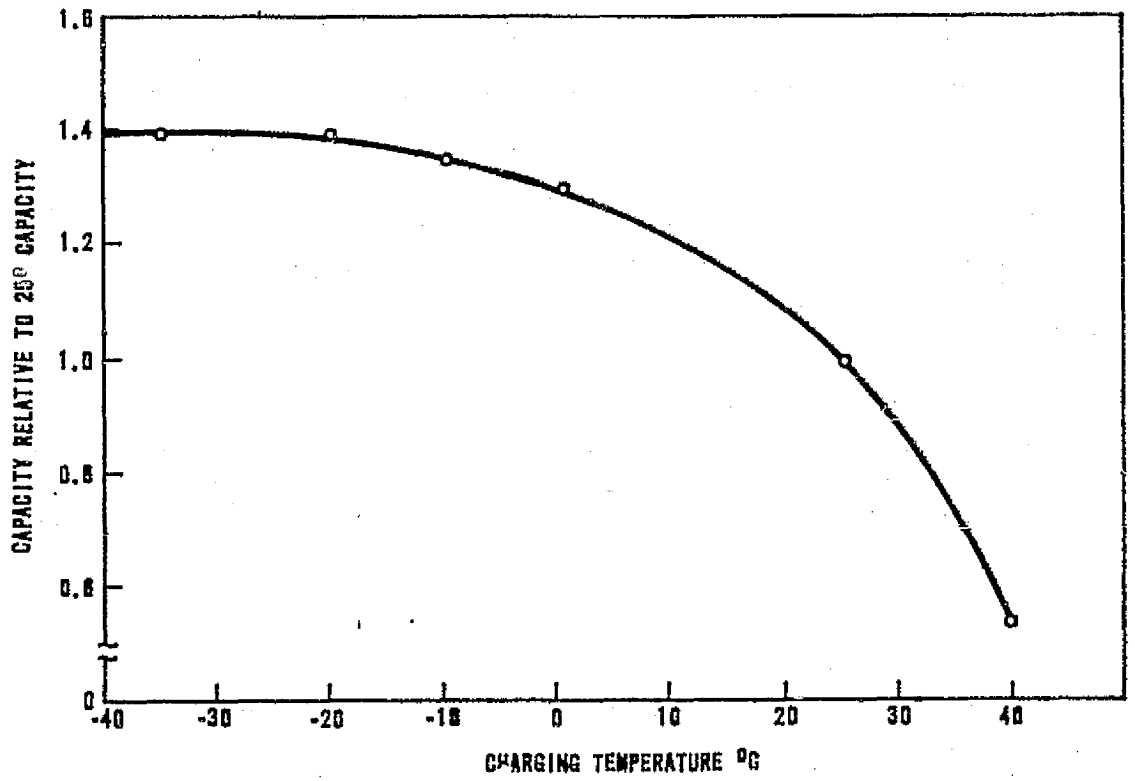

FIGURE 2. POSITIVE PLATE CHARGE ACCEPTANCE (DISCHARGES AT 25°C)

2.2.2 Maximum allowable cell voltage. The maximum allowable cell voltage is limited to the hydrogen evolution potential which is reported to be somewhere between 1.47 and 1.55 volts per cell at room temperature. An additional variable is the negative temperature coefficient of the cell emf, which is reported to be 2.5 millivolts (mV) /°C/cell. This value reflects changes in overvoltage, equilibrium potential, potential drops across the electrode, and the impedance of the electrolyte and electronics. On a 24-cell basis, the battery voltage values as a result of the temperature coefficient would be 35.4 volts at 20°C, 36.3 volts at 0°C, and 34.2 volts at 40°C.

2.2.3 Third electrode charge termination signal. In the nickel-cadmium cell, charging reactions are always accompanied by other reactions that consume current, but do not result in charging the electrode. These reactions are in large part the electrolytic decomposition of electrolyte to form hydrogen and oxygen. In spacecraft cells, which are positive limited, oxygen evolution is of primary concern in the normal operating range.

The gassing behavior of the positive nickel-hydroxide electrodes during charging shows that the onset of gassing between 40 to 80 percent of full charge is highly variable and unpredictable, even in experiments using the same electrode,

charging rate,and temperature. The rate of gassing at 100 percent state of charge is never 100 percent because of the delay in gas evolution. Gas is evolved at a relatively high rate for some time after charging is stopped. This may represent a loss of usable capacity in the plate.

For sealed operation, the oxygen evolved from the nickel-hydroxide electrode must be recombined at the cadmium electrode if excessive pressure is to be prevented. The actual rate of oxygen recombination at the cadmium electrode is known to be fast, so that the controlling factor is the rate of transport of oxygen to the cadmium electrode.

An important method for increasing the rate of oxygen recombination in sealed cells is by the use of auxiliary electrodes which promote the electrochemical reduction of oxygen. Passive auxiliary electrodes, known as fuel cell electrodes, are used primarily for gas recombination. Active auxiliary electrodes, known as adhydrode electrodes, are used primarily to provide a signal for initiating charge control.

Active auxiliary electrodes differ from the passive electrodes mentioned previously by having provision for taking a signal from the auxiliary electrode circuit. A current or voltage signal can be obtained. During charging all of the charging current passes through the nickel-hydroxide electrode; all of the current passes through the cadmium electrode until oxygen starts to evolve at the nickel-hydroxide electrode. This oxygen reacts at the auxiliary electrode and current thus flows into the auxiliary electrode circuitry, shunting the current flowing through the cadmium electrode. This shunt current depends upon the oxygen pressure, size of auxiliary electrode, auxiliary electrode circuit impedance, temperature, and the specific auxiliary electrode parameters, such as catalyst type, loading, and waterproofing. The output from this signal electrode is proportional to the partial pressure of evolved oxygen.

The fuel cell type of electrode is designed to be insensitive to oxygen pressure and carry large currents per unit area of surface. This electrode has a current flow that is a direct function of the rate of gas evolution in the cell up to the saturation level. Using a large area auxiliary electrode, with a low circuit impedance, the oxygen produced on charging will be reduced as fast as it arrives at the auxiliary electrode until the rate of oxygen production exceeds the capacity of the fuel cell electrode circuit. This electrode will also recombine hydrogen.

In summary, gassing information related to charging is as follows:

(a) The onset of gassing between 40 and 80 percent of full charge is highly variable and unpredictable.

(b) Two types of auxiliary electrodes, an adhydrode and a fuel cell type, are being used to detect the oxygen pressure or to recombine the oxygen.

(c) Oxygen evolution from the nickel-hydroxide electrode increases with an increase in temperature.

2.2.4 Memory. The memory phenomena is defined as a reversible battery capacity degradation. The phenomena is reversible in the sense that the lost capacity can be recovered through special charge and discharge techniques. It has been proposed that the memory phenomena is caused by a crystal growth on the cadmium plate. As previously noted, cadmium hydroxide dissolves and is redeposited at the negative electrode as cadmium metal during charge. The crystal size is dependent on several parameters: low current and high temperature give a coarse deposit of larger crystals; high current and low temperature give a finely divided deposit.

2.3 Summary of Research Data. The information available on Ni-Cd cells or batteries was rather general in nature. Typical voltage levels were limited to 1.47 to 1.55 volts during charge to prevent hydrogen evolution. Charge current was limited by hydrogen evolution possibilities on the high side and by inefficient charge acceptance on the low side. Charge termination control was suggested by a third electrode signal, however, no specific load values or control limits were available. Memory phenomena was discussed but no specific recovery or delay techniques were recommended.

A test program was initiated to determine more specific values on Ni-Cd cells and batteries and to ascertain if the values were compatible with the ATM mission specifications.

3. TEST PROGRAM

3.1 Test Specimens. Each test battery was composed of 24 series-connected, 20-ampere-hour Ni-Cd cells manufactured by General Electric Company. The three types of 20-ampere-hour cells that were tested are shown in table I. The AB09 cell provides only the negative and positive electrodes and does not have auxiliary signal or recombination electrodes. The AB10 cell, in addition to the two main electrodes, contains a third adhydrode electrode which develops an electrical signal that is proportional to the partial pressure of oxygen which is generated during normal cell operation. The oxygen is recombined at the negative plate in this cell. Any hydrogen which might evolve is not recombined. The negative to positive electrode capacity ratio is approximately 1.2 to 1. Excess negative capacity insures that the cell is positive limited and only oxygen is evolved during normal cell operation when the cell becomes fully charged. The AB12 cell contains a precharged negative electrode, a third adhydrode electrode, and a fourth (fuel cell) electrode. The third electrode is similar to the AB10 cell third electrode. The fourth electrode recombines oxygen at high rates up to its design limits. It will also recombine any hydrogen which might evolve during cell operation.

One of the major differences between the AB10 and AB12 type cell is the 20 percent of precharged cadmium plate surface area in the AB12 cell as shown in figure 3. The purpose of precharge, which increases the effective cadmium electrode area, is to maintain the useful battery capacity for longer periods of cyclic operation. The apparent deficiency of oxygen recombination area in the AB12 cell is offset by the fourth electrode which provides rapid recombination of oxygen and hydrogen.

TABLE I. NICKEL-CADMIUM CELL TYPES

Leading Particulars	Type AB09	Type AB10	Type AB12
Capacity (Ampere-hour)			
Rated	20	20	20
Average	25	25	25
Third Electrode	None	Type B, C	Type C
Recombination Electrode	No	No	Yes
Precharged Cd Plate	No	No	Yes
Electrolyte Volume (34% KOH)	68 cubic centimeters (cc)	68 cc	72 cc
Weight (grams)	889	889	889
Dimensions (centimeters)			
Height	18.176 ± 0.0381	18.176 ± 0.0381	18.176 ± 0.0381
Width	7.6073	7.6073	7.6073
Thickness	2.2936	2.2936	2.2936

The third electrode of the AB10 cell is either a type B or type C electrode. The third electrode for the AB12 cell is a type C. The basic differences of the type B and type C electrodes are as follows:

Item		Type B Electrode	Type C Electrode
Nickel substrate	:	40 square centimeters	10 square centimeters
Catalyst	:	Platinum	None
Oxygen diffusion barrier	:	Electrolyte	1/2-mil teflon film pressed onto electrode

The diffusion barrier stabilizes the third electrode response as a function of life. The catalyst function in the type B electrode is to recombine oxygen with some hydrogen recombination also.

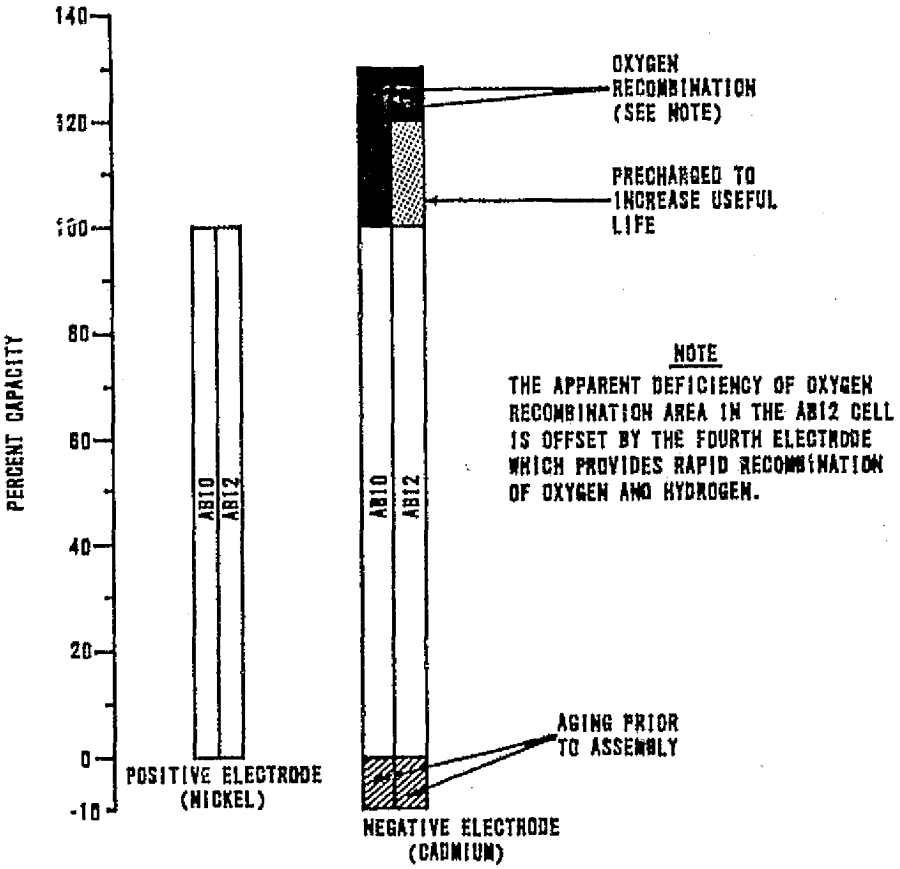

FIGURE 3. COMPARISON OF PLATE CAPACITIES - GENERAL ELECTRIC COMPANY AB10 CELL AND AB12 CELL

There were nine batteries used in the ATM test program as follows:

(a) GE1, GE2, and GE2M. The GE1 and GE2 batteries contained 21 AB09 cells and 3 AB10C cells. These batteries were the initial test batteries utilized to investigate the optimum ATM charge regime. Because of capacity degradation and cell divergence at the end of charge, the most nearly matched cells of GE1 and GE2 were combined to make GE2M.

(b) GE1C, GE2C, and GE3C. The GE1C, GE2C, and GE3C batteries consisted of 24 AB10C cells which had been 5 percent matched on an ampere-hour charge and discharge basis prior to delivery.

(c) GE1AB12, GE2AB12, and GE3AB12. The AB12 cell was chosen for the ATM flight batteries and these flight-type test batteries were subjected to extensive ATM cyclic and diagnostic tests.

3.2 Test Procedures. The primary test procedure followed throughout the test program was to conduct operational tests under simulated ATM orbit conditions, evaluate the battery parameters and performance, and then perform specific tests for investigation of particular characteristics or parameters. The ATM test cycle was as follows:

(a) Charge time: 58 minutes

(b) Discharge time: 36 minutes

(c) Temperature: 25 ± 5°C

The 24-cell test batteries were mounted in a restrainer designed by the battery manufacturer. Thermal control of the cells was accomplished by maintaining an airflow over heat sinks located on the large face of each cell. The temperature was maintained within ± 1°C with a temperature chamber.

The cells were electrically connected in series. Control of the battery was by an ATM flight-type electronic control package or by an ATM orbit simulating power supply programmer. A 700-watt power supply simulated the ATM solar array output. The ATM electrical load was simulated with an electronically controlled load bank. Cyclic timing was performed with two tandem controlled clocks.

Data were normally collected with a data acquisition system which recorded individual cell voltages, total battery voltage, third electrode voltage, and battery current. In addition, a strip chart recorder continuously monitored the total voltage, battery current, and the third electrode signal. Another multipoint recorder was used to record all test specimen temperatures.

Data processing was controlled by a magnetic tape unit associated with the data acquisition system. A 25-channel data acquisition system with a punched paper tape output was used for special tests.

4. TEST RESULTS

4.1 Test Data Presentation. Because of the sometimes concurrent battery tests, related test sequences, and generally simultaneous data collection of various operational parameters, the results of all battery tests are presented under primary operational characteristics headings.

Specifically, the test results are presented as follows:

(a) Maximum Voltage Characteristics (4.2)

(b) Charge Rate (4.3)

(c) Third Electrode Signals (4.4)

(d) Recharge Requirements (4.5)

(e) Capacity Degradation Characteristics (4.6)

4.2 Maximum Voltage Characteristics. The original battery charge regime was a combination of a constant current and constant voltage charge. The initial charge regime is shown in figure 4. The charge, which was 58 minutes in length, was initially a 10-ampere constant current. This charge level was maintained until the total battery voltage reached a preset level. This level was determined by the maximum allowable individual cell voltage of 1.47 volts. When the voltage of any cell reached 1.47 volts during the first charge cycle, the charger was adjusted to convert the charge from constant current to constant voltage. During the remaining charge time, the battery voltage remained constant. During the 36-minute discharge time (see figure 4, the 58 to 94 minute period), the battery load was maintained at 200 watts.

The types of individual cell voltage characteristics resulting from the initial charge regime are shown in figures 5 and 6. The initial tests were performed with AB09 cells. Figure 5 depicts the relationship between the charge current and several individual cell voltages. Of particular importance is the individual cell voltage divergence after 100 percent of the previous discharge has been delivered to the cells. Figure 6 shows the charge cycle of the same cells shown in figure 5 except that the data of figure 6 were recorded earlier. Comparison of both figures indicates consistent performance of the cells, i.e., cell 10 will remain the high cell and cell 8 will remain the low cell as long as the battery is subjected to continuous cyclic operation.

4.2.1 Cell voltage divergence - AB09 tests. The AB09 tests indicated that the cell voltage divergence characteristics appeared to be a function of the number of cycles to which a battery has been subjected. An example of the cell voltage divergence characteristic is shown in figure 7. As indicated, the cell divergence increased from 8 to 38 mV. Note the consistent order of the cells, with the voltage of cell 8 being the lowest and the voltage of cell 10 being the highest. The four phases shown in figure 7 are test sequences related to capacity degradation characteristics and are discussed elsewhere.

Cell voltage divergence is caused by a difference in the capacity of the individual cells of a battery. The capacity difference may be caused by an initial cell capacity mismatch during battery assembly or as a result of a memory phenomena.

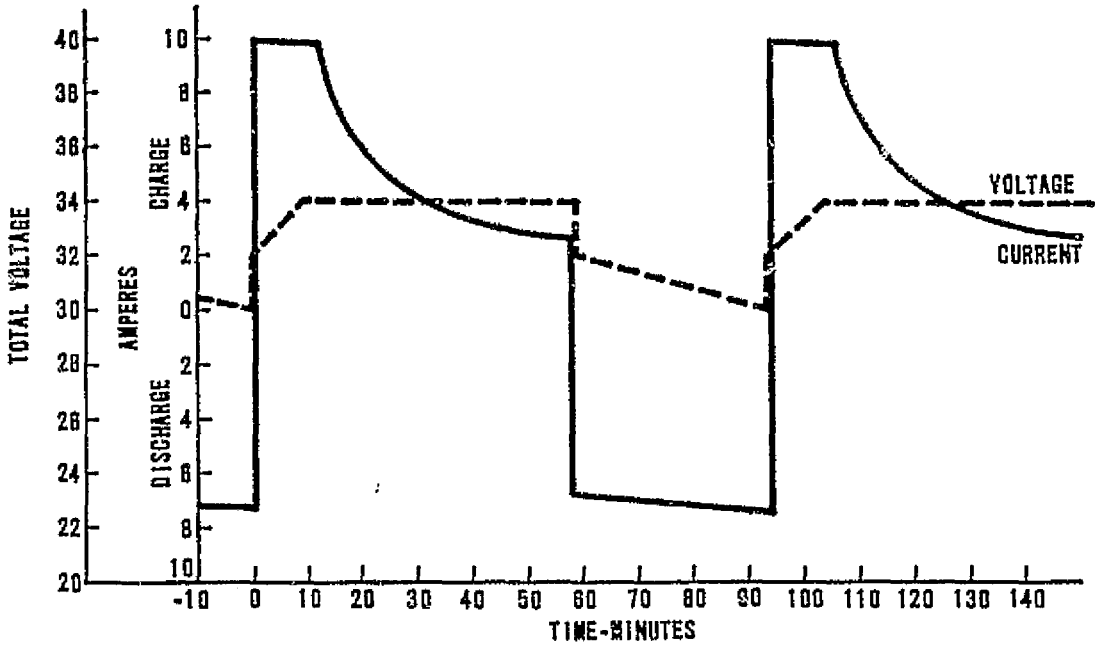

FIGURE 4. INITIAL CHARGE REGIME-AB09 BATTERY

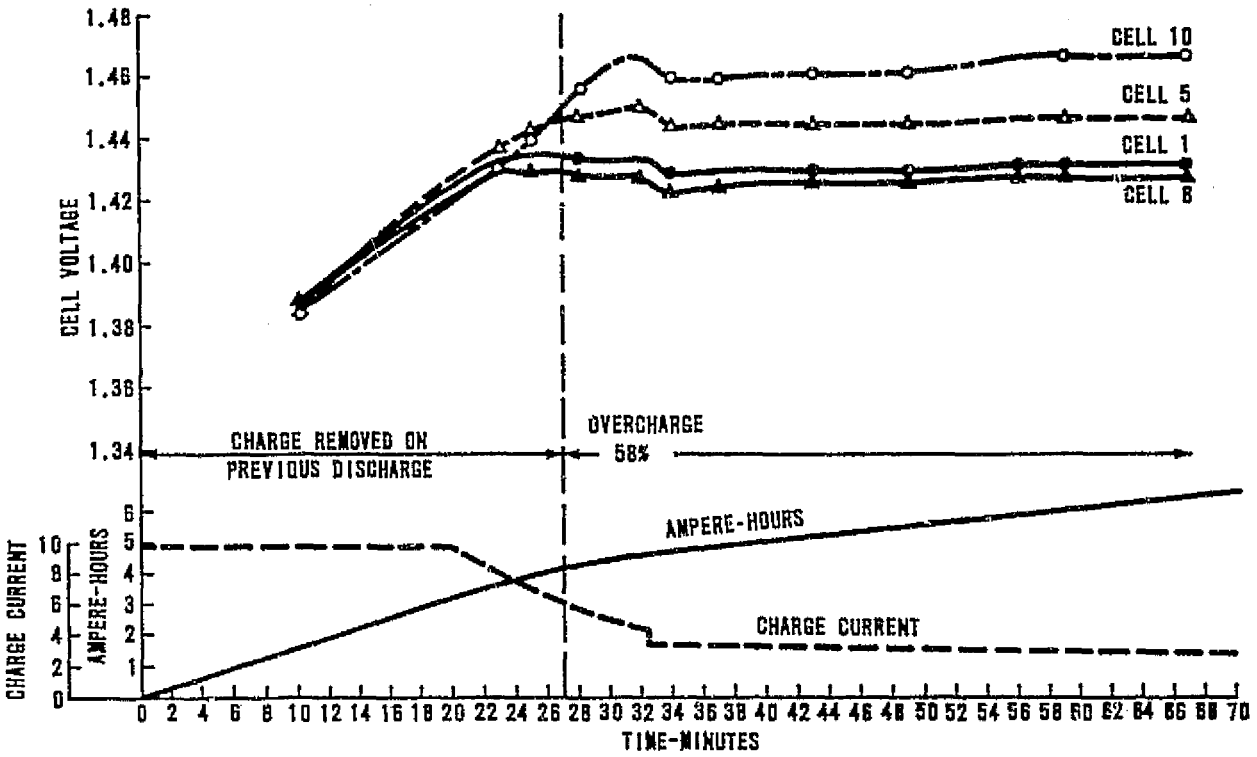

FIGURE 5. INITIAL CHARGE REGIME-CELL CHARACTERISTICS, AB09 BATTERY (CYCLE 247)

4014244

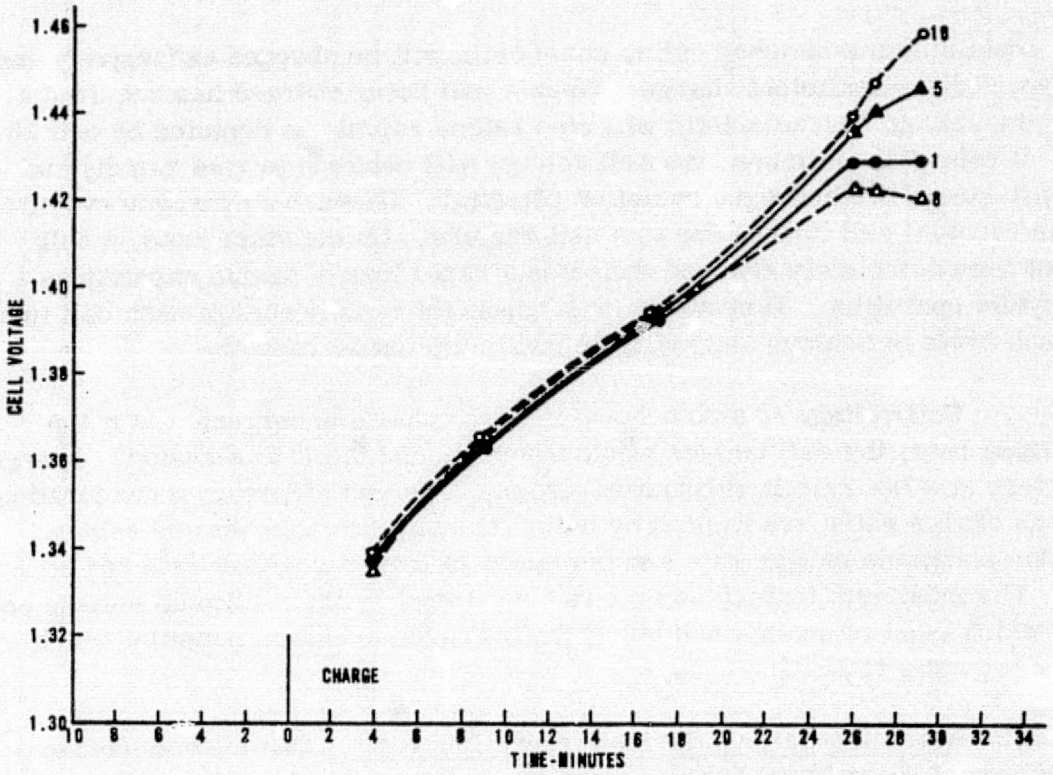

FIGURE 6. INITIAL CHARGE REGIME-CELL CHARACTERISTICS, AB09 BATTERY (CYCLE 134)

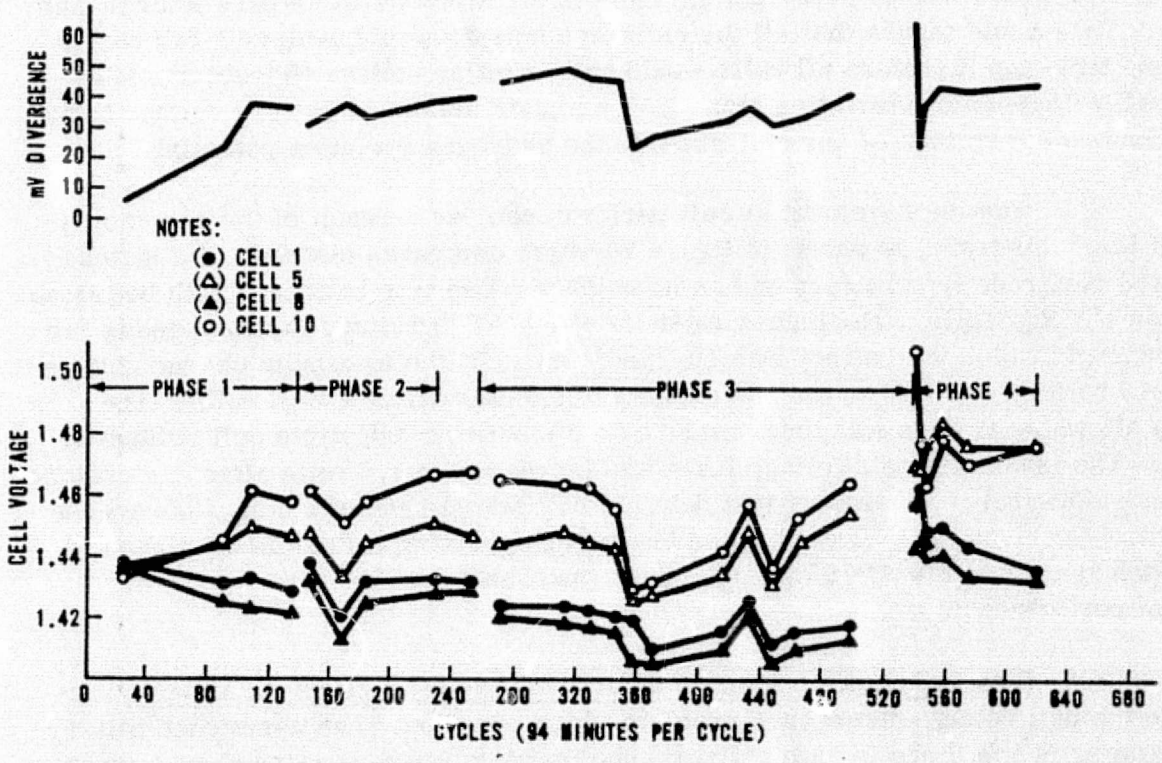

FIGURE 7. CELL DIVERGENCE CHARACTERISTICS, AB09 BATTERY

40M 22411

In a battery containing mismatched cells, some cells will be charged excessively and others will not acquire sufficient charge. When a cell being charged has acquired a full charge, the voltage characteristic will rise rather rapidly as depicted by cell 10 in figure 6. If charging continues, the cell voltage will continue to rise rapidly and eventually will exceed the hydrogen evolution potential. Excessive hydrogen evolution will result in eventual cell failure due to a cell rupture. On the other hand, a cell which has not been completely charged indicates a rapid loss of usable capacity as a function of cyclic operation. Therefore, it is important to fully charge each cell in a battery in each cycle to achieve and maintain maximum useful capacity.

Cell voltage is also a function of the charging current. At a 1.5 ampere charging rate, the cell voltage would never exceed the 1.5 volt level. Charging a cell or battery at a low rate is impractical from a time and efficiency consideration. However, high charge rates are limited by the maximum allowable battery voltage. This limits the maximum charge rate and the length of time a constant rate can be maintained. The maximum battery voltage is determined by the maximum voltage on any one cell which must be maintained below the hydrogen evolution potential which reportedly is 1.5 volts at 25°C.

4.2.2 Recommendations derived from AB09 tests. One method used to reduce the effects of the voltage divergence shown in figure 8 is to reduce the constant voltage charge by at least 0.6 volt below the maximum voltage to which the battery is charged. This method is shown graphically in figure 9. A second method used to reduce the divergence was to match all the cells in a battery on an ampere-hour in-and-out basis. This would insure that all the cells in a battery would achieve a full charge at the same time and therefore all cells would have similar voltage characteristics. Similar cell voltage characteristics also allow a higher maximum battery voltage to be achieved before the voltage of any cell exceeds the hydrogen evolution potential.

The improvement in cell performance, as a result of the recommendations of the AB09 tests, is shown in figure 10 which compares test data of a matched AB10, third electrode type battery and an unmatched AB09 type battery. Both batteries are the same electrically. The higher capacity of the AB10 battery is attributed to the higher voltage to which the battery was charged. At 20°C the maximum charge voltage on the AB10 battery was 35.4 volts and on the AB09 battery it was 34.8 volts. The maximum allowable voltage was determined by the maximum allowable cell voltage of 1.5 volts. The maximum cell voltage limit was increased to 1.5 volts after discussions with the manufacturer. Subsequent test data did not indicate adverse cell performance as a result of the increase. The increase in battery operating voltage is attributed to the 24 matched cells of the AB10 battery. Subsequent matched batteries which were tested also performed as well.

4.2.3 Effect of cyclic operation on cell voltage divergence-AB10 tests. In addition to the cell voltage divergence problem which occurred in an unmatched battery at the beginning of life there is also a divergence problem which appears to be a function

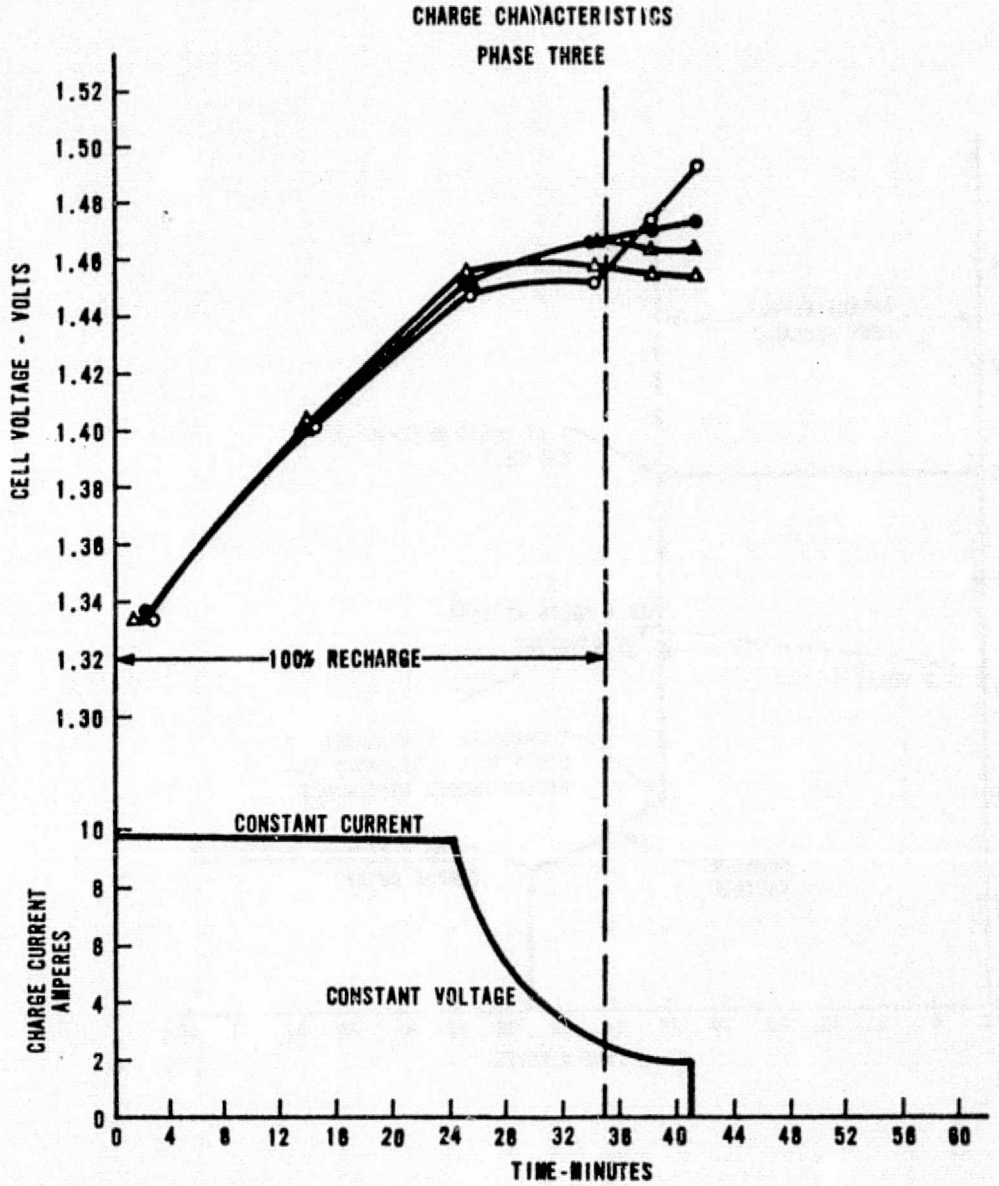

FIGURE 8. CELL DIVERGENCE DURING CONSTANT VOLTAGE CHARGE

40M22411

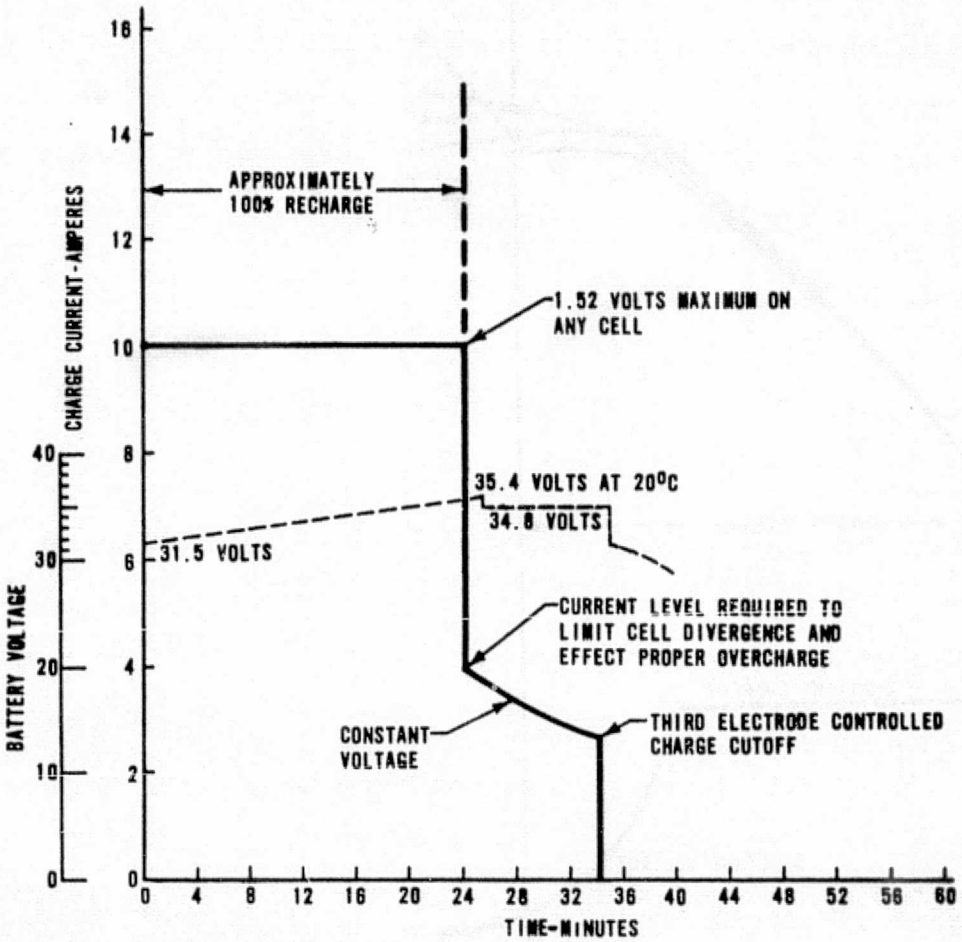

FIGURE 9. RECOMMENDED CHARGE REGIME AS A RESULT OF INITIAL AB09 TESTS

40M22411

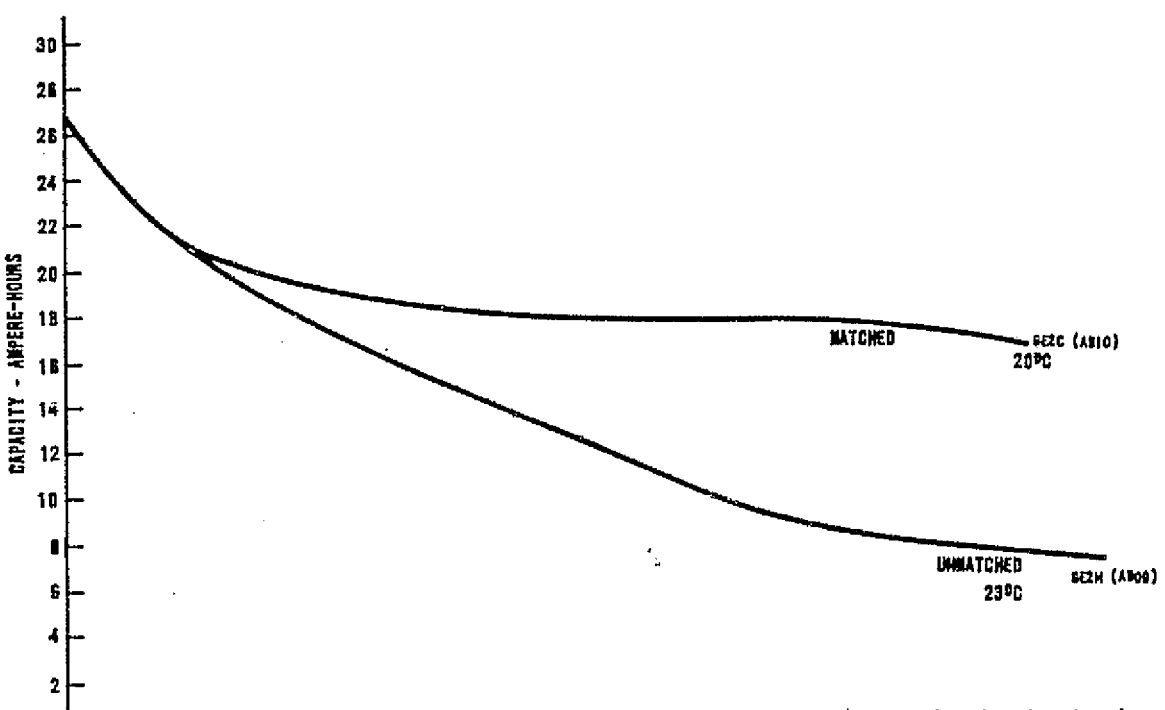

FIGURE 10. BATTERY CHARACTERISTICS-CELL MATCHING EFFECTIVENESS

of cycle life. This problem was observed in the operation of AB10 cells. Two AB10 batteries were being subjected to simulated ATM orbital conditions at 20°C as shown in figure 11. During the initial battery voltage adjustments, all cells were checked during charge to insure that 1.5 volts per cell was never exceeded and that all cell voltages were within acceptable limits.

During the course of normal ATM cycling, test batteries GE2C and GE3C contained cells which exceeded the maximum operating voltage of 1.5 volts. The following list of figures detail individual cell performance before and after action was taken to correct the overvoltage condition:

AB10 Battery				Remarks
GE2C Figure	Cycle	GE3C Figure	Cycle	
12	18	16	73	Normal and diverging cells
13	36	17	156	Decrease in cell voltage prior to trip after the maximum battery trip voltage is reduced.
14	109			High cell voltage after trip
15	260	18	305	Acceptable cell voltage after the constant voltage had been reduced

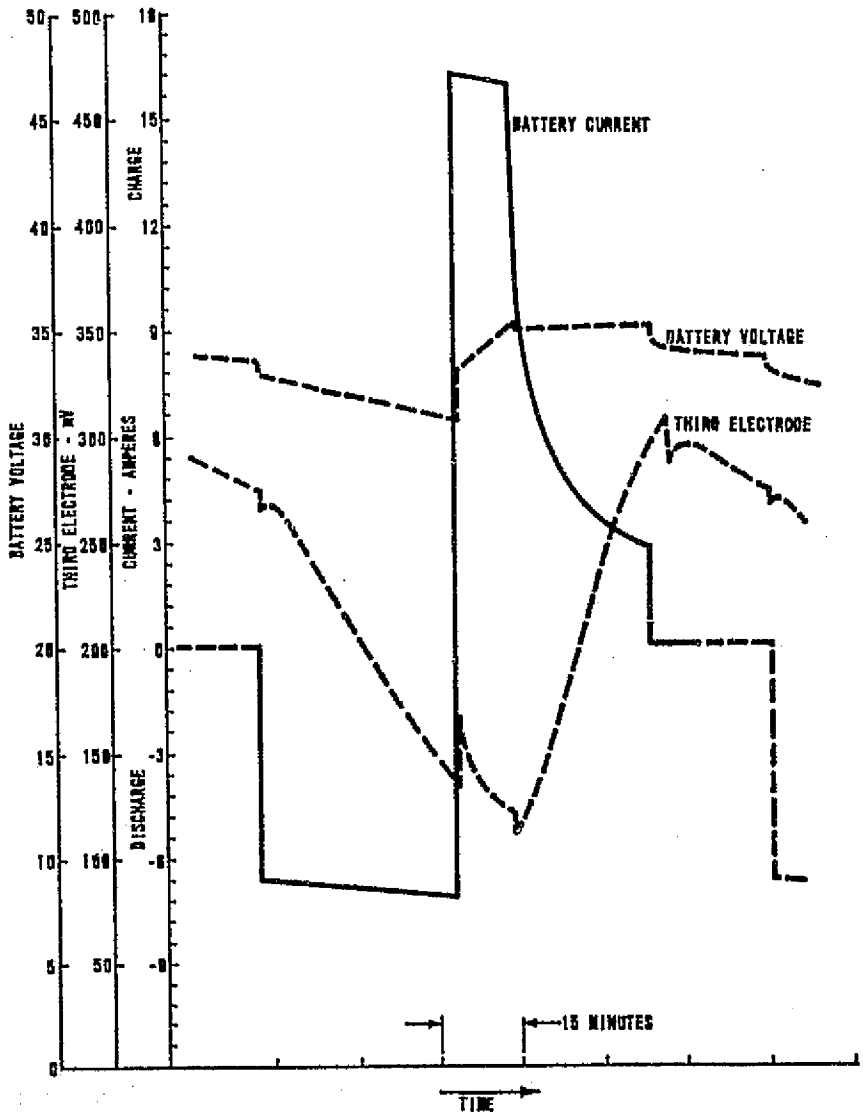

FIGURE 11. SIMULATED ATM CYCLE - AB10 BATTERY

40Y 22 SH

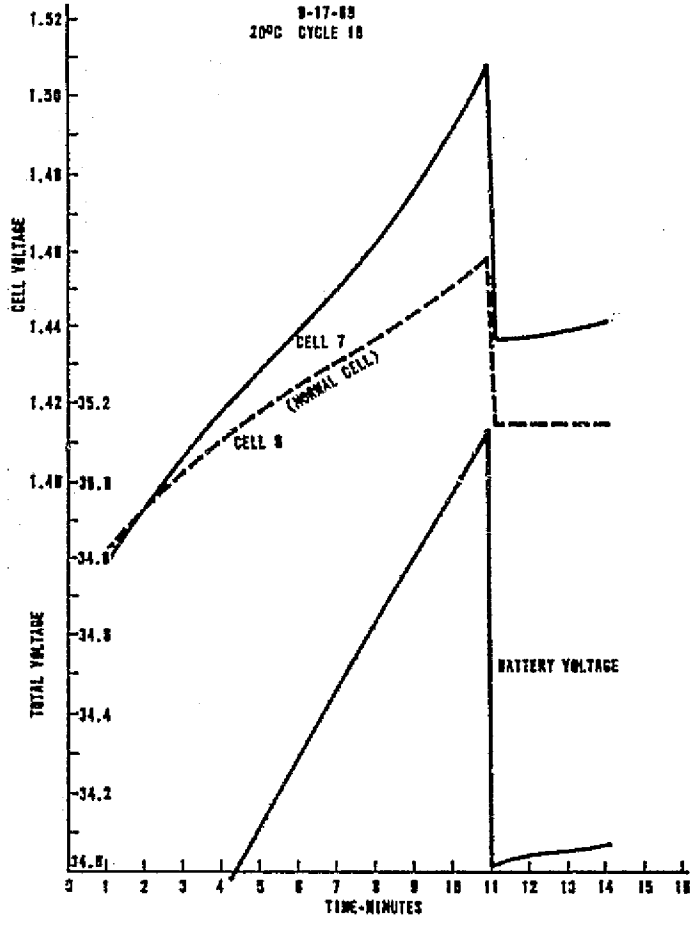

FIGURE 12. CELL DIVERGENCE DURING CONSTANT VOLTAGE CHARGE, AB10 BATTERY, CYCLE 18

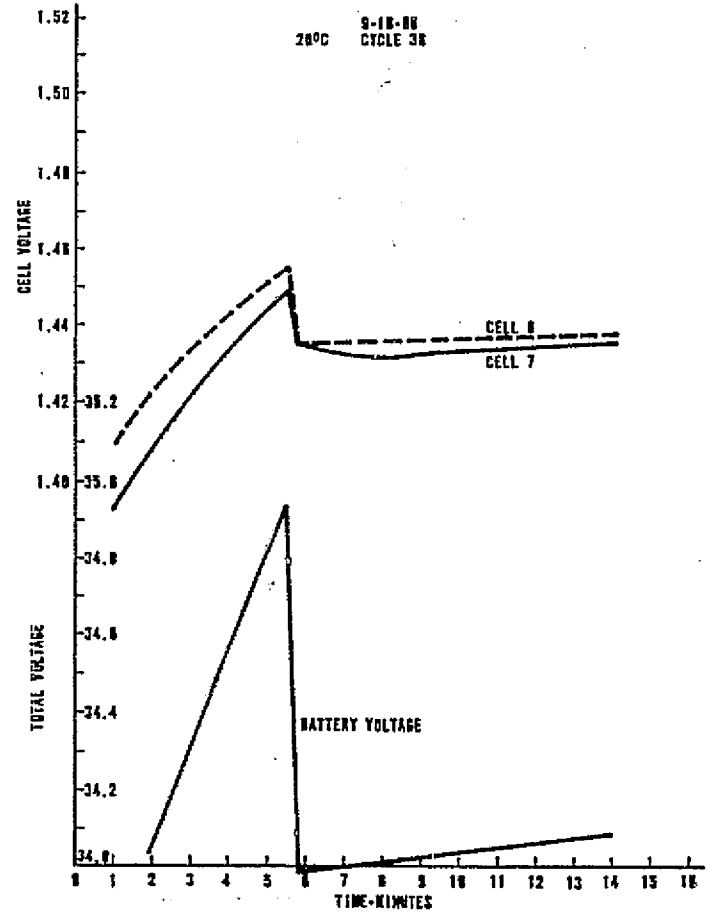

FIGURE 13. CONTROL OF CELL DIVERGENCE (FIGURE 12) BY REDUCING MAXIMUM CHARGE VOLTAGE, AB10 BATTERY

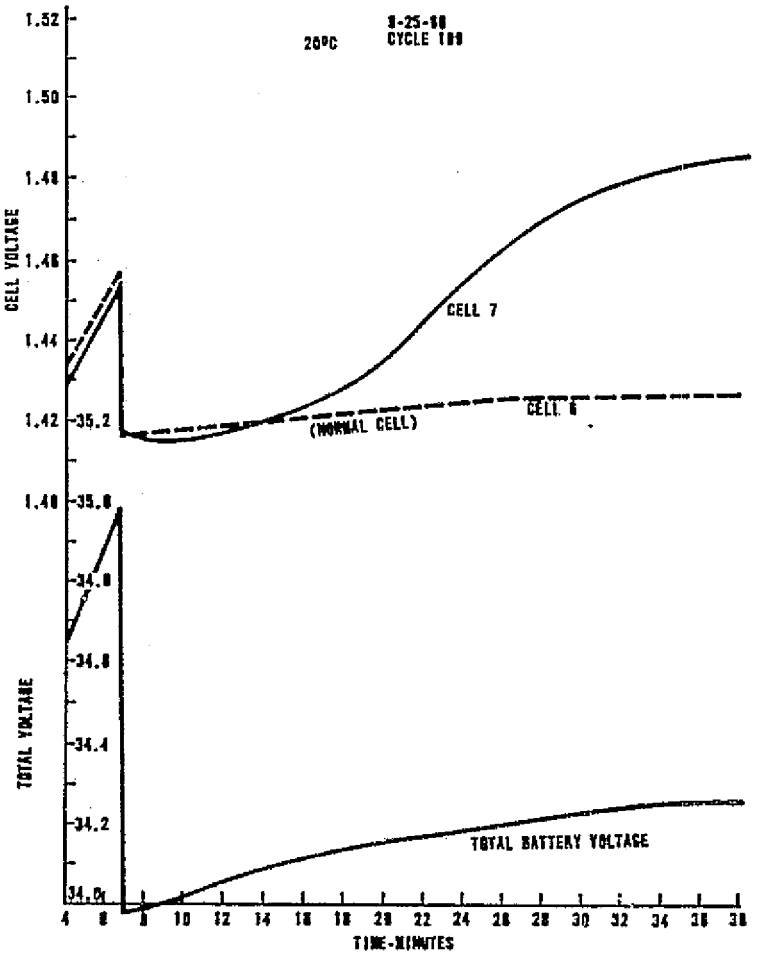

FIGURE 14. CELL DIVERGENCE DURING CONSTANT VOLTAGE CHARGE, AB10 BATTERY, CYCLE 109

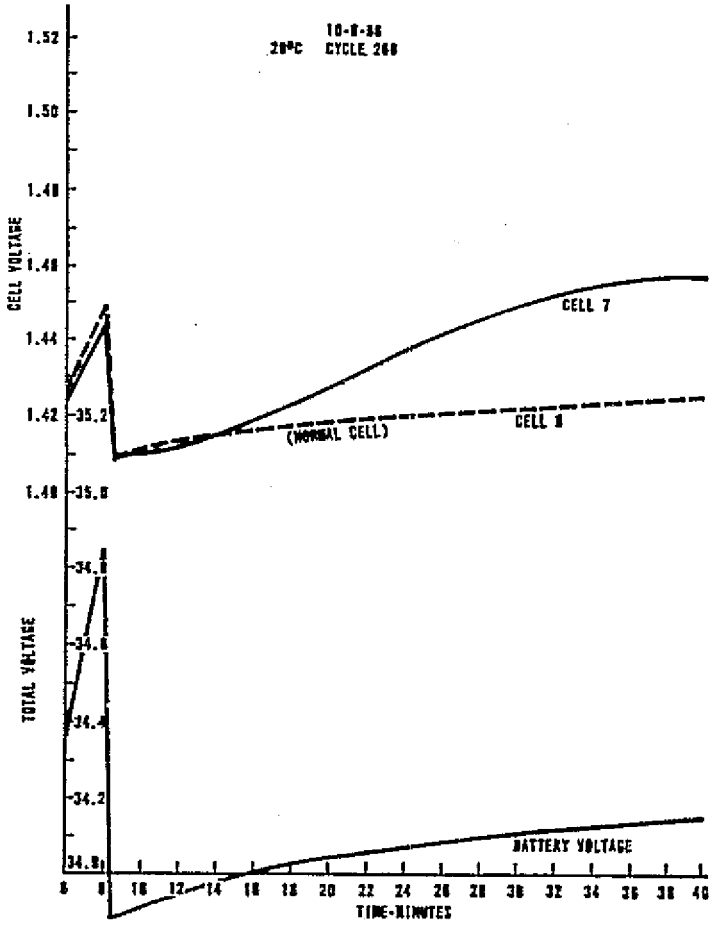

FIGURE 15. CONTROL OF CELL DIVERGENCE (FIGURE 14) BY REDUCING LEVEL OF CONSTANT VOLTAGE CHARGE, AB10 BATTERY

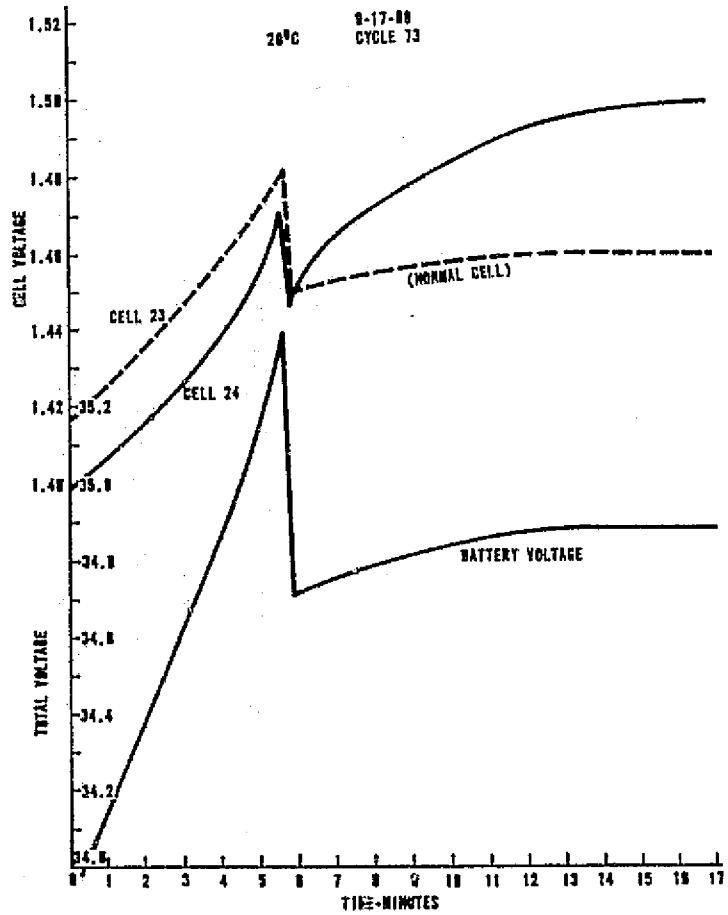

FIGURE 16. CELL DIVERGENCE DURING CONSTANT VOLTAGE CHARGE, AB10 BATTERY, CYCLE 73

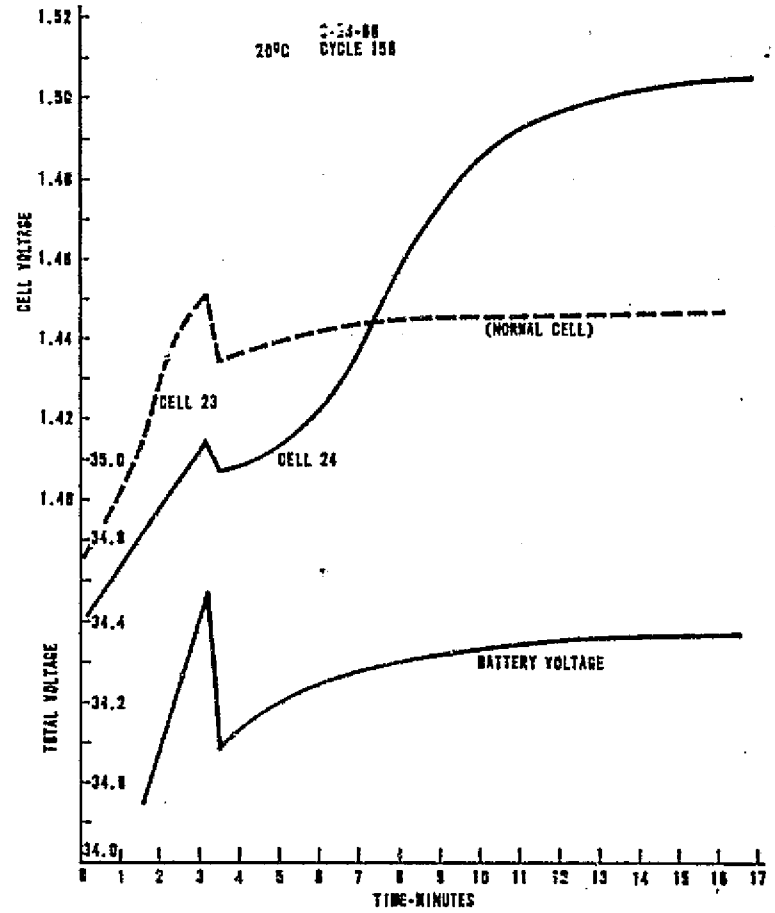

FIGURE 17. CELL DIVERGENCE (FIGURE 16) NOT AFFECTED BY MAXIMUM CHARGE VOLTAGE REDUCTION, AB10 BATTERY

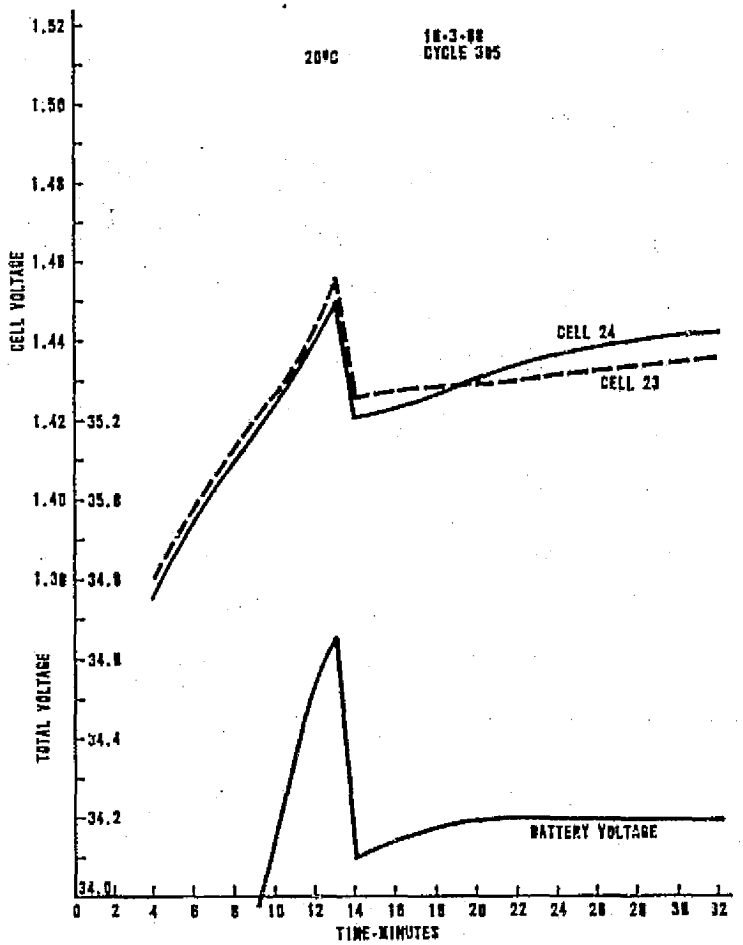

FIGURE 18. CONTROL OF CELL DIVERGENCE (FIGURE 16) BY REDUCING LEVEL OF CONSTANT VOLTAGE, AB10 BATTERY

The cell voltage changes noted in figures 12 through 15 for GE2C occurred during normal ATM cycling. Extensive cycling under these high cell voltage conditions could result in hydrogen gas evolution and in eventual battery failure. It is to be noted, however, that excessively high cell voltage can be remedied by reducing the maximum battery voltage (trip), and by reducing the constant charge voltage.

4.2.4 Summary-maximum voltage characteristics. As a result of the cell performance noted in these tests, several problem areas have become apparent:

(a) High individual cell voltages occur as a result of long-term, steady-state cycling. In addition, the time of onset and the particular cell or cells effected cannot be reliably predicted at the start of cycling. This problem may require that critical battery voltage adjustments during charge must be set to levels which would maintain safe voltage levels over long-term cycling.

(b) A factor observed and measured during these and other tests was the reduction of useful battery capacity over long periods of continuous cycling. This phenomena is attributed to the onset of memory. The effects of memory were found to be reduced by initially charging the battery to its full capacity prior to cycling and by adjustments of the battery voltage trips and the constant voltage charge rate at cycle 1 to their maximum allowable safe operating levels. This procedure causes the effective capacity to remain above useful levels for longer periods of cycling. If, after an initial charge, the critical voltage points are reduced to levels which will be safe at cycle 1000, the useful capacity decreases at a much faster rate with continuous cycling.

(c) The data show that the safe charge voltage operating levels are significantly higher at cycle 1 than at cycle 1000 for the AB10, type C, cells. The problem becomes one of selecting a set of operating limits which will limit individual cell voltages to safe levels over the intended cycling period and still maintain acceptable capacity during the cycle life.

Test data indicated that further tests were required to determine the effect of safe level operation on the capacity degradation and on cell voltage characteristics as a function of long-term cycling. Maximum voltage tests of AB09 and AB10 batteries, especially data on maximum voltage during charge and cell matching requirements, were applied to subsequent tests on AB12 batteries. The effects of temperature on the anomalies observed were not determined since all the testing was conducted at 20°C. It is probable, however, that higher temperatures will accelerate the onset of high cell voltages and memory, and that lower temperatures will reduce this effect.

For best possible operating characteristics all the battery test data indicate that the battery should be charged to the highest possible value to achieve the highest operating efficiency. Not only is the efficiency maximized but the capacity degradation characteristics are minimized as discussed under capacity degradation.

The only maximum voltage limiting factor is the hydrogen evolution potential. As previously noted, this potential is reported to be temperature dependent and at present is one of several values, depending on the reference source consulted. The conversion from constant current to constant voltage is determined by the maximum allowable battery voltage which is reported to be 1.47 volts per cell at room temperature. Reference 1 indicates 1.55 volts as the hydrogen gassing potential. The battery manufacturer uses a 1.5 volt upper operational limit on their AB10 cell and a 1.52 volt limit on their AB12 cell at 20°C. However, no absolute hydrogen evolution potential has been determined to date.

An additional variable is the negative temperature coefficient of the cell emf, which is reported to be 2.5 mV/°C/cell. This value reflects changes in overvoltage, equilibrium potential, potential drops across the electrolyte, and electronic impedances. On a 24-cell basis, the battery voltage values as a result of the

temperature coefficient are shown in figure 19. These values were empirically determined. What this figure does not reflect is the effect of prolonged cycling. MSFC data have indicated that after extended cyclic operation, the cell voltages will increase above acceptable limits when the battery temperature is decreased. Conversely, on the first cycle the cells will perform normally when the temperature is decreased. No remedy has yet been developed for this problem.

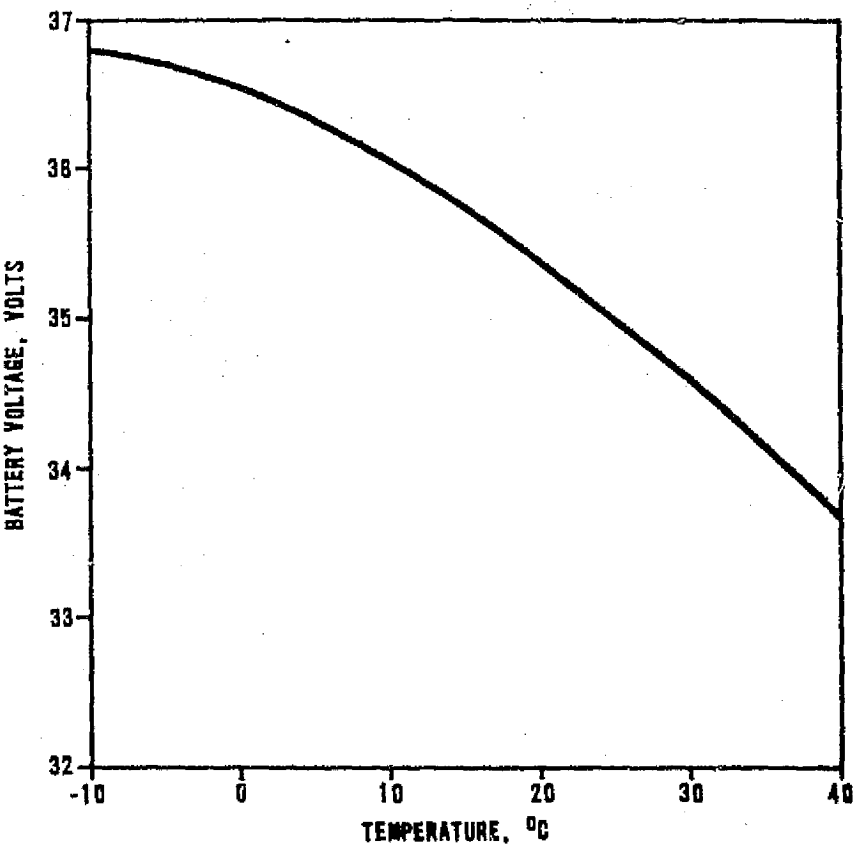

FIGURE 19. VOLTAGE LEVEL AS A FUNCTION OF TEMPERATURE

4.3 Charge Rate. Charge acceptance efficiency has been determined to be a function of current rate and temperature. As shown in figure 20, charge acceptance is maximum at a 2C charge rate. Although charging a battery at a 2C rate is most efficient, high charge rates are detrimental to the battery when the battery is at a low temperature. Hydrogen evolution reportedly occurs at low temperature (0°C or less) whenever the charge rate exceeds a particular level. The maximum allowable charge rate is a function of temperature, thus a 15-ampere charge rate was chosen for ATM batteries because the charge rate had to be compatible throughout the temperature range encountered in ATM. Charge rates of 15 amperes at minus 20°C were performed and found to be acceptable.

40M22411

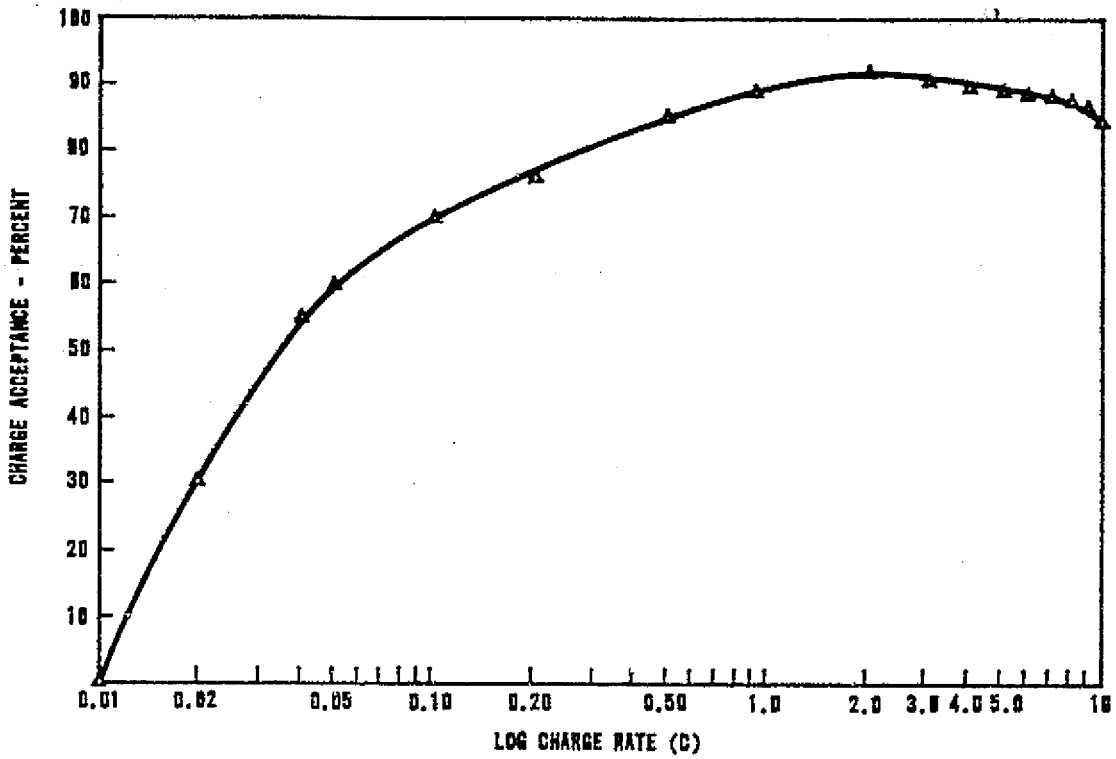

FIGURE 20. CHARGE ACCEPTANCE

4.4 Third Electrode Signals.

4.4.1 Comparison of AB10 and AB12 third electrode signals. During the ATM battery tests the third electrode signals of the AB10 and AB12 cells were evaluated and compared. The AB10 cell contains an auxiliary electrode while the AB12 cell contains an auxiliary electrode and a fuel cell (recombination) electrode. Figure 21 presents a comparison of the AB10 and AB12 third electrode signals when both cell types were subjected to the identical charge conditions. The AB12 cell has a higher response rate than the AB10. The response is due, in part, to the presence of the fourth electrode in the AB12 cell. During operation, the fourth electrode will recombine all evolved oxygen until it becomes saturated. At this time, the third electrode signal begins to rise. The rapid rise time allows greater tolerance in the charge control electronics.

4.4.2 Charge termination control-AB12 tests. Tests were performed on a battery with AB12 type cells to determine a method whereby three redundant charge termination control third electrodes could be chosen in a flight battery. The third electrode of each of the 24 cells in the test battery was terminated with a resistance load, and the battery was subjected to simulated cyclic operation in a thermal chamber. The third electrode signal voltages and total battery current were monitored and recorded. The recorded data were processed and plotted by a computer.

40M 22411

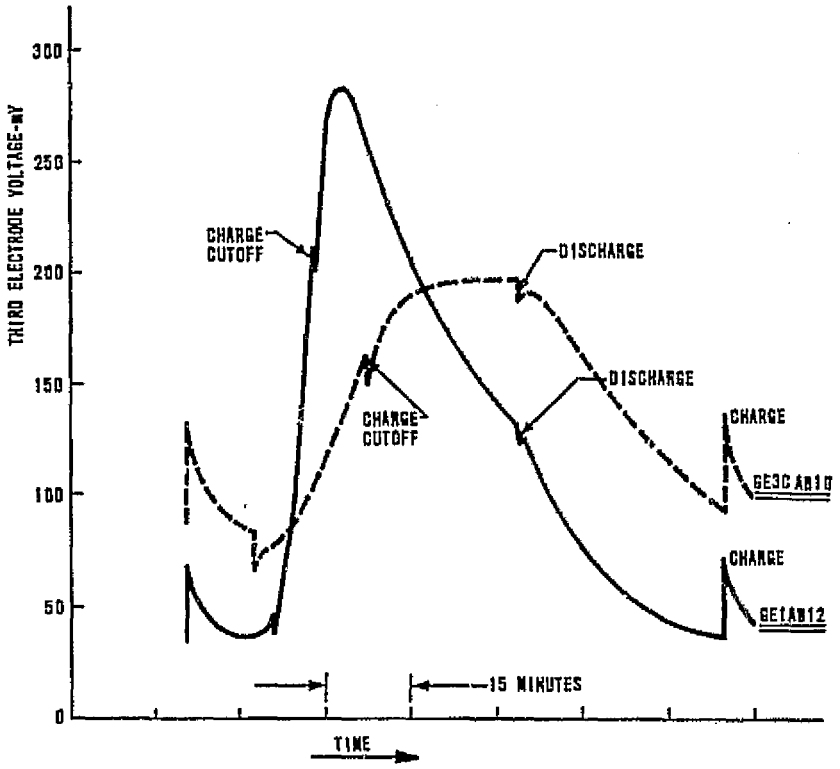

FIGURE 21. COMPARISON OF AB10 AND AB12 CELL THIRD ELECTRODE SIGNAL

During each data run, the battery was subjected to steady-state simulated ATM cycling. Each cycle was composed of a 36-minute discharge followed by a 58-minute charge. A 200-watt load was maintained throughout the discharge, the 58-minute charge was composed of a 15-ampere constant current charge followed by a constant voltage charge. Changeover from a constant current charge to a constant voltage occurred when the battery voltage reached a preset level (1.5 volts on any cell at 20°C). The preset voltage level is temperature dependent as previously shown in figure 19. The constant charge voltage level was 0.8 volt less than the preset level.

Charge termination occurred when the third electrode signals reached 200 mV. The charge termination control cell third electrode was terminated with a 150-ohm resistor. This load was maintained on cell 1 throughout the test to provide a base line for the data obtained.

A sample of third electrode data is shown in figure 22, which depicts the current profile and typical third electrode response for a single cell. The third electrode signal, as noted previously, is a function of the partial pressure of oxygen which begins to evolve when the nickel electrode approaches 80 percent state of charge.

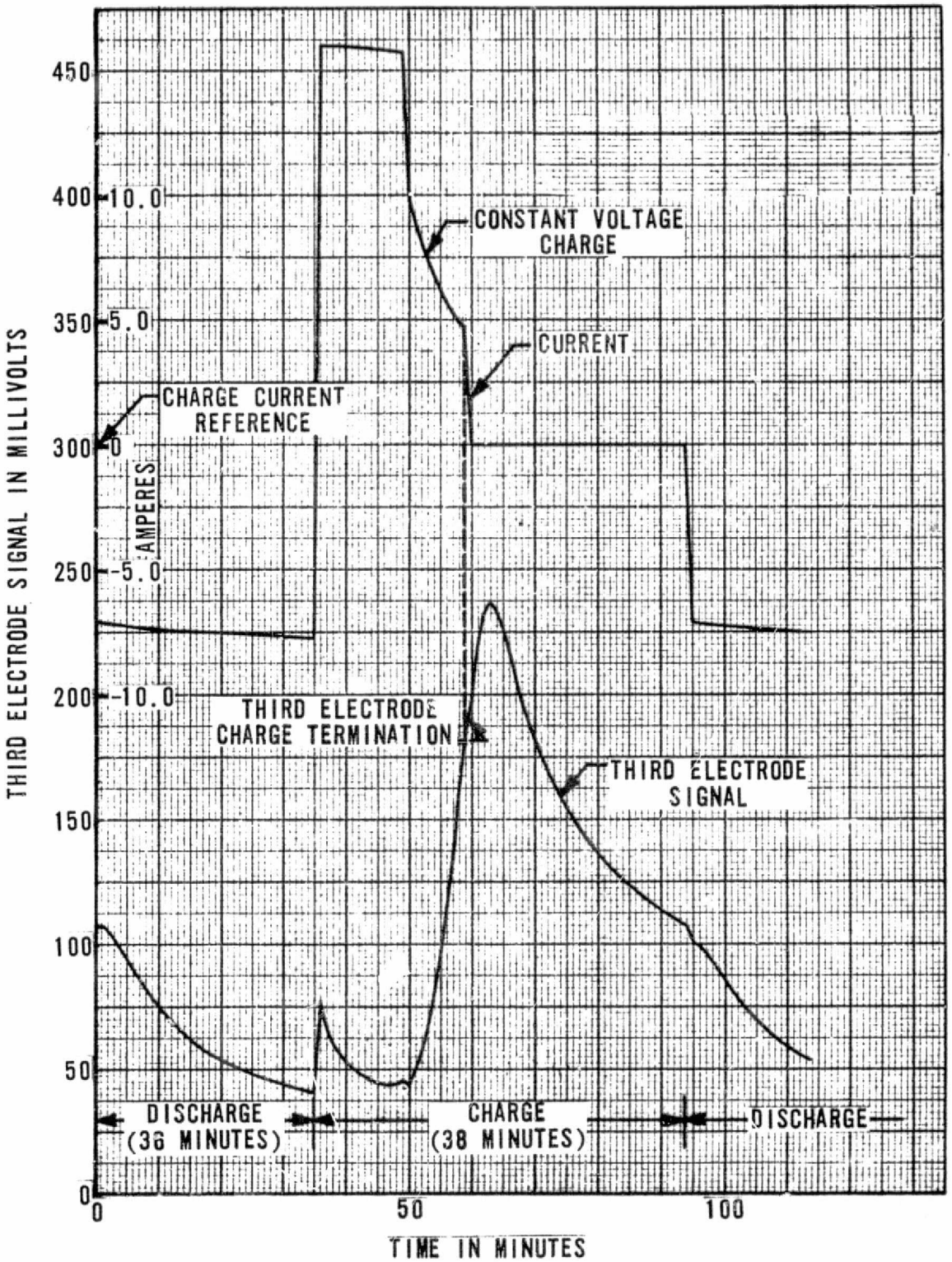

FIGURE 22. TYPICAL THIRD ELECTRODE SIGNAL DATA TAKEN AT STEADY-STATE CONDITIONS, AB12 BATTERY

40M22411

In the AB12 type cell, the signal is also a function of the oxygen recombination capability of the fourth electrode. During normal operation, the fourth electrode will recombine all the evolved oxygen until it becomes saturated, at which time the third electrode signal begins to rise. The third electrode signal will continue to rise until oxygen stops evolving. Oxygen continues to evolve sometime after charge is terminated. Since the third electrode signal is measured from the negative battery terminal to the cell case, the signal indicates an IR variation whenever the battery current varies. These variations are shown in figure 22 where the battery current changes from discharge to charge, from constant current to constant voltage charge, and when charge is terminated.

Typical signal data from the battery third electrodes are shown in figure 23. The figure depicts 24 individual third electrode signals recorded during cycle 62 and cycle 63 under steady-state cyclic conditions at 20°C and 150-ohm load resistance. Figure 24 depicts 6 of the 24 cells shown in figure 23. The most significant factor in figures 23 and 24 is the difference in third electrode signal among 24 cells when all cells are subjected to identical cyclic conditions. The difference is such that the peak millivolt signal varies by as much as 3.5 (ratio of highest to lowest peak third electrode signal).

Figure 25 illustrates the performance of the third electrode in cell 21 under steady-state cyclic conditions at 20°C with third electrode load resistors having values between 75 and 1000 ohms. It should be noted that although the third electrode produces a higher signal for higher terminating impedances (as would be expected), the increase is not linear due to a change in the effective internal resistance.

Figures 26, 27, 28, and 29 illustrate the deviation of all 24 third electrode signal voltages for temperatures of 0, 10, 20, and 30°C with a constant load of 400 ohms. Note that both the shape and the relative position of the curves change with an increase in temperature. The peaks of the third electrode curves tended to flatten out as the temperature increased. There was also an upward shift in the curves with the increase in temperature, particularly significant for those cells which were the least responsive at the lower temperature.

Figures 30, 31, 32, and 33 illustrate the response of cell 7 as a function of temperature and load. Each figure shows curves for 0, 10, 20, and 30°C with corresponding loads of 400, 300, 200, and 75 ohms. The same effects are noted in these figures as was noted in figures 25 through 29.

From the representative data shown in figures 22 through 33, the following third electrode operating characteristics can be determined:

(a) The variation of third electrode signal with load resistance.

(b) The effect of temperature upon third electrode response.

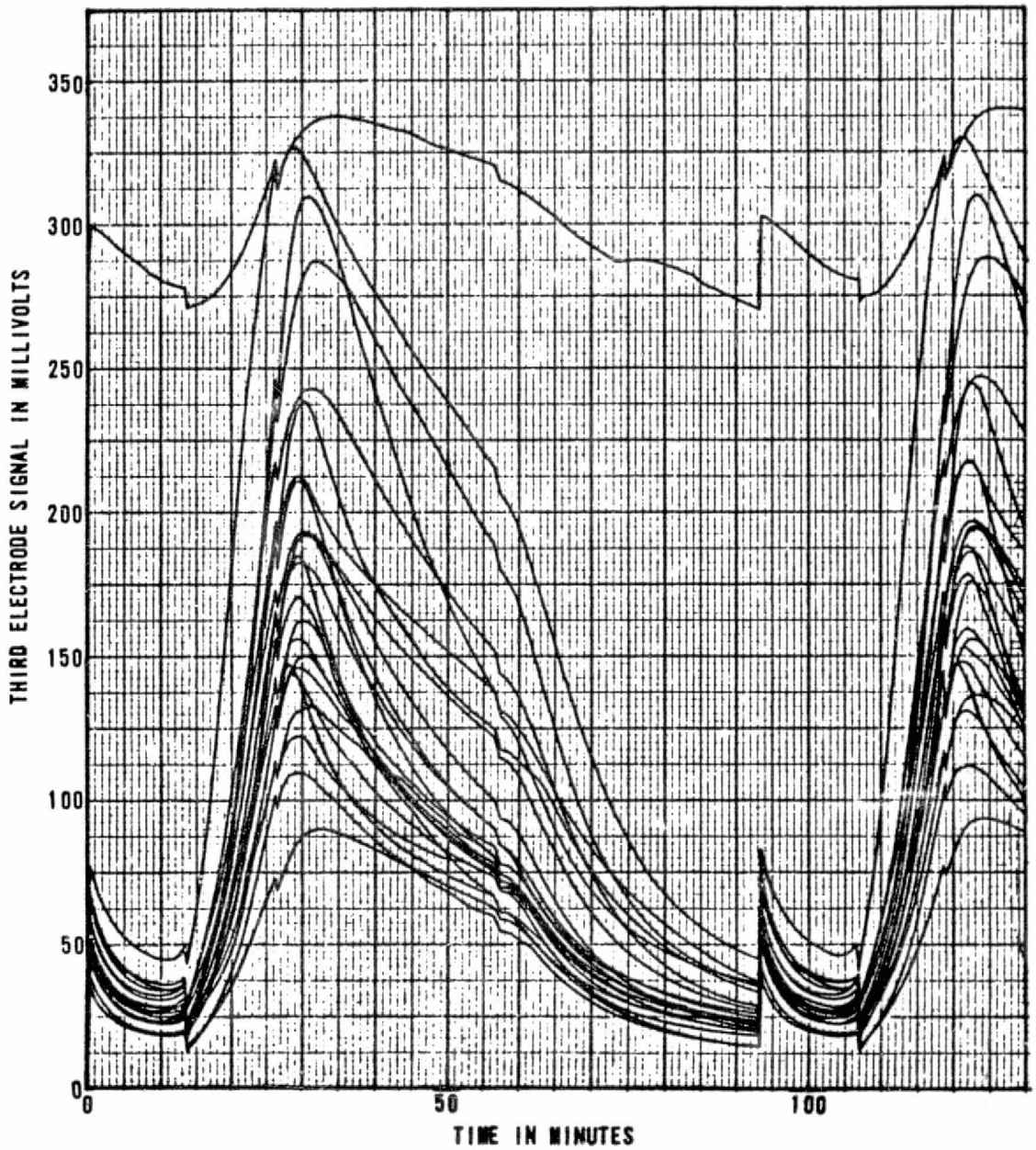

FIGURE 23. THIRD ELECTRODE SIGNAL FOR 24 CELLS AT 20° C, CYCLES 62 AND 63, LOAD RESISTANCE 150 OHMS (AB12 CELLS)

40M22411

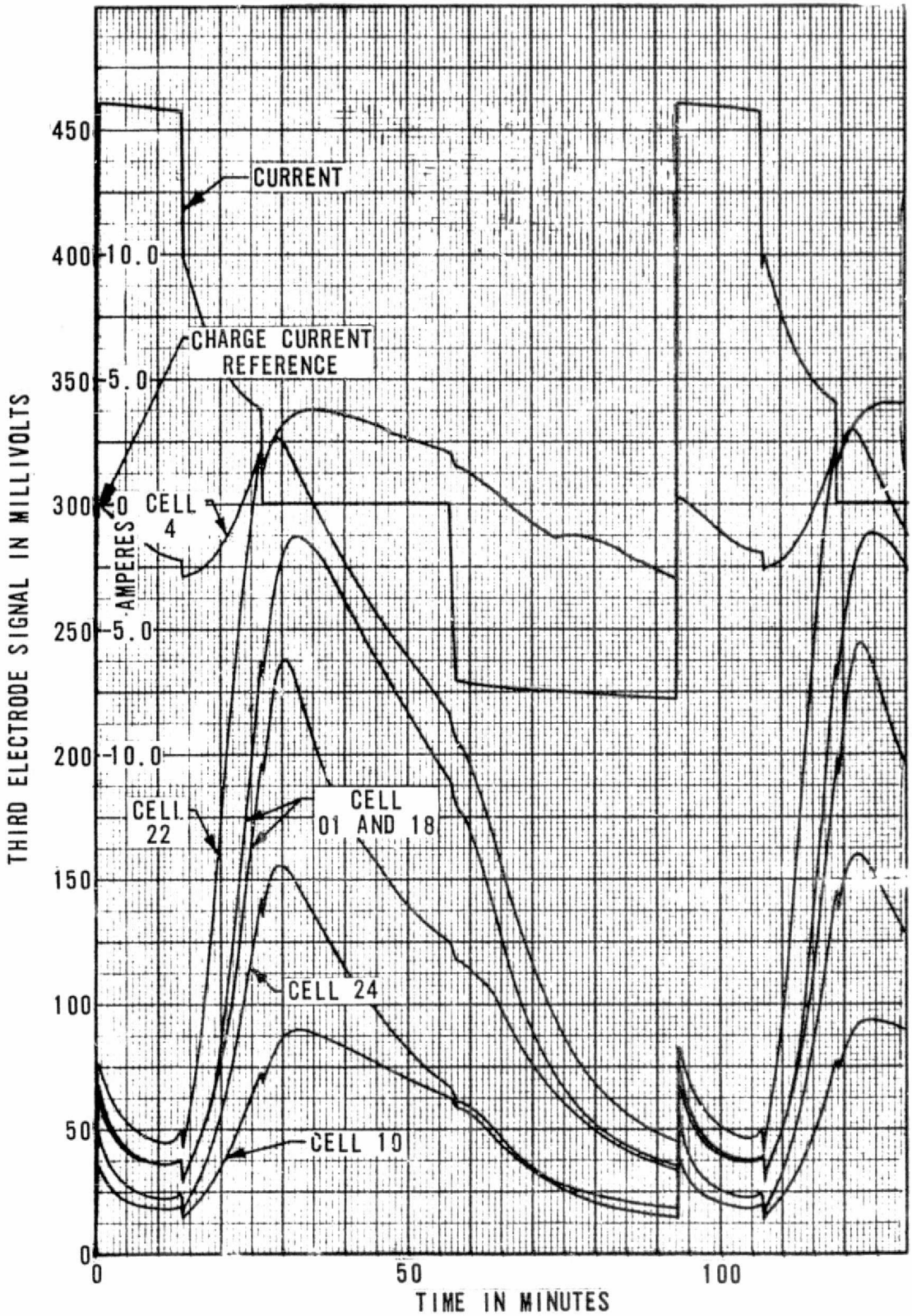

FIGURE 24. THIRD ELECTRODE SIGNAL FOR SIX CELLS AT 20°C, CYCLES 62 AND 63, LOAD RESISTANCE 150 OHMS (AB12 CELLS)

40M22411

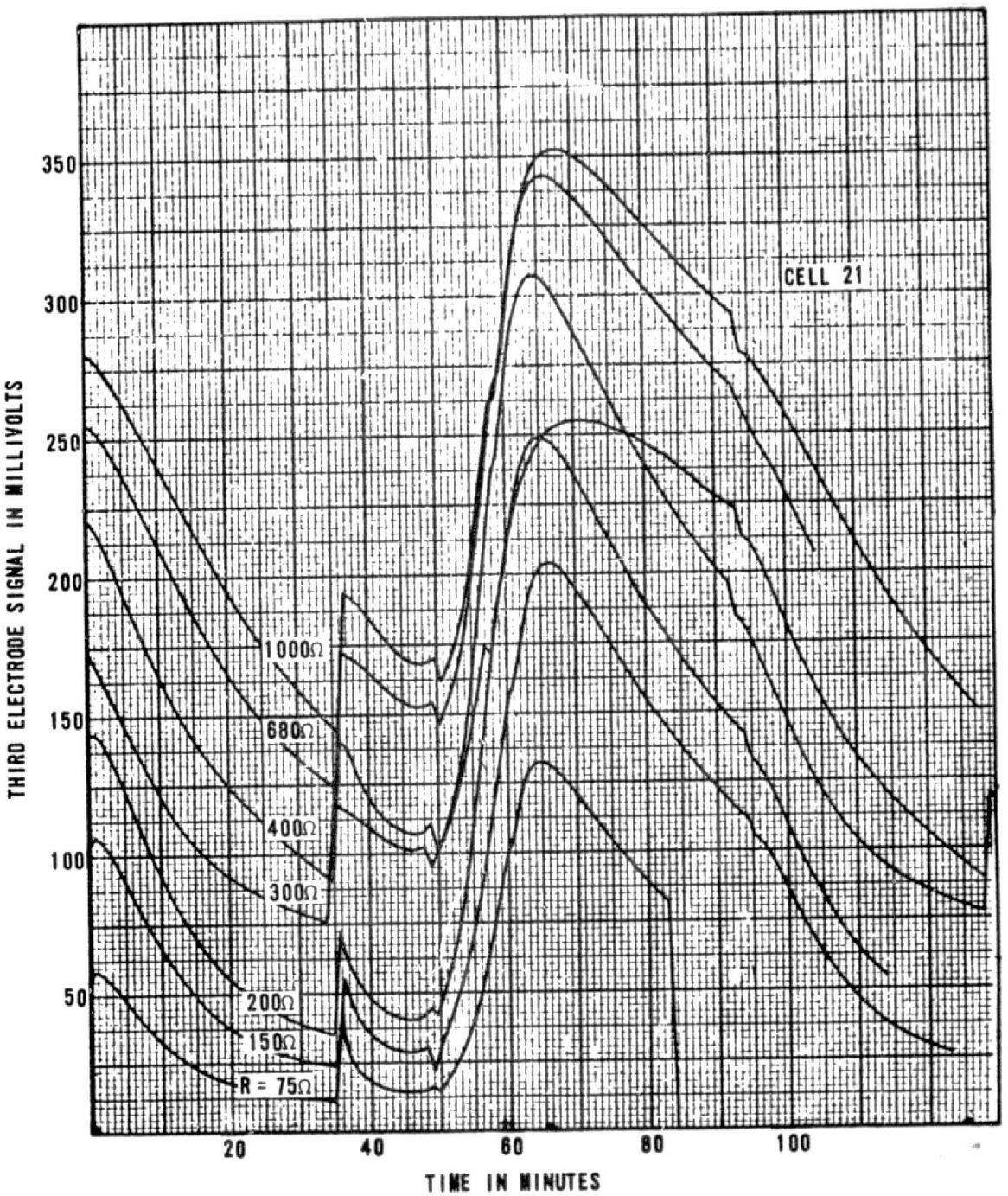

FIGURE 25. THIRD ELECTRODE SIGNALS FOR A SINGLE CELL AT 20°C AND VARYING LOAD RESISTANCES (AB12 CELL)

40M22411

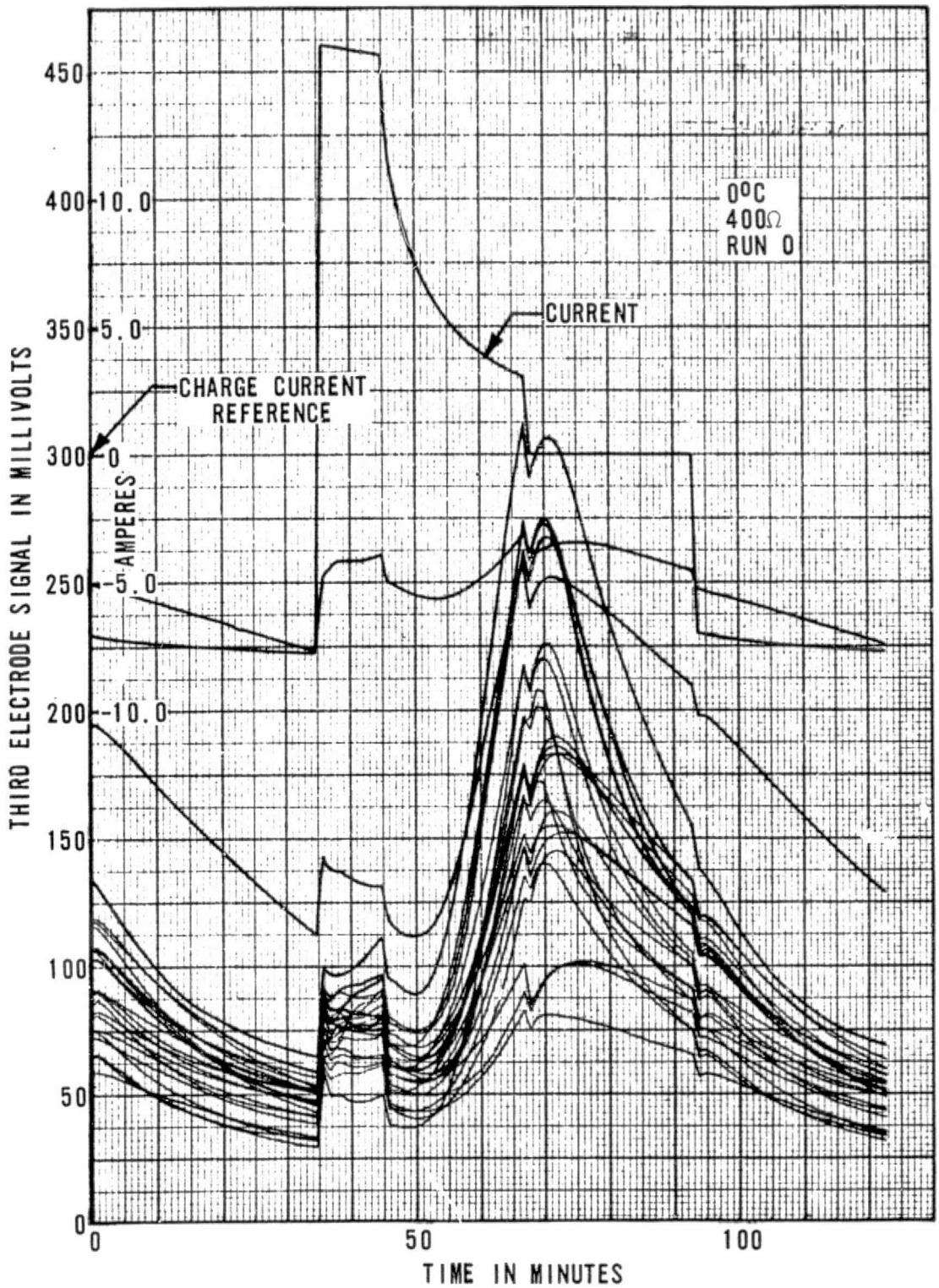

FIGURE 26. THIRD ELECTRODE SIGNAL FOR CELLS AT 0°C AND 400-OHM LOAD (AB12 CELLS)

40M 22411

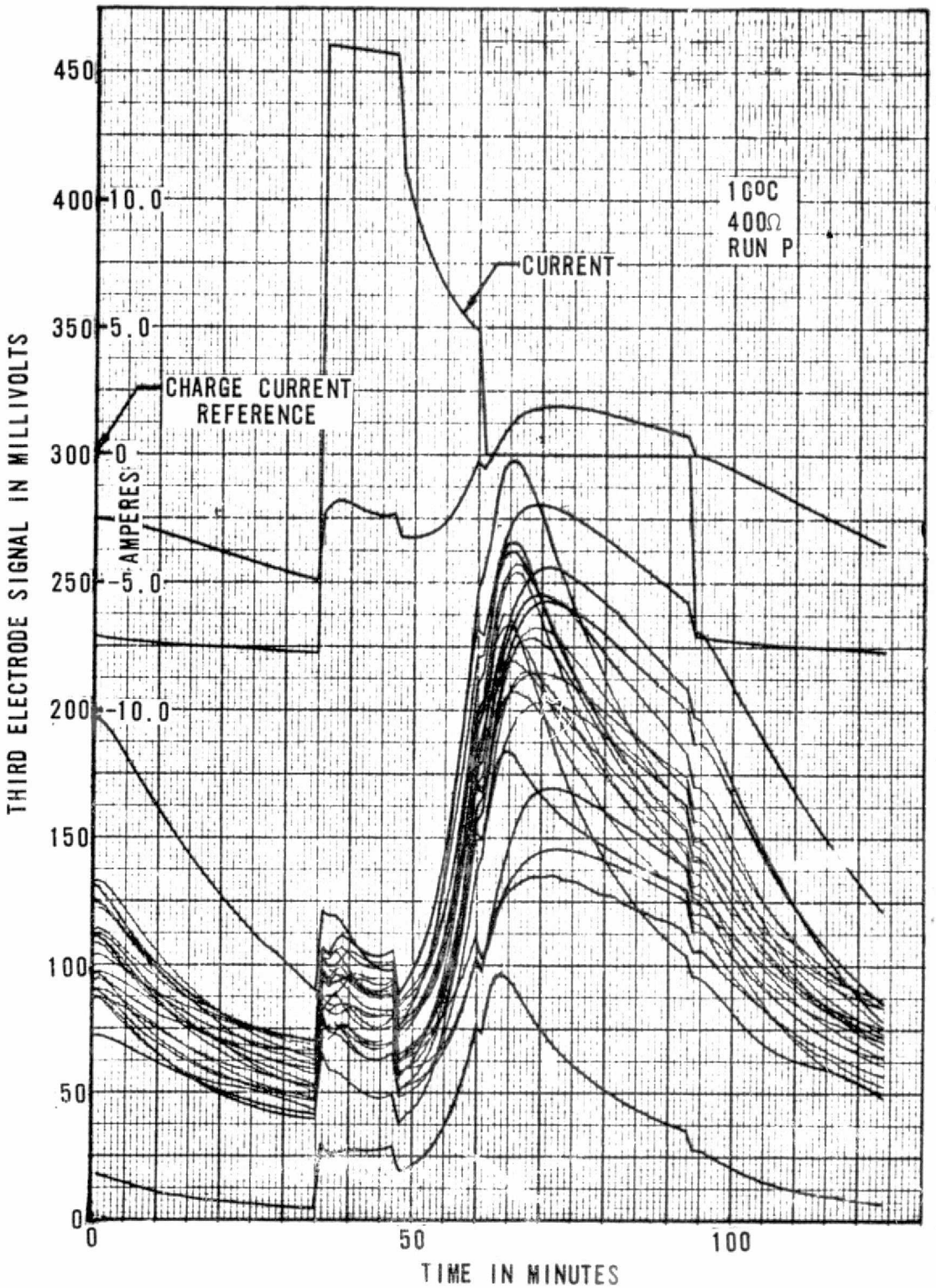

FIGURE 27. THIRD ELECTRODE SIGNAL FOR CELLS AT 10°C AND 400-OHM LOAD (AB12 CELLS)

40M22411

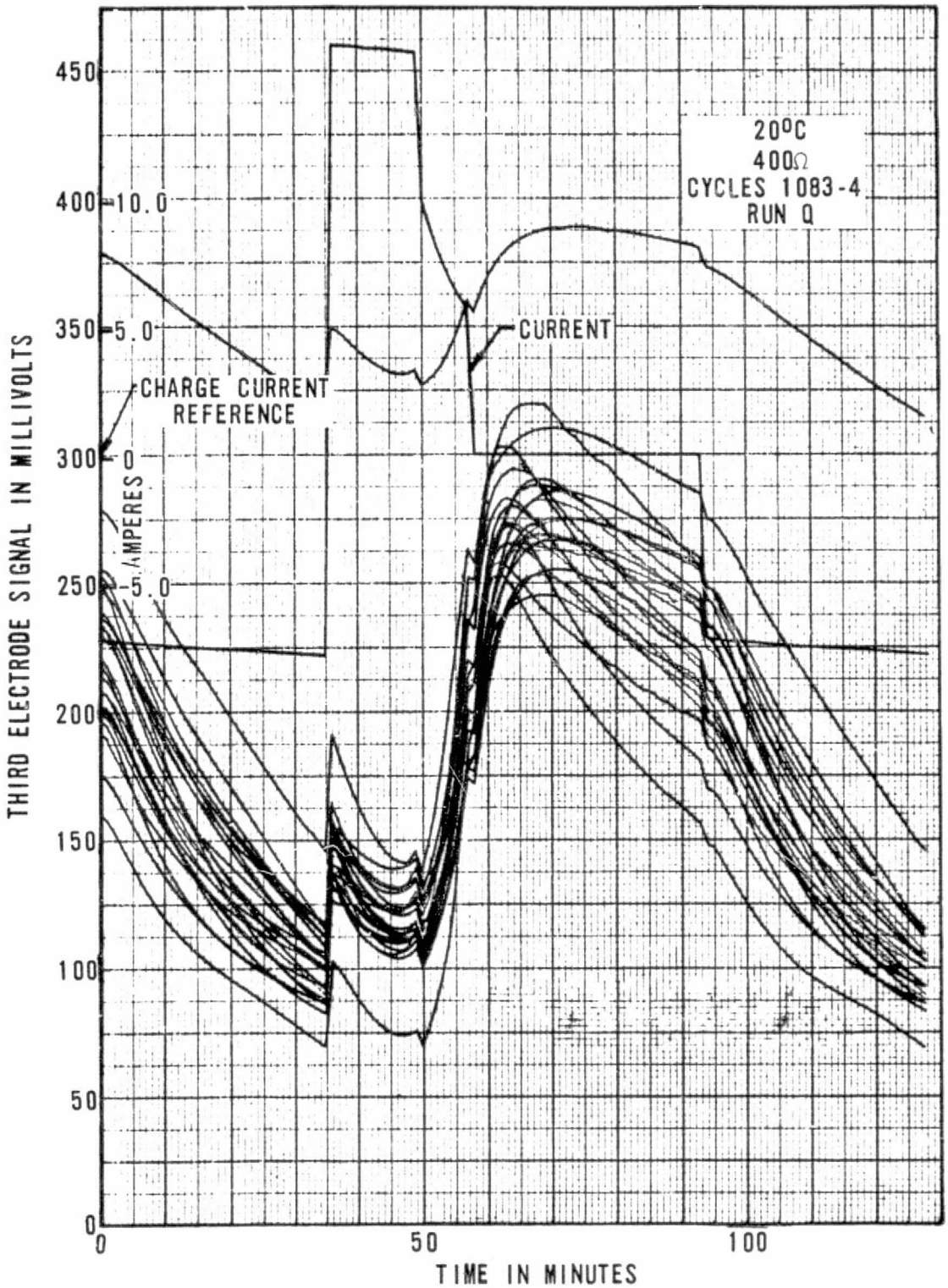

FIGURE 28. THIRD ELECTRODE SIGNAL FOR CELLS AT 20° C AND 400-OHM LOAD (AB12 CELLS)

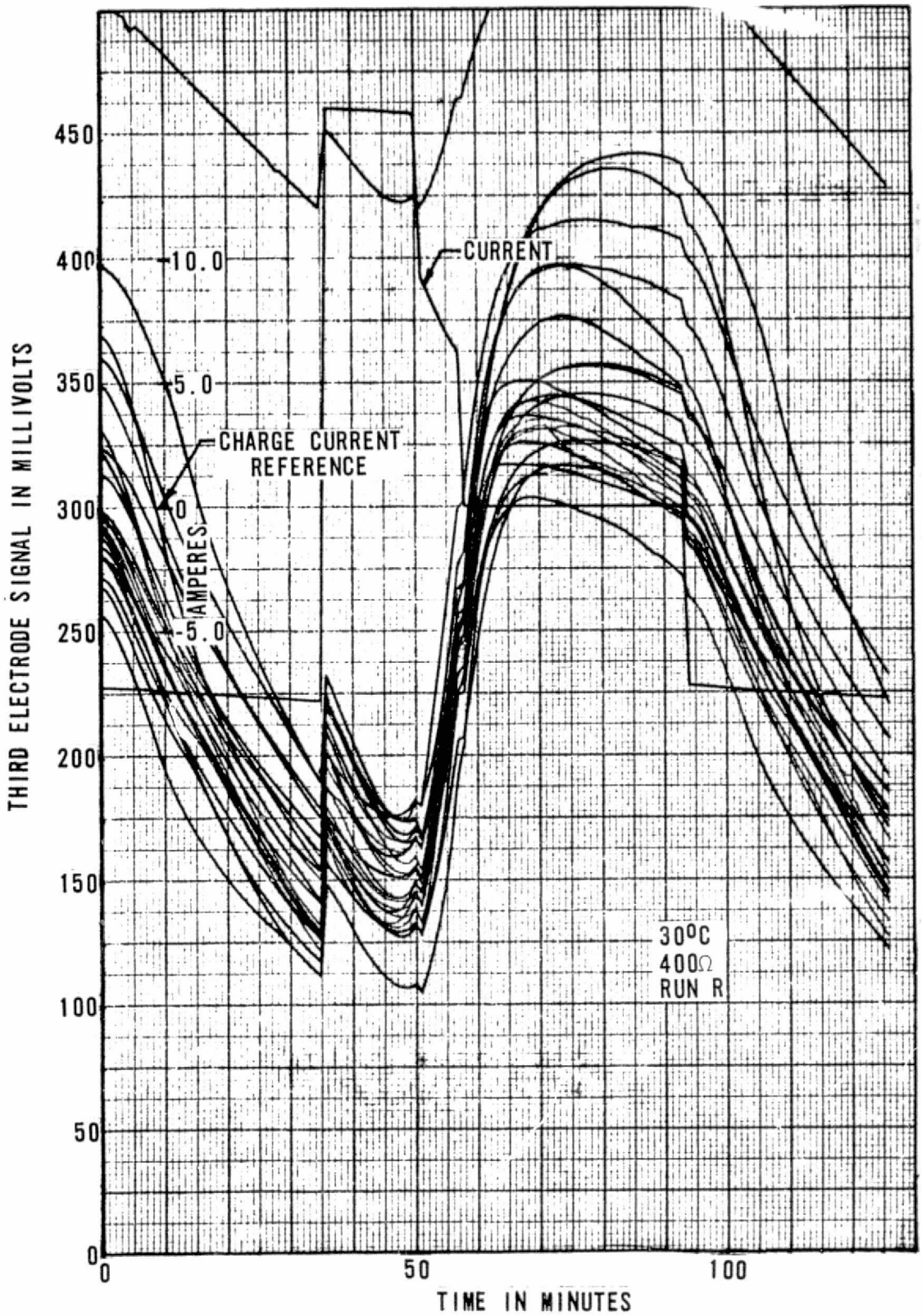

FIGURE 29. THIRD ELECTRODE SIGNAL FOR CELLS AT 30°C AND 400-OHM LOAD (AB12 CELLS)

40M22411

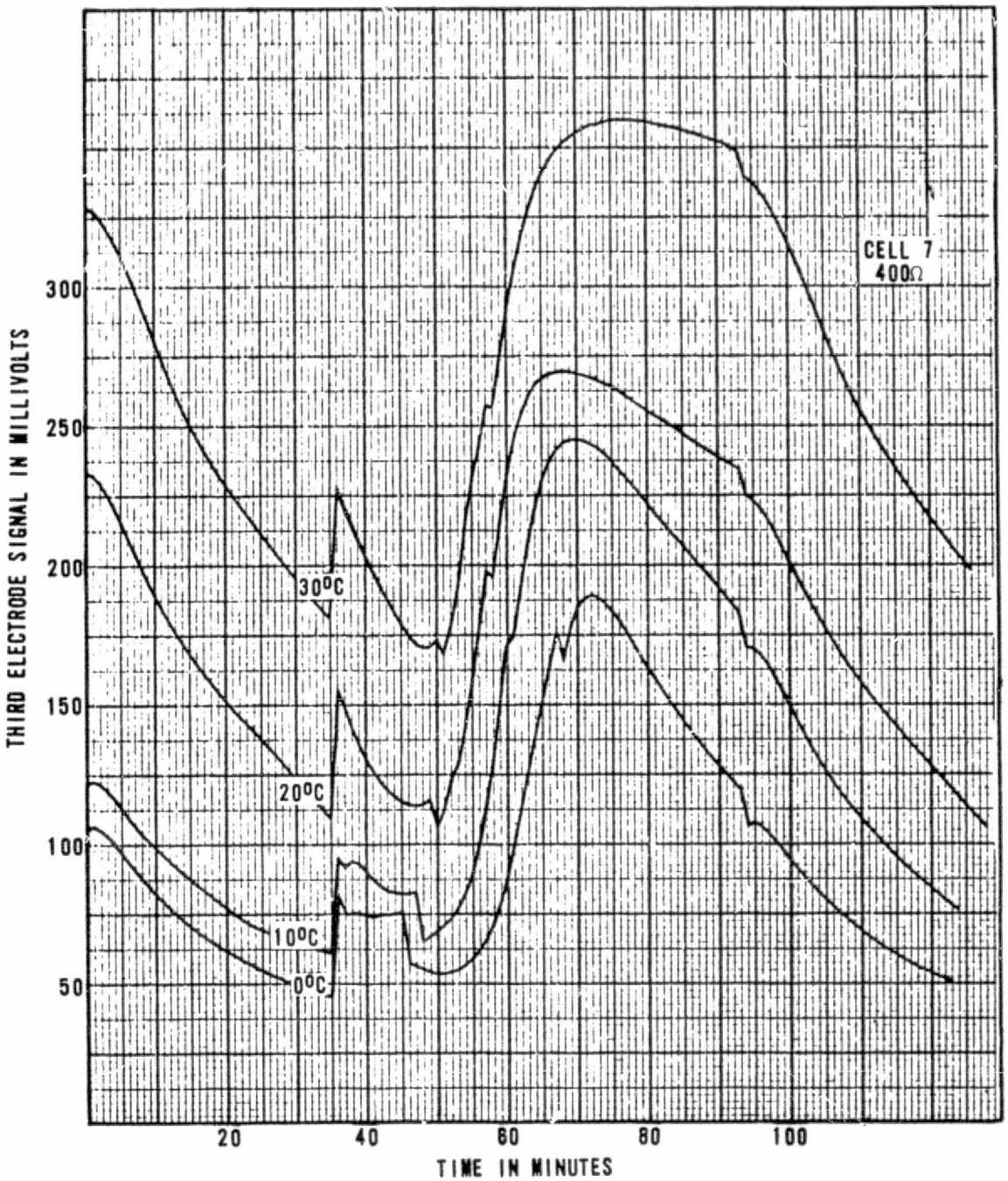

FIGURE 30. THIRD ELECTRODE SIGNAL FOR CELL 7 AT 400-OHM LOAD AND VARYING TEMPERATURES (AB12 CELLS)

40M22411

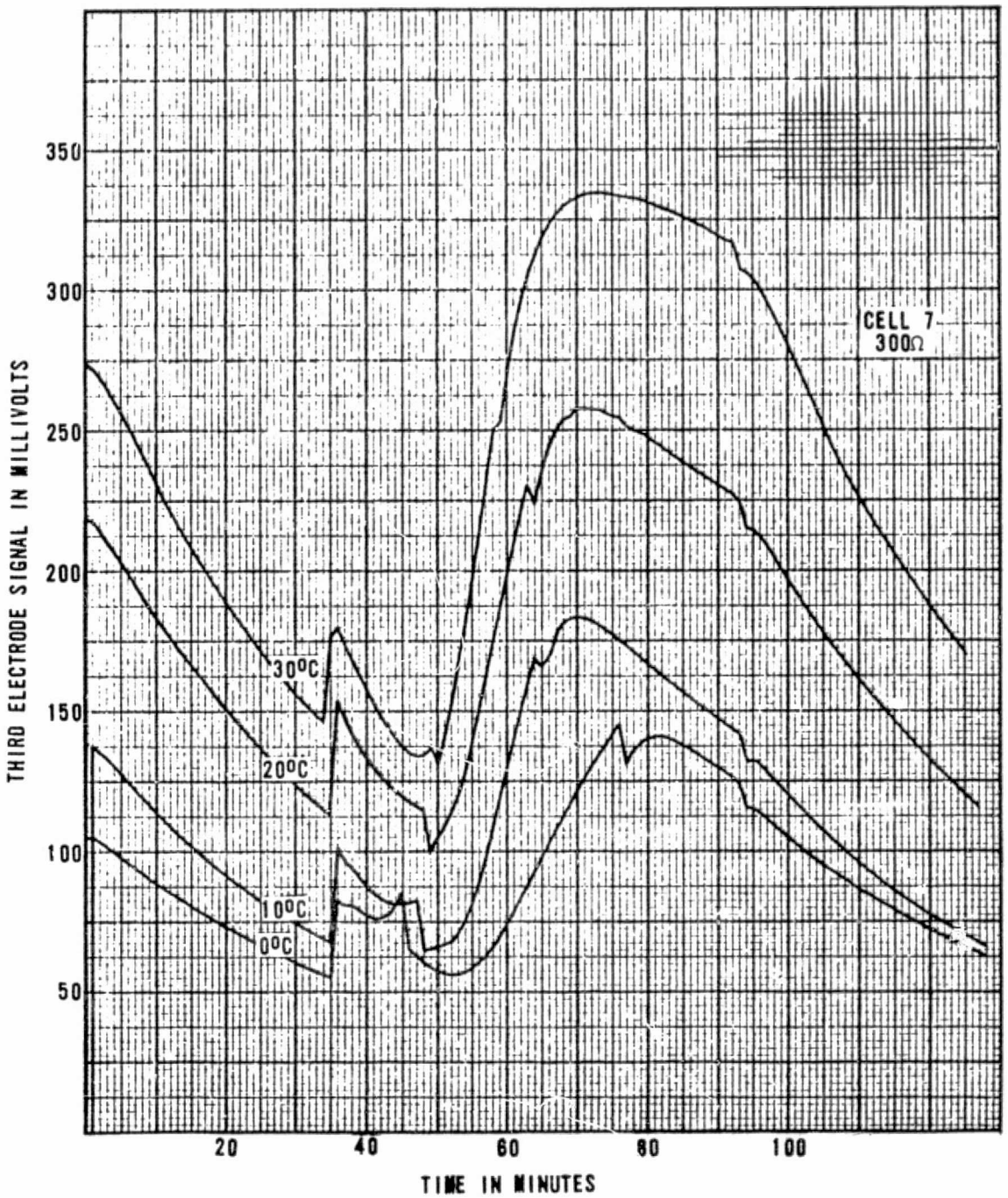

FIGURE 31. THIRD ELECTRODE SIGNAL FOR CELL 7 AT 300-OHM LOAD AND VARYING TEMPERATURES (AB12 CELLS)

40M 22411

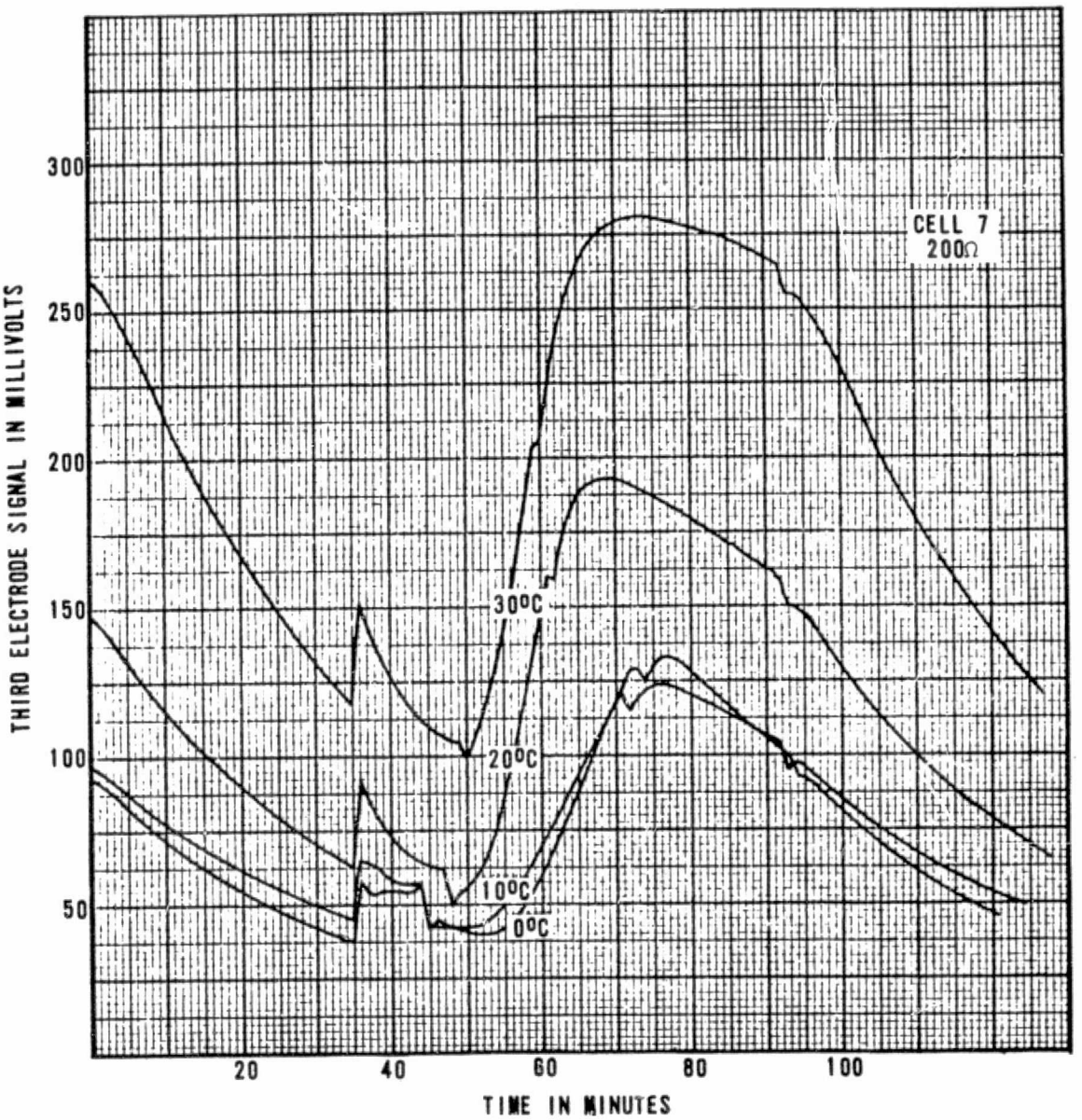

FIGURE 32. THIRD ELECTRODE SIGNAL FOR CELL 7 AT 200-OHM LOAD AND VARYING TEMPERATURES (AB12 CELLS)

40M2241

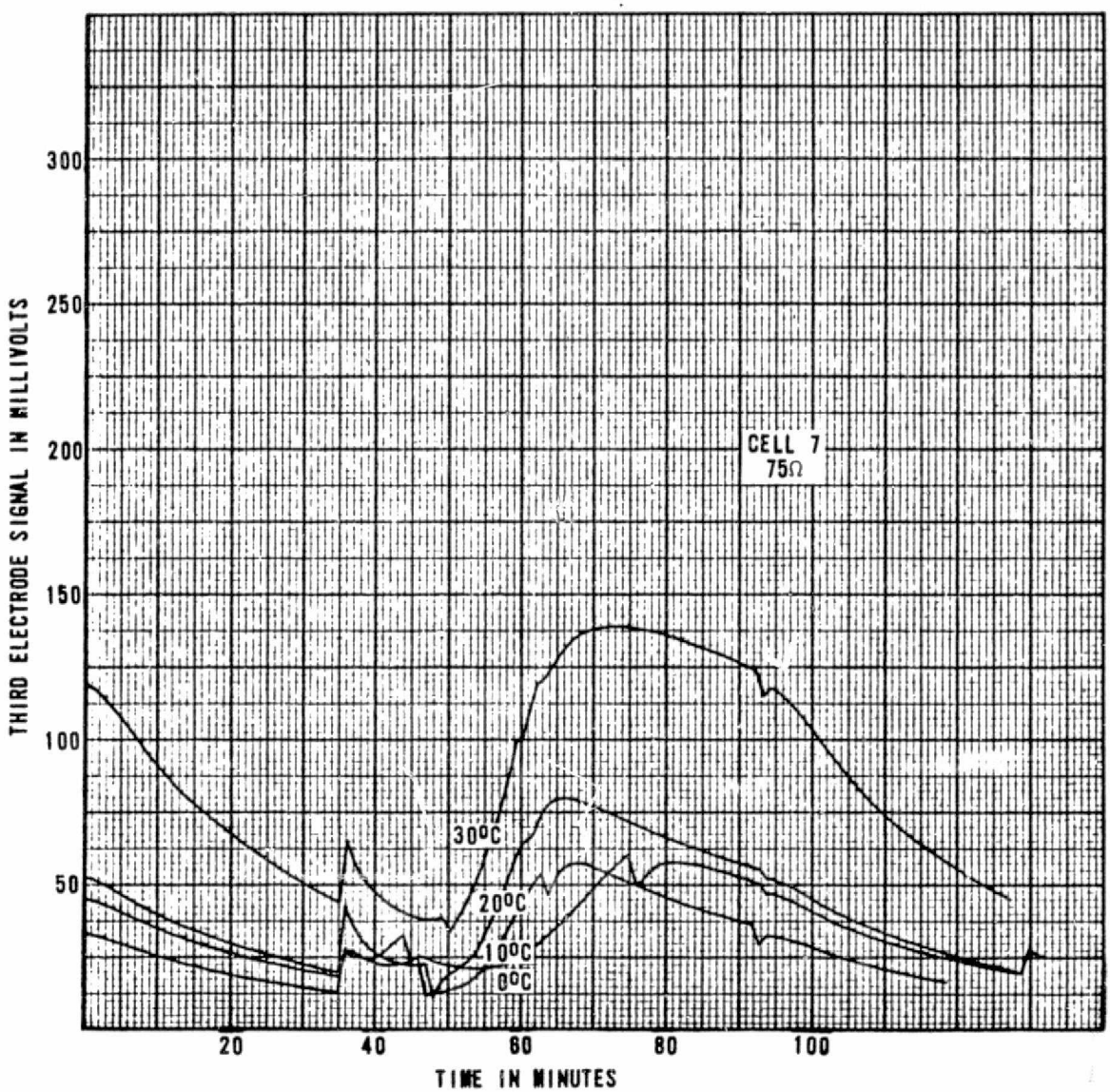

FIGURE 33. THIRD ELECTRODE SIGNAL FOR CELL 7 AT 75-OHM LOAD AND VARYING TEMPERATURES (AB12 CELLS)

40M22411

An analysis of third electrode operating characteristics was performed to determine the following information:

(a) Internal resistance characteristics.

(b) Recommended third electrode terminating resistance.

(c) A method by which the third electrode signals can be equalized.

The data and analysis presented here for several cells are representative of that obtained for each cell in the battery. The analysis was limited to several cells since all the cells have similar basic response characteristics.

4.4.3 Internal resistance characteristics. The third electrode may be considered as the following circuit:

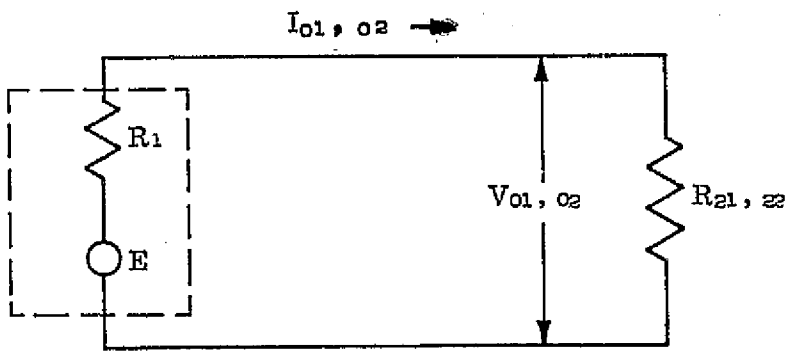

where:

E	=	internal generator
R_1	=	internal resistance
R_{21}	=	a particular load resistance
R_{22}	=	a load resistance not equal to R_{21}
I_{o1}	=	load current associated with the resistance R_{21}
I_{o2}	=	load current associated with the resistance R_{22}
V_{o1}	=	potential measurement across the resistance R_{21}
V_{o2}	=	potential measurement across the resistance R_{22}

4044.2.241

Assuming the internal generator to be a constant voltage source, the internal resistance appears as a variable resistor whose value may be determined by measurement of the voltage across the external load resistance.

Then:

$$E = R_1 I_{o1} + R_{s1} I_{o1} \text{ and } E = R_1 I_{o2} + R_{s2} I_{o2},$$

$$R_1 I_{o1} + R_{s1} I_{o1} = R_1 I_{o2} + R_{s2} I_{o2}$$

Since:

$$V_{o1} = R_{s1} I_{o1} \text{ and } V_{o2} = R_{s2} I_{o2},$$

$$R_1 I_{o1} + V_{o1} = R_1 I_{o2} + V_{o2}$$

Therefore:

$$R_1 = \frac{V_{o1} - V_{o2}}{I_{o2} - I_{o1}} = \frac{\Delta V_o}{\Delta I_o} = \frac{V_{o1} - V_{o2}}{\frac{V_{o2}}{R_{s2}} - \frac{V_{o1}}{R_{s1}}}$$

The internal resistance characteristics of cell 21 were determined by using figure 25 and the preceding derivation. The results of this analysis are shown in figure 34. The figure is a family of curves which illustrate the internal electrode resistance characteristics during the control portion of the charge cycle. Time as shown on figure 34 can be correlated with the time axis in figure 25. The divergence of several data points is attributed to battery parameter changes which occurred as a result of the time difference between recorded data (data were taken at various points over a 2000 cycle period).

The third electrode internal resistance is equal to the negative slope of the curves shown in figure 34. As shown, maximum internal resistance occurs when the external load is between 150 and 300 ohms. At the point of maximum internal resistance, the internal signal generator approaches a constant current source. The data of figures 30 through 33 were replotted to depict the internal resistance characteristics of cell 7 at equal states of charge as a function of temperature. These data are shown in figure 35. Maximum internal resistance again occurs when the external load is between 150 and 300 ohms at all temperatures.

Figure 36 depicts the internal resistance characteristics of cell 3 throughout the control portion of the charge cycle. This curve was calculated in a similar fashion to figure 34. It is evident from the figures that maximum internal resistance also occurs when the external load is between 150 and 300 ohms.

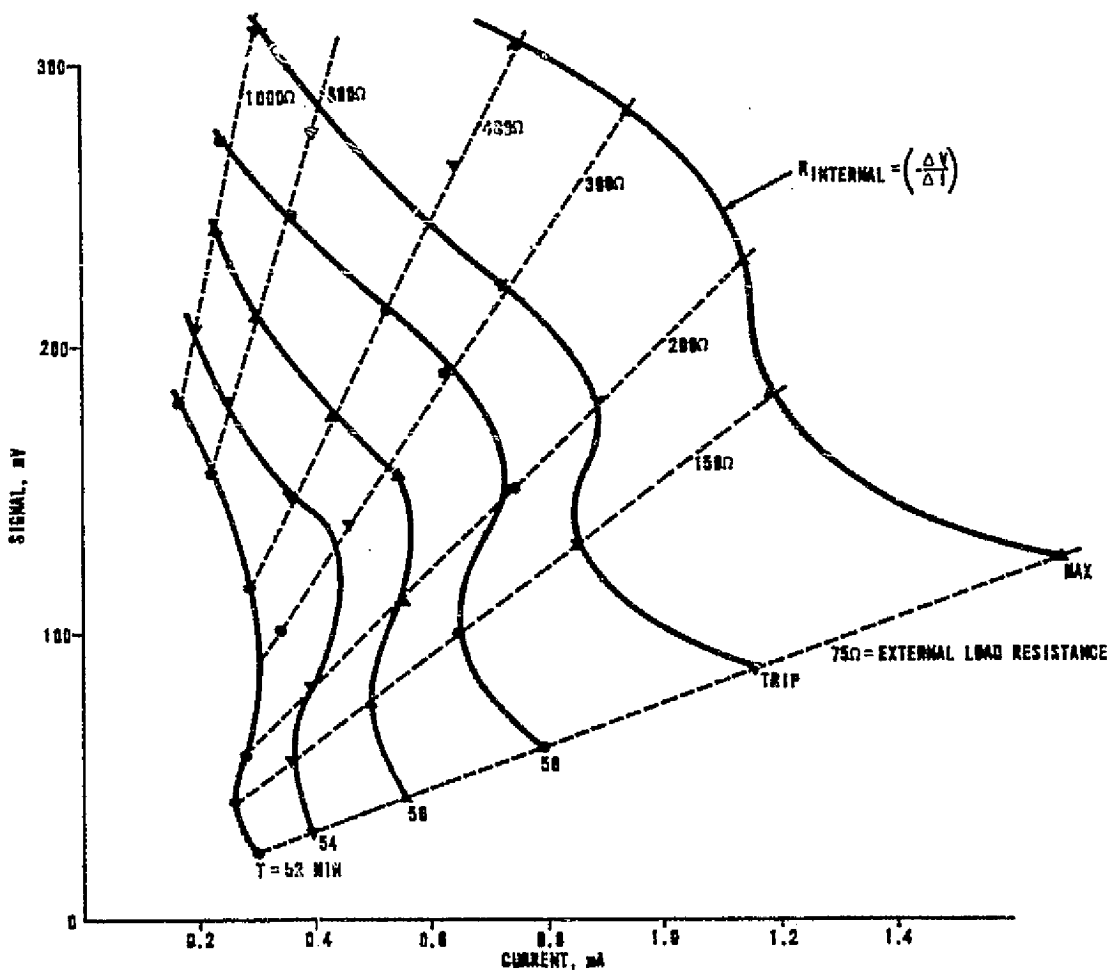

FIGURE 34. INTERNAL RESISTANCE CHARACTERISTICS FOR CELL 21 AT 20°C (AB12 CELL)

40M 22411

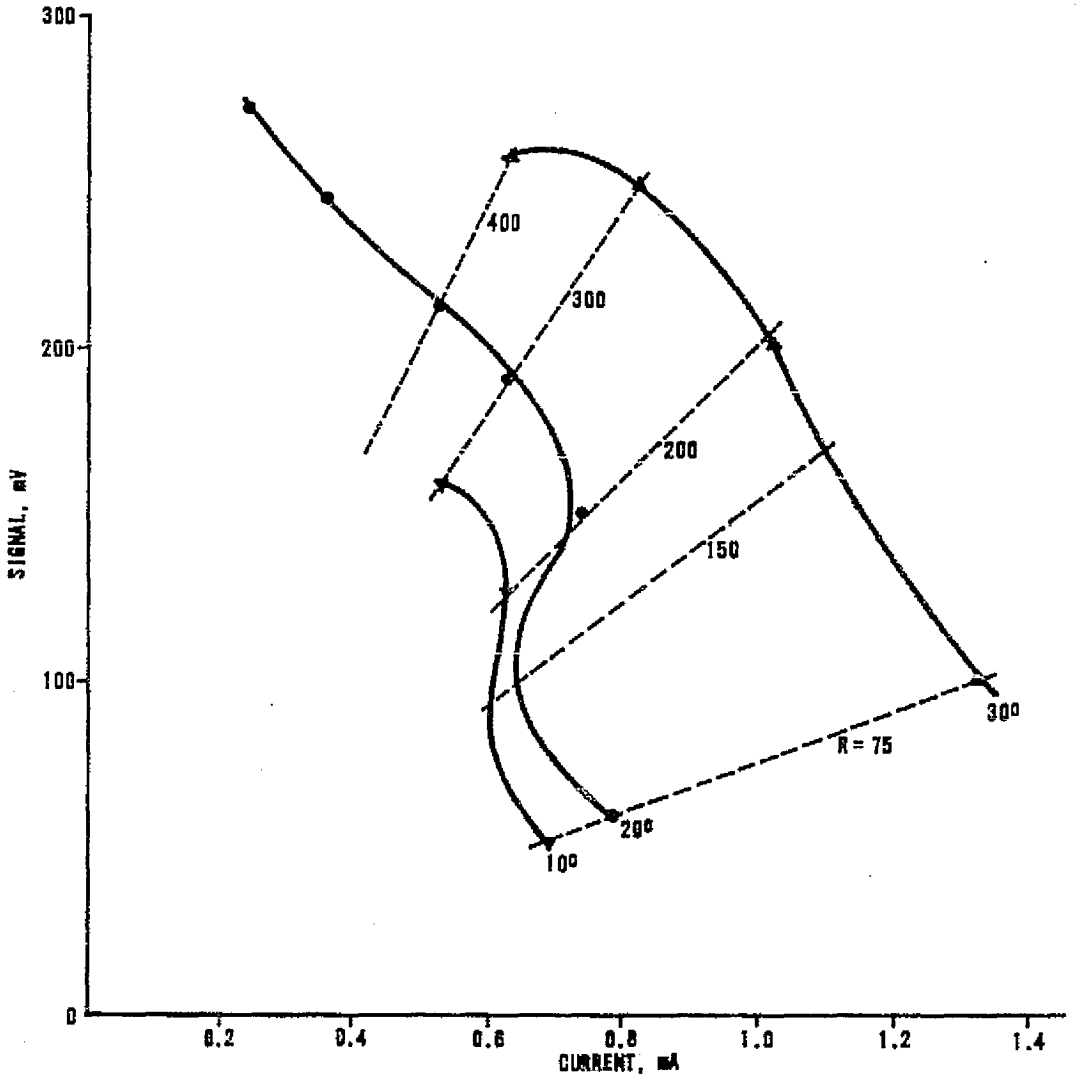

FIGURE 35. INTERNAL RESISTANCE CHARACTERISTICS FOR CELL 7 AT VARYING TEMPERATURES AND A PARTICULAR STATE OF CHARGE (AB12 CELL)

40M 22411

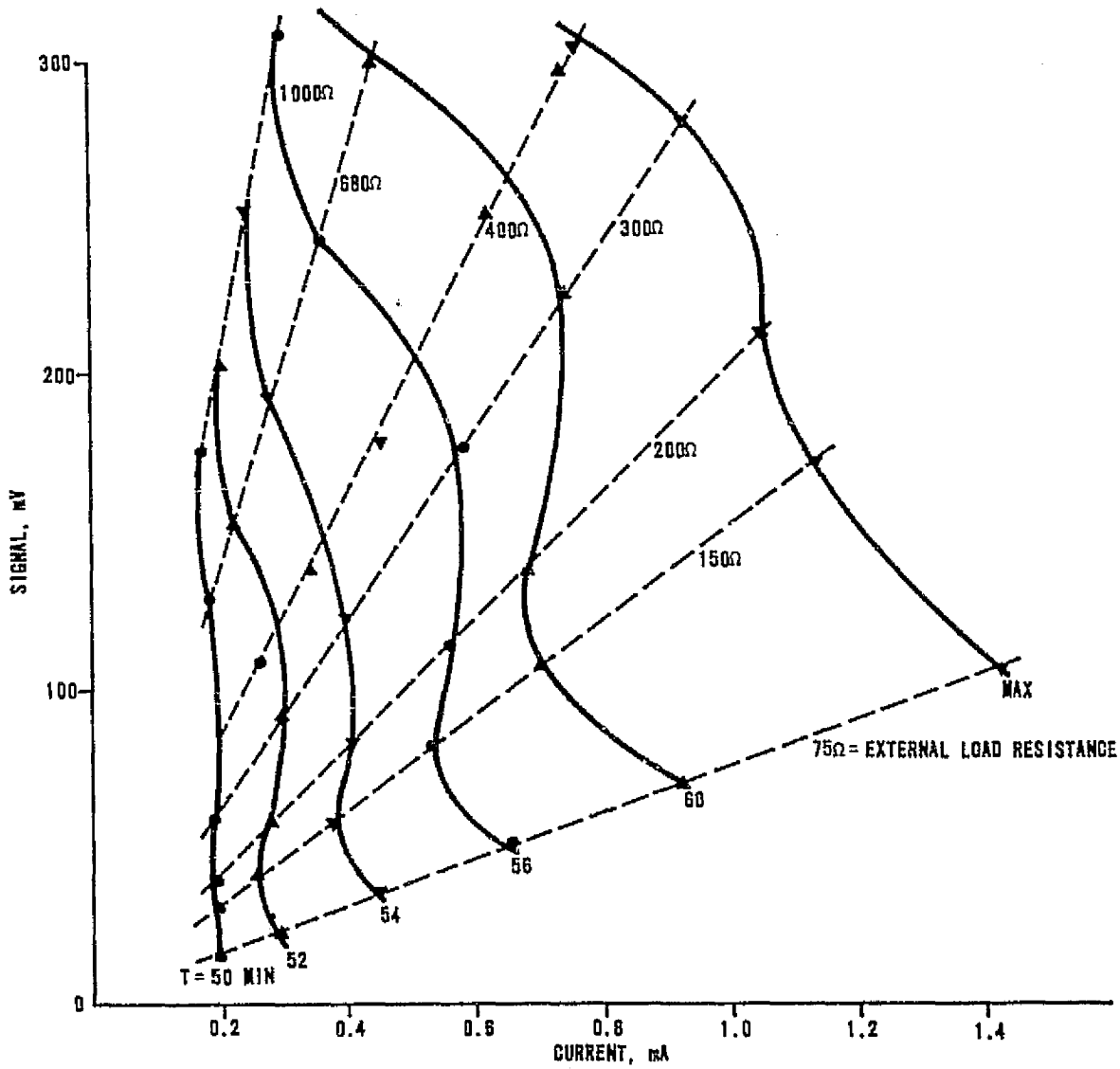

FIGURE 36. INTERNAL RESISTANCE CHARACTERISTICS FOR CELL 3 AT 20°C

AD-A 22 441

A comparison of cells 2, 3, and 7 is shown in figure 37. The cells are shown at an equal state of charge. Although the cells all exhibit maximum internal resistance within the same external load ranges, the figure illustrates the nonuniformity of the third electrode response.

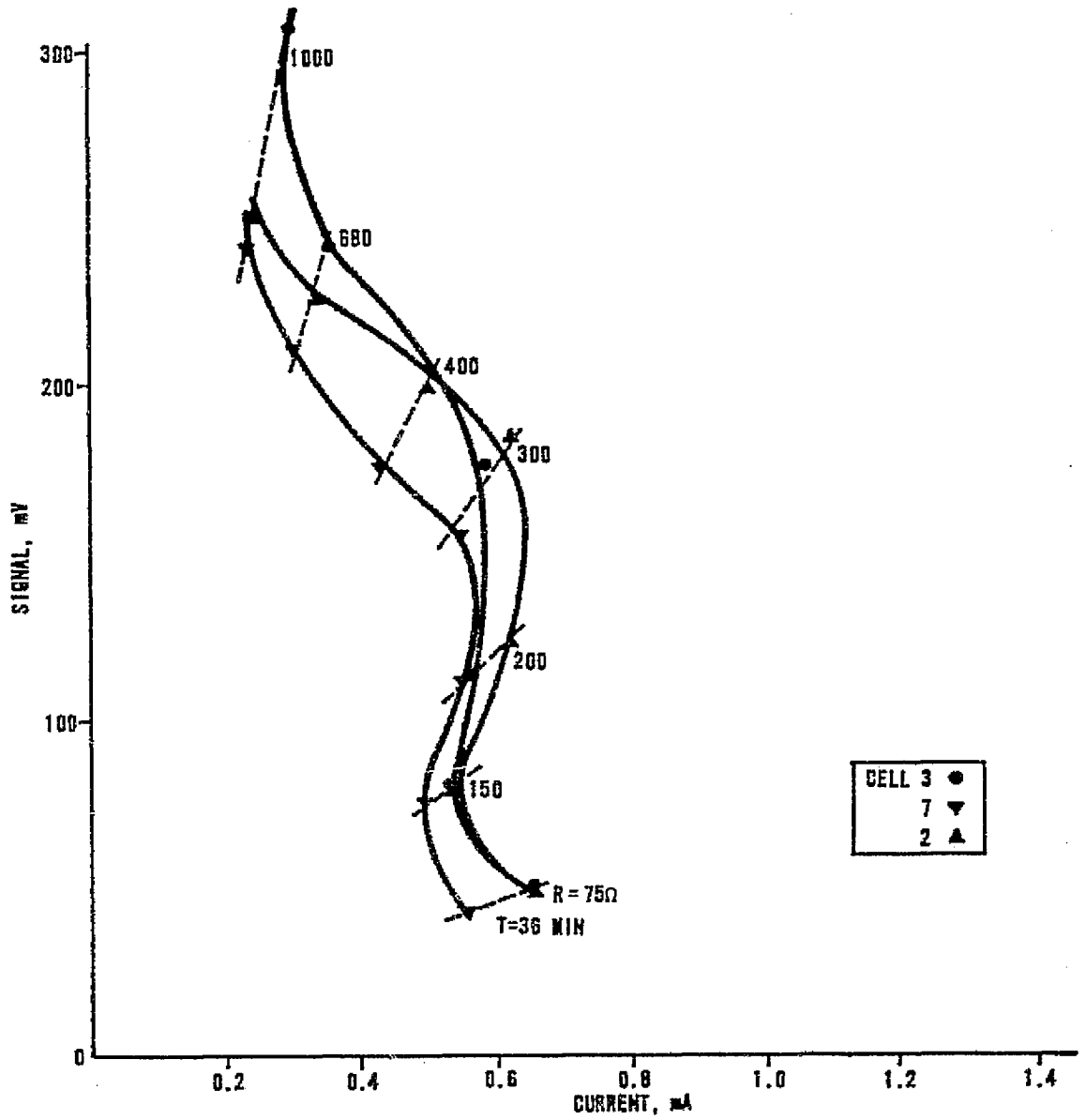

FIGURE 37. INTERNAL RESISTANCE CHARACTERISTICS FOR THREE CELLS AT A PARTICULAR STATE OF CHARGE (AB12 CELLS)

40M 22411

4.4.4 Comparison of third electrode response for four cells tested under same conditions. Signal values for four cells were taken at test conditions of 20°C with a 200-ohm third electrode load at various states of charge. These values were compared to see if the signal deviation from cell to cell at a particular state of charge was uniform throughout the cycle. The results as shown in table II indicate that the signal deviations were not uniform and varied at each state of charge, i.e., the deviation of one signal from another at the beginning of charge was in no way related to their deviation at the end of charge. This rules out the possibility of matching third electrode responses by adjustment of load resistances based on signal variation under a given set of conditions.

TABLE II. SIGNAL IN MILLIVOLTS AT VARIOUS STATES OF CHARGE FOR FOUR CELLS, 200-OHM LOAD AND 20°C

Cell	Signal mV		
	Begining of Constant Current Charge	Constant Voltage Charge	Maximum Signal After Charge Termination
2	44	175.0	237.5
3	38.0	162.0	217.0
7	45.0	47.5	175.0
21	42.5	175.0	248.0

4.4.5 Selection of battery third electrodes. When the third electrode is considered as a black box and the internal generator as a constant voltage source, the internal resistance appears as a variable resistor whose value is determined by the value of the external electrical load. As shown in figure 34, 35, and 36 the internal resistance changes from positive values through negative values with the maximum resistance occurring between 150 and 300 ohms external load. Although all cells tested indicated maximum internal third electrode resistance between 150 and 300 ohms external load, the signal values of each third electrode were not equal. Non-uniformity of the signal values must be eliminated in the flight battery which requires three redundant third electrode charge termination control signals. To achieve signal uniformity, the external load resistors will be chosen so that at charge termination all three signals will be equal. The mean value of the external load will be 200 ohms since this is the constant current point which facilitates calculation.

Assembly of the flight battery with three redundant charge termination electrodes can be achieved in the following manner. All flight cells will be subjected to several simulated ATM cycles at 20°C with 200-ohm third electrode load resistors. After steady-state cycling is achieved, the ampere-hour charge/discharge

ratio can be determined. All the third electrode signals are recorded when the charge/discharge ratio is equal to 110 percent at 20°C. During flight battery assembly the previously recorded third electrode data will be available from which three charge terminations control cells can be chosen.

4.4.6 Temperature dependence of third electrode signal. Figures 38, 39, 40, and 41 are log plots of the third electrode signal as a function of temperature and load. These figures were plotted from data similar to that depicted in figures 30 through 33 for cell 7, AB12 type battery. Each log plot is a family of curves which depicts the signal value of cell 3 at various states of charge with a given load resistor. The time associated with each curve in the figures corresponds to a state of charge.

A replot of cell 3 at a given state of charge is shown in figure 42. Each curve in the figure represents the temperature response of the third electrode for the indicated load values.

Figure 43 was plotted to depict the relative signal values of three cells at two states of charge. The state of charge corresponds to the time values indicated in the figure. The significant factor in this figure is the nonuniformity of the cells response when all three cells are subjected to a 400-ohm load resistor.

The log plots of third electrode signal as a function of temperature has possible future application. Plots of the type shown in figure 42 for cells with similar temperature sensitivities should yield parallel lines. By adjustment of third electrode load resistances, with a mean value of 200 ohms, cells with similar sensitivities could be made to give identical responses. A suggested cell matching procedure based on similar temperature sensitivities is as follows:

(a) Record third electrode signals of each cell at two different temperatures and at equal states of charge.

(b) Calculate the slope of the log signal versus temperature curve.

(c) Group the cells according to similarity of temperature sensitivities.

(d) Match cell group signals through adjustment of third electrode load resistances.

Calibration of third electrode signal versus pressure would provide a means for predicting pressures in these temperature ranges. Such a calibration would also make it possible to determine pressure rates from data similar to figure 22 and the effect of temperature upon these rates.

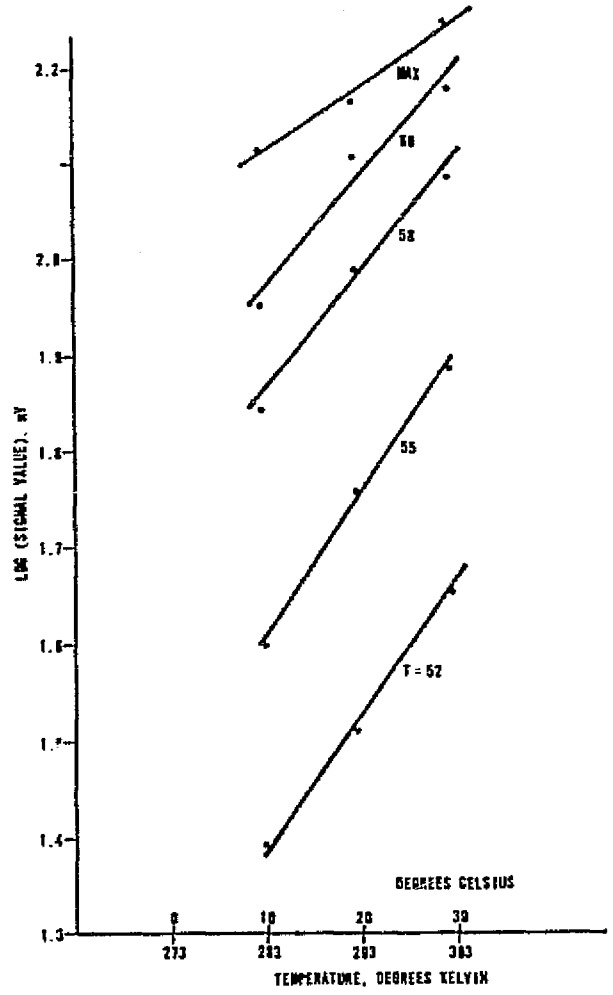

FIGURE 38. TEMPERATURE SENSITIVITY OF CELL 3 AT VARIOUS STATES OF CHARGE WITH 75-OHM LOAD

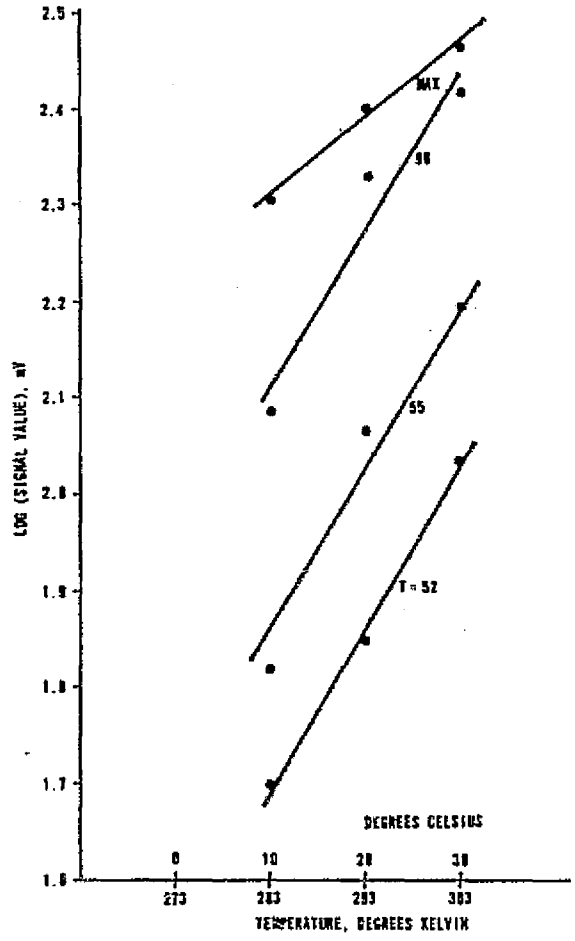

FIGURE 39. TEMPERATURE SENSITIVITY OF CELL 3 AT VARIOUS STATES OF CHARGE WITH 200-OHM LOAD

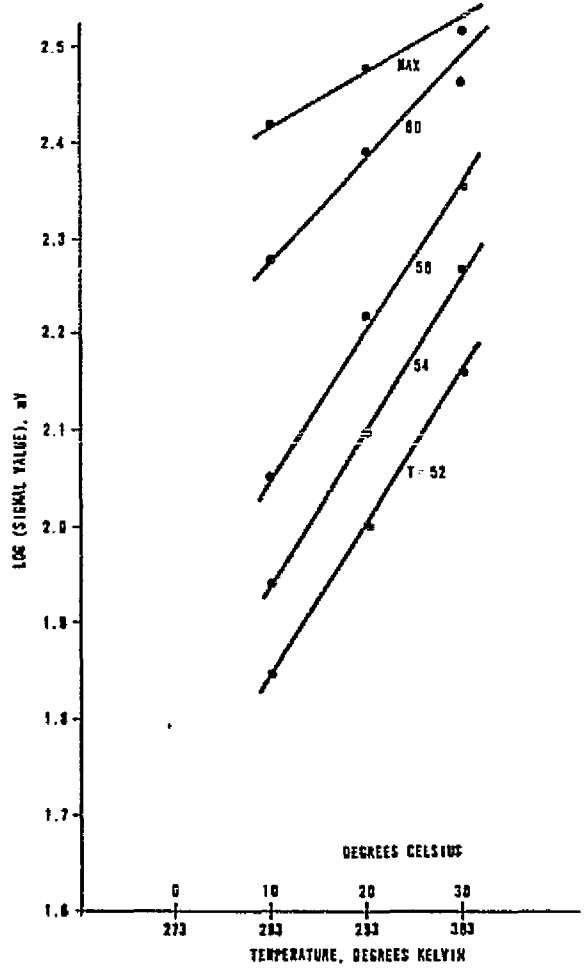

FIGURE 40. TEMPERATURE SENSITIVITY OF CELL 3 AT VARIOUS STATES OF CHARGE WITH 300-OHM LOAD

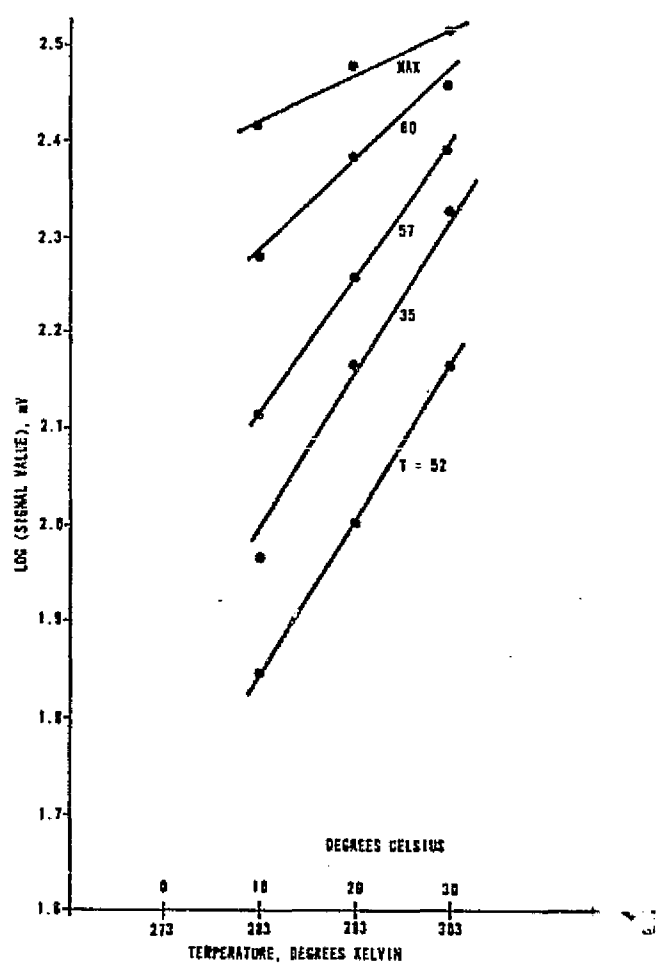

FIGURE 41. TEMPERATURE SENSITIVITY OF CELL 3 AT VARIOUS STATES OF CHARGE WITH 400-OHM LOAD

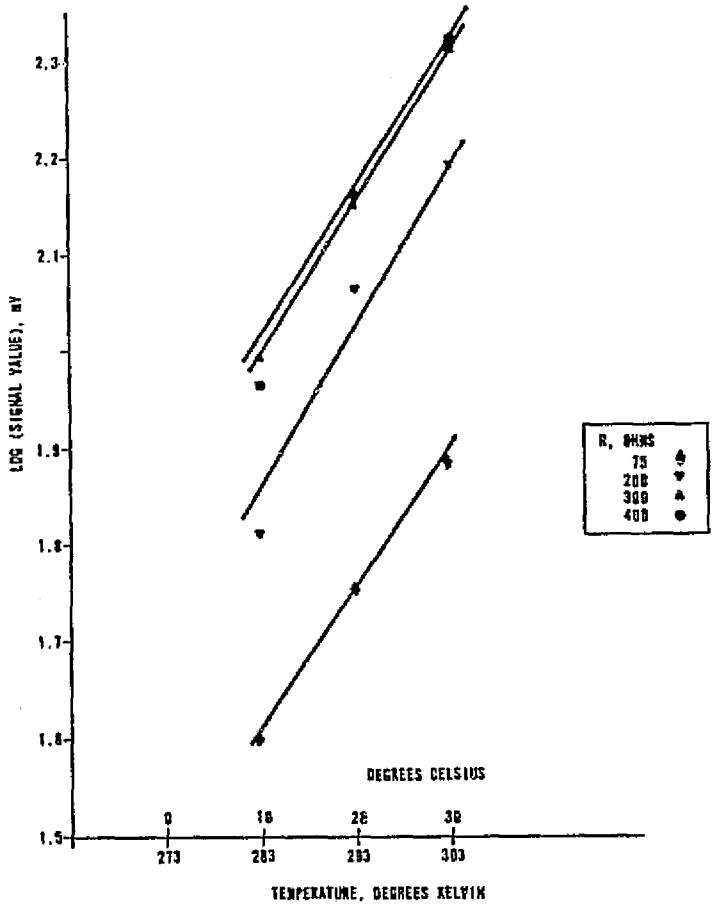

FIGURE 42. TEMPERATURE SENSITIVITY OF CELL 3 AS A FUNCTION OF LOAD AT A PARTICULAR STATE OF CHARGE

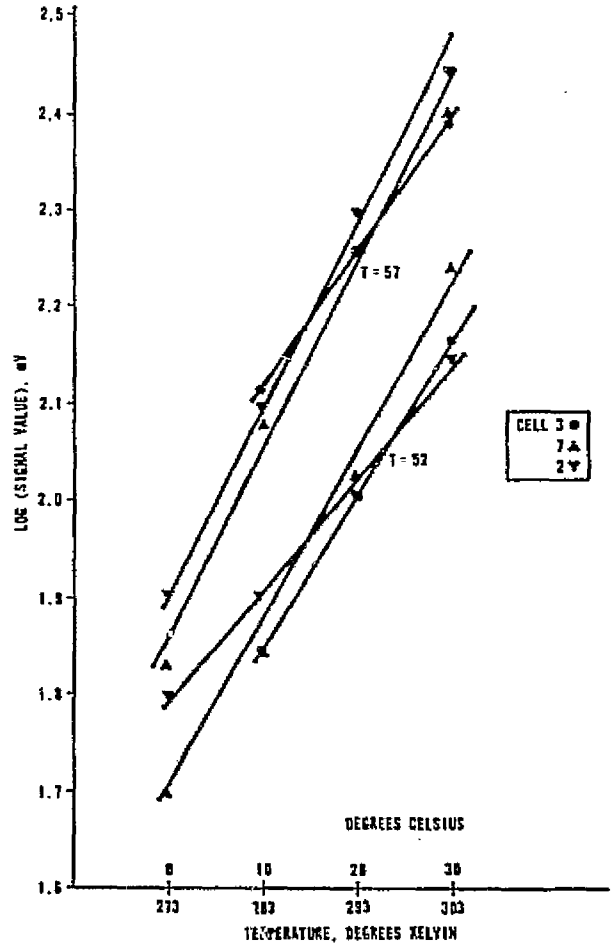

FIGURE 43. TEMPERATURE SENSITIVITIES OF THREE CELLS AT THE SAME STATE OF CHARGE WITH 400-OHM LOAD

4.4.7 Summary - third electrode signals. Several important third electrode operating characteristics were determined during testing: one of these is the internal resistance of the third electrode, another is the temperature response, and a third is the nonuniformity of cell response when cells are subjected to identical cyclic conditions. These characteristics have determined the methods to be used which will enable the optimized choice of charge termination control third electrode.

4.5 Recharge Requirements. The cyclic operation (charge/discharge) of a Ni-Cd battery requires that more electrical energy be replaced during charge than is removed during discharge. The basic source of inefficiency is in the energy conversion process which, during charge, converts electrical energy to chemical energy, thermal energy, and gas; and during discharge converts chemical energy to electrical and thermal energy. Thermal energy, which is dissipated as heat and is therefore not part of the desired energy conversion process, must be replaced during the charge cycle. However, energy replacement, beyond the amount necessary to completely charge the battery and replace the losses, will generate additional thermal energy and gas. The charge criterion therefore, is to maintain an electrical energy in-out ratio which will maintain a given state of charge.

A convenient unit specifying the electrical energy removed and replaced during discharge and charge, respectively, is the ampere-hour. The ratio of ampere-hours-in to ampere-hours-out is defined as the recharge fraction. State-of-the-art Ni-Cd battery information at the initiation of the ATM program indicated a minimum recharge fraction requirement of 120 percent at 20°C operating temperature with a nominal electrical load of 200 watts. This recharge fraction will result in approximately 28 watts of excess heat being generated by a 24-cell, 20-ampere-hour Ni-Cd battery. With an ATM electrical power system design constraint precluding the use of an active cooling system, the maximum battery generated heat that could be dissipated under the environmental boundary was 19 watts, corresponding to a 110-percent recharge fraction. The development effort was therefore concerned with reducing the required recharge fraction consistent with acceptable and reliable Ni-Cd battery operation.

Tests were conducted to establish acceptable recharge fraction values which would result in operation of the battery within the ATM electrical and thermal specifications. The basic test procedure was to subject the test specimen to simulated ATM orbital conditions and observe and record usable battery capacity as a function of cycles, temperature, and electrical load. The recharge fraction was adjusted to an equivalent value of 107 percent at 20°C with a 200-watt electrical load.

To acquire the required data, the 24-cell battery was subjected to simulated ATM orbital conditions as shown in figure 44. Charge time was 58 minutes and discharge time was 36 minutes. The charge was composed of a constant current charge followed by a constant voltage charge. Conversion from a constant current to a constant voltage charge occurred when the battery voltage reached a preset level. This

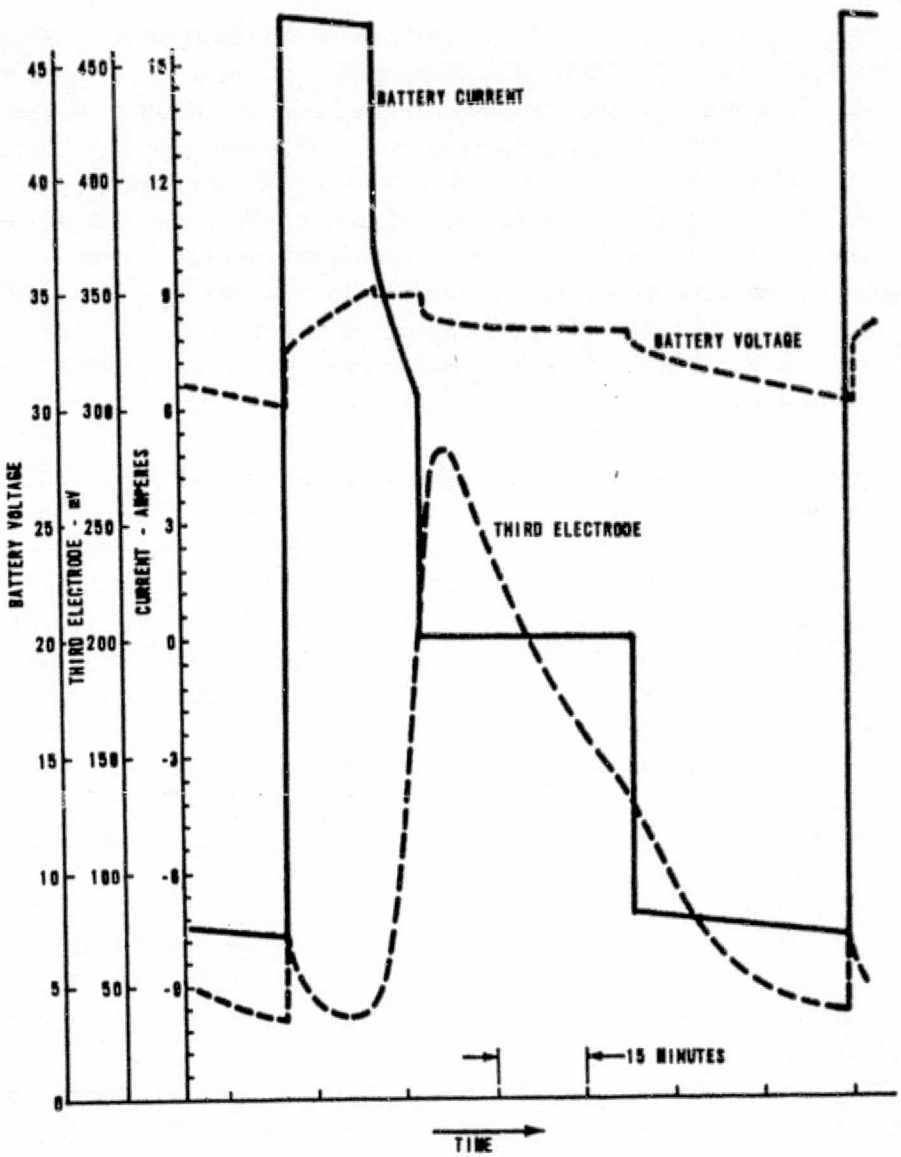

FIGURE 44. ATM TEST CYCLE - AB12 BATTERY

40M22411

preset voltage level is a function of temperature as previously shown in figure 19. The constant voltage charge was 0.8 volt less than the preset level. Charge termination occurred when the third electrode signal from the most negative cell in the battery reached 200 mV. The 200-ohm third electrode load and the charge termination voltage level remained constant throughout the test.

The test specimen was subjected to 2000 simulated ATM orbital cycles prior to recording the recharge fraction data. The purpose of the pretest cycles was to establish proper battery performance at 0°C. Test data were recorded at four temperatures: 0, 10, 20, and 30°C. At each temperature, the battery was subjected to five different loads ranging from 100 to 291 watts. The battery was cycled for 4 hours at each load prior to recording test data. All the data points were based on an average of three cycles each. The charge/discharge ampere-hours were determined with an ampere-hour integrator. All voltages, battery current, and third electrode signals were monitored with a data acquisition system.

The results of the pretest cycles are noted in figure 45. Although the indicated cycles were recorded primarily at 0°C, several data points reflect 20°C and 30°C cyclic performance. Since the measured capacity at cycle 2000 was above the rated battery capacity, it was assumed that the battery was being sufficiently recharged. This assumption was based on the capacity degradation from cycle 0 to 2000 which was less than anticipated based on all previous battery test data.

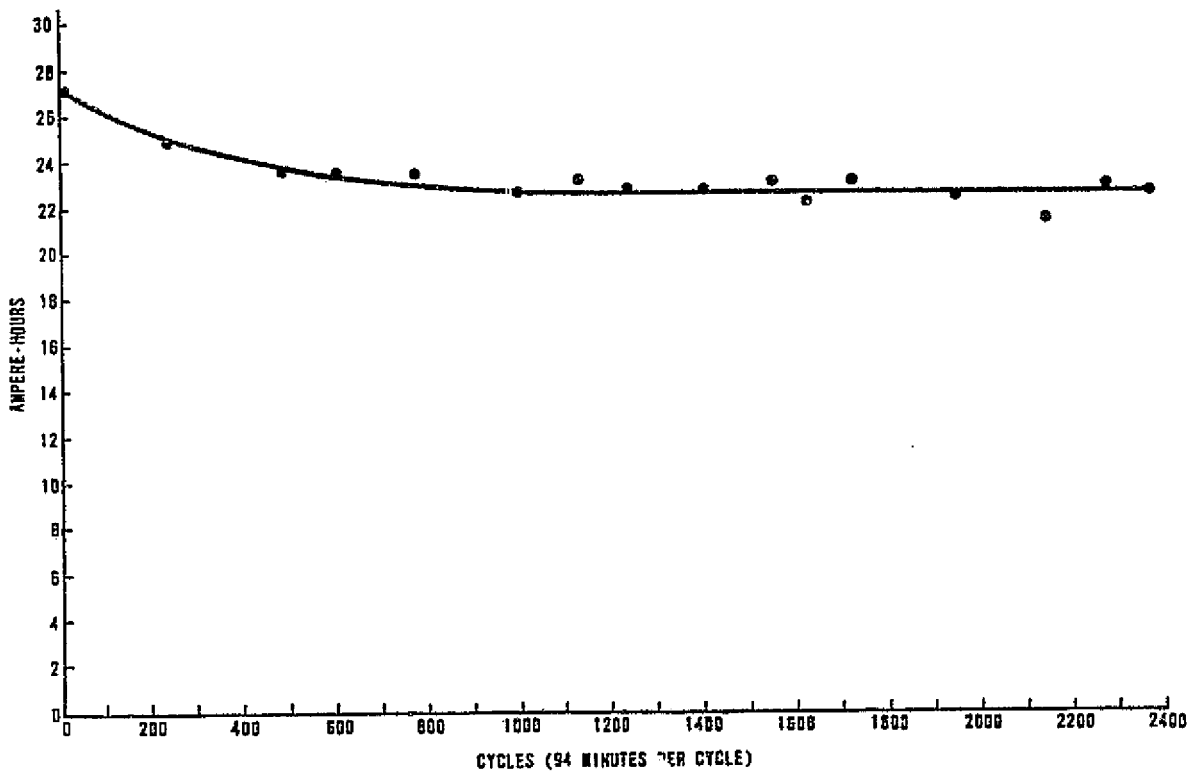

FIGURE 45. CAPACITY CHARACTERISTICS, ATM 2000 CYCLE TEST PRIOR TO RECHARGE FRACTION TEST, AB12 BATTERY

The results of the recharge fraction tests are shown in figure 46. As shown, the required recharge varies as a function of load and temperature. The variation is the result of battery response to external conditions such as load and temperature.

A Ni-Cd battery has the highest charge efficiency when the state of charge is 80 percent or less. Conversely, the charge efficiency decreases when the state of charge increases above 80 percent. At 100 percent state of charge, the charge efficiency is zero. This factor accounts for the increase in the measured recharge fraction as the load was decreased. At light loads, the battery is cycled at a high state of charge, therefore charging is less efficient.

Charge efficiency is also a function of temperature. As temperature increases, the charging efficiency decreases. This factor caused the rise in the recharge fraction as the battery temperature was increased.

The results of the recharge fraction test, together with the 2000 pretest cycles at 0° C and the 1500 post-test cycles at 20°C, has indicated acceptable battery operation with an associated recharge fraction that reduces total battery heat to acceptable ATM levels. The battery capacity characteristic at 20°C during the 1500 post-test cycles is shown in the 3000 to 4500 cycle test period of figure 53.

The battery heat generated at a 20°C cyclic operation with a 200-watt electrical load is approximately 17 watts per cycle. This value is the result of operation at 107-percent recharge fraction and is within the ATM thermal specifications.

To achieve maximum battery operating efficiency, the charge termination control third electrode must be chosen so as to provide a proper signal for termination. An example of the response of third electrode signals is shown in figures 47 and 48. When cell 3 is used for charge termination, the recharge fraction is 105.7 percent. Conversely, when cell 1 is used the recharge fraction is 113 percent. The conclusion to be derived from this data is that the choice of the controlling third electrode determines the recharge fraction. Charge termination of the ATM flight cells will be determined by use of the above information.

4.6 Capacity Degradation Characteristics.

4.6.1 Capacity as a function of temperature and cyclic history. The most important phase of the Ni-Cd battery investigation was to establish the useful battery capacity as a function of temperature and cyclic history. Absolute battery capacity tests were conducted on battery GE3CAB10. Each test cycle consisted of 30 ampere-hours of charge followed by a complete discharge and strapout. The charge was delivered to the battery at a 15-ampere constant current. When the battery voltage had increased to a preset level of 35.4 volts, the charge was converted from a constant current charge to a constant voltage charge. The constant voltage, which was 0.7 volt

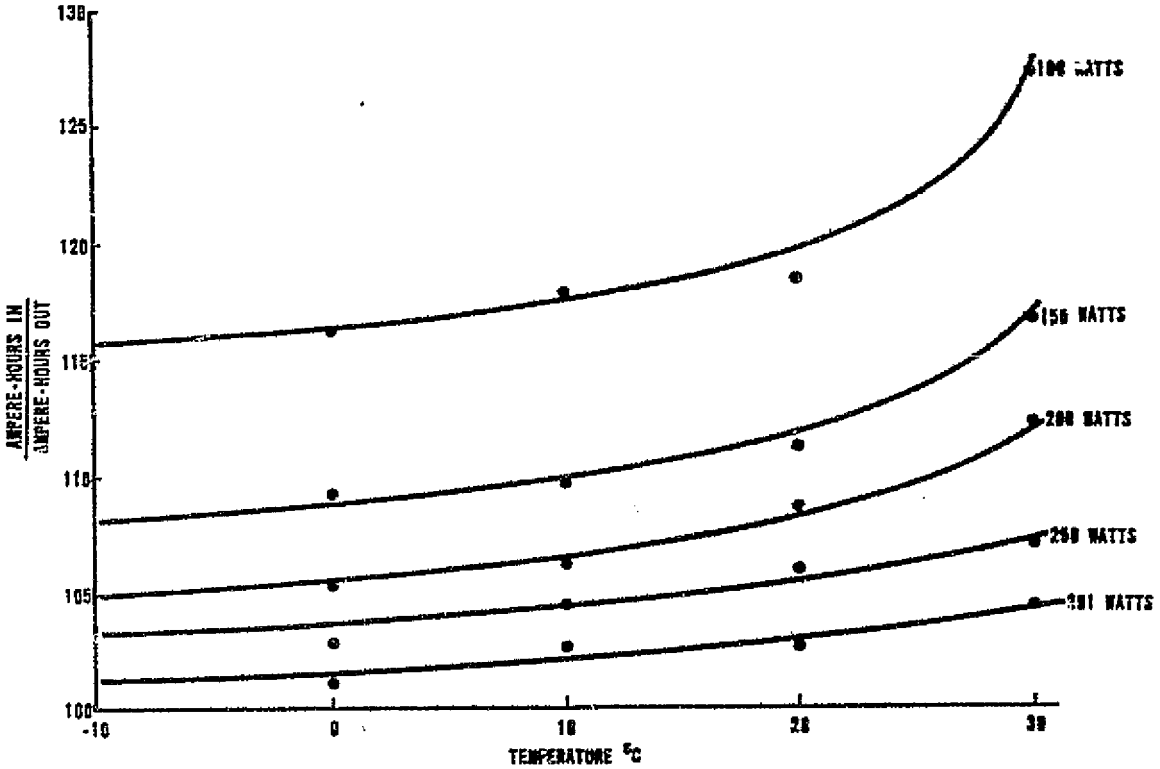

FIGURE 46. RECHARGE CHARACTERISTICS, AB12 BATTERY

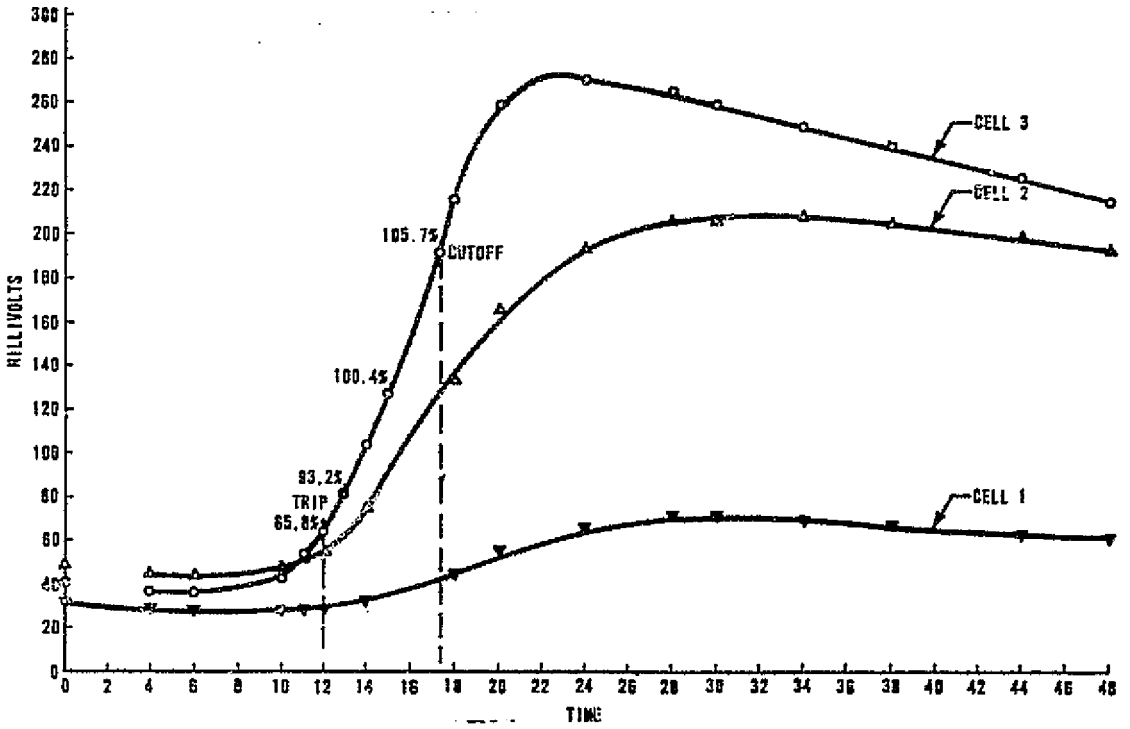

FIGURE 47. THIRD ELECTRODE CHARACTERISTICS, 50-OHM LOAD, 20°C, AB12 BATTERY

40M 22411

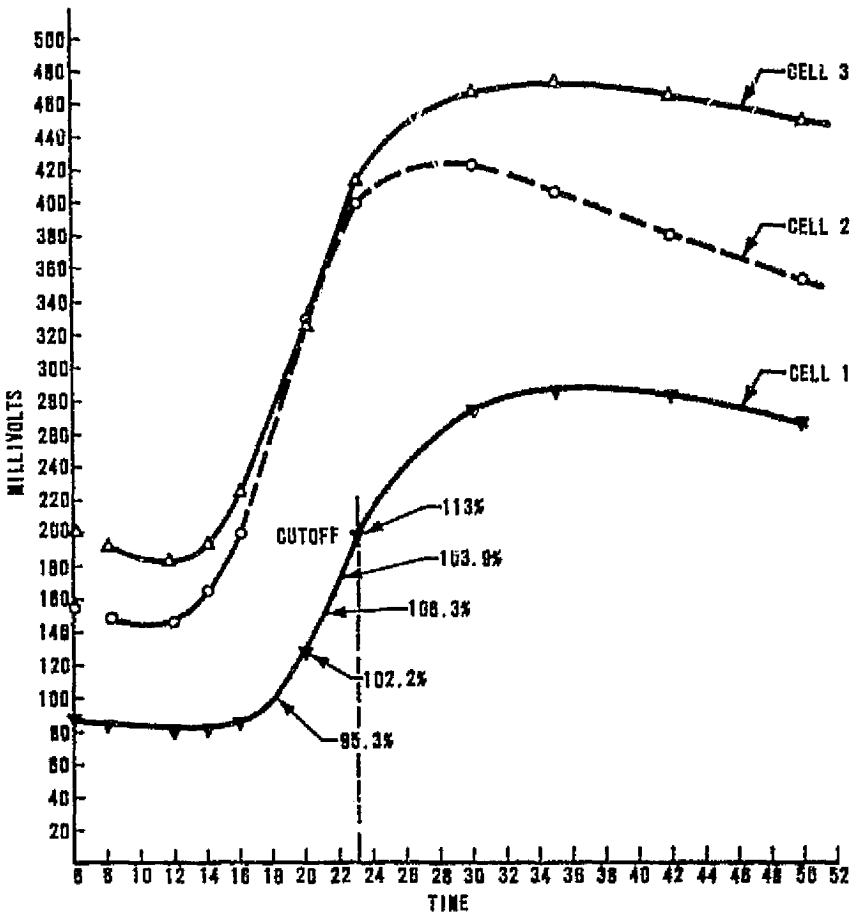

FIGURE 48. THIRD ELECTRODE CHARACTERISTICS, 200-OHM LOAD, 20° C, AB12 BATTERY

below the trip level, was maintained until 30 ampere-hours had been delivered to the battery. Capacity was measured by discharging the battery at a constant 10-ampere rate until the voltage of any one cell decreased to 1.0 volt. Following the capacity test, each cell was shunted with a 1-ohm resistor until the cell voltage decreased to 0.9 volt at which time the cells were individually shorted electrically. The short was maintained for 72 hours. Prior to application of the short, the temperature was changed to the subsequent test temperature to assure battery equilibrium prior to the next charge cycle.

Absolute battery capacity as a function of temperature is shown in figure 49. Each capacity test is depicted by an individual point. The numbers associated with each point indicate the order in which the tests were conducted. The data indicate that the battery contains rated capacity at temperatures between 0°C and 40°C. However, note that the tests depicted in figure 49 were single cycle tests and that steady-state cycling at the test temperatures would not result in the capacity levels indicated.

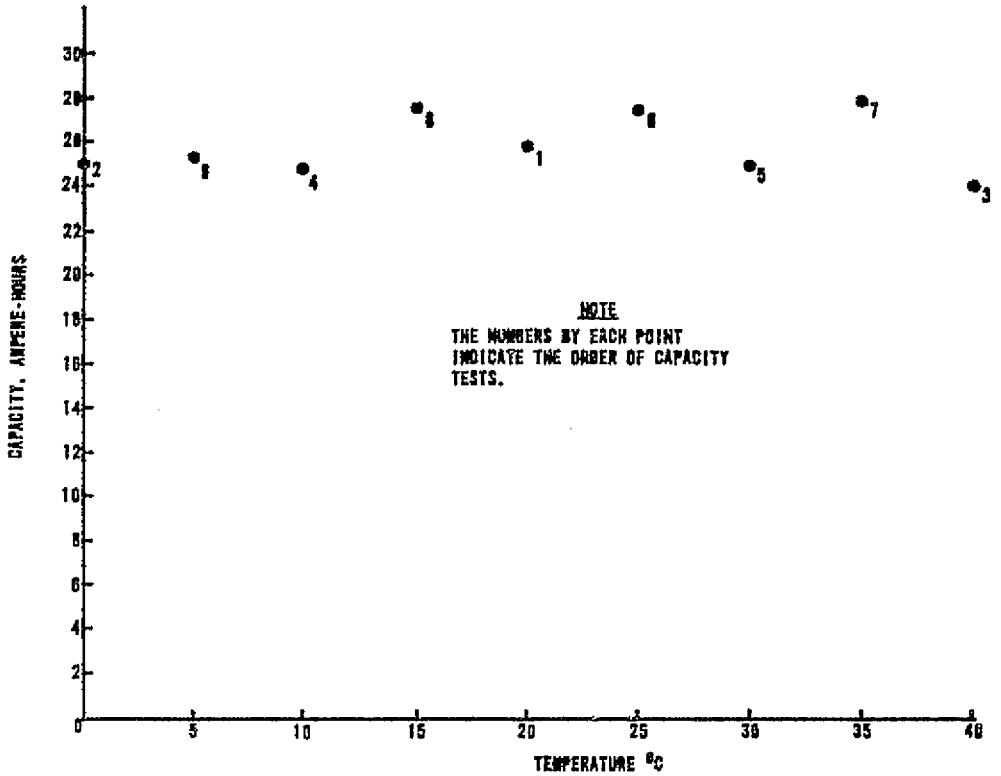

FIGURE 49. CAPACITY CHARACTERISTICS, AB10 BATTERY

Cyclic capacity degradation was measured to acquire information to assist in optimizing the charging technique. The initial capacity characteristics were determined with an AB09 type battery. The test cycle and the resulting capacity characteristics of the AB09 test were previously shown in figure 11 and figure 10, respectively. As previously shown in figure 10, a change in the charge regime and an increase in trip voltage for the AB10 type battery tests resulted in improved capacity. The only difference between the two cell types was that the AB10 cells contained a third electrode. The AB09 battery test was conducted at 23°C and the AB10 battery test was conducted at 20°C. The increase in trip voltage was possible through the improved cell matching as noted in paragraph 4.2.

Additional capacity degradation tests were performed on the AB12 type cell which contains a third electrode and a fourth electrode. These tests were intended to demonstrate the useful battery capacity characteristics. The test cycle used in this test was previously shown in figure 44. This test also included a temperature compensated maximum charge voltage. The general test procedure was to subject the test specimens to continuous simulated ATM orbital cycling with a fixed set of charge and discharge control parameters. After a definite capacity trend or

goal was established, one parameter was changed and the test was continued. Battery capacity was determined by discharging the battery immediately following the completion of a charge at a 10-ampere rate until the voltage of any cell decreased to 1.0 volt. If testing was to continue after the 10-ampere discharge, the battery would be fully charged by extended ATM charge, and cycling would continue.

In general, battery capacity characteristics are affected by two considerations: the response to temperature and the possible capacity recovery techniques once degradation had occurred.

Temperature characteristics of the three ATM flight-type test batteries (AB12 cells) are shown in figure 50. The 20°C and 30°C curves depict the expected performance of a battery which is subjected to continuous cycling at the indicated temperature. In this respect, the curves depict worse case battery performance at the respective temperature. Although the 0°C curve reflects primarily 0°C data, the curve also reflects battery performance when the battery is subjected to temperatures between 0° C and 40° C. The 0°C curve data were taken from a test sequence which consisted of a high temperature test for up to 4 days, preceded and followed by at least 4 days of 0°C cycling. As shown in figure 50, the average capacity degradation is not greatly affected by the high temperature. The high temperature cycling was performed to acquire third electrode characteristics data.

One obvious conclusion from figure 50 is the rapid battery capacity degradation as a function of steady-state cycling at high temperatures. Another factor is the nonlinear temperature response of the battery. What is not well defined, however, is the battery response to a variation in temperature and loads. The 0°C curve is an example of this type of response but it does not define precisely what the relationship is.

The capacity degradation of a battery imposes limitations on mission objectives. Capacity degradation can be defined as the decrease in available battery capacity within usable voltage limits. The total battery design capacity is always available but after the onset of memory much of it is below usable levels. Part of the capacity degradation test program was to determine if a capacity recovery technique could be devised which would effectively recover any or all of the battery capacity below usable voltage levels.

4.6.2 Capacity recovery techniques. It has been theorized that the useful battery capacity is a function of the battery discharge rate. The theory was tested by subjecting a rated 20-ampere-hour AB09 battery, which had a useful capacity of 14 ampere-hours, to a series of sequential capacity tests where each capacity test would be preceded by 50 simulated ATM cycles and be conducted at different discharge rates. The results of this test are illustrated in figure 51. The 2-ampere-hour difference shown in the figure is attributed to instrumentation error.

40M 22411

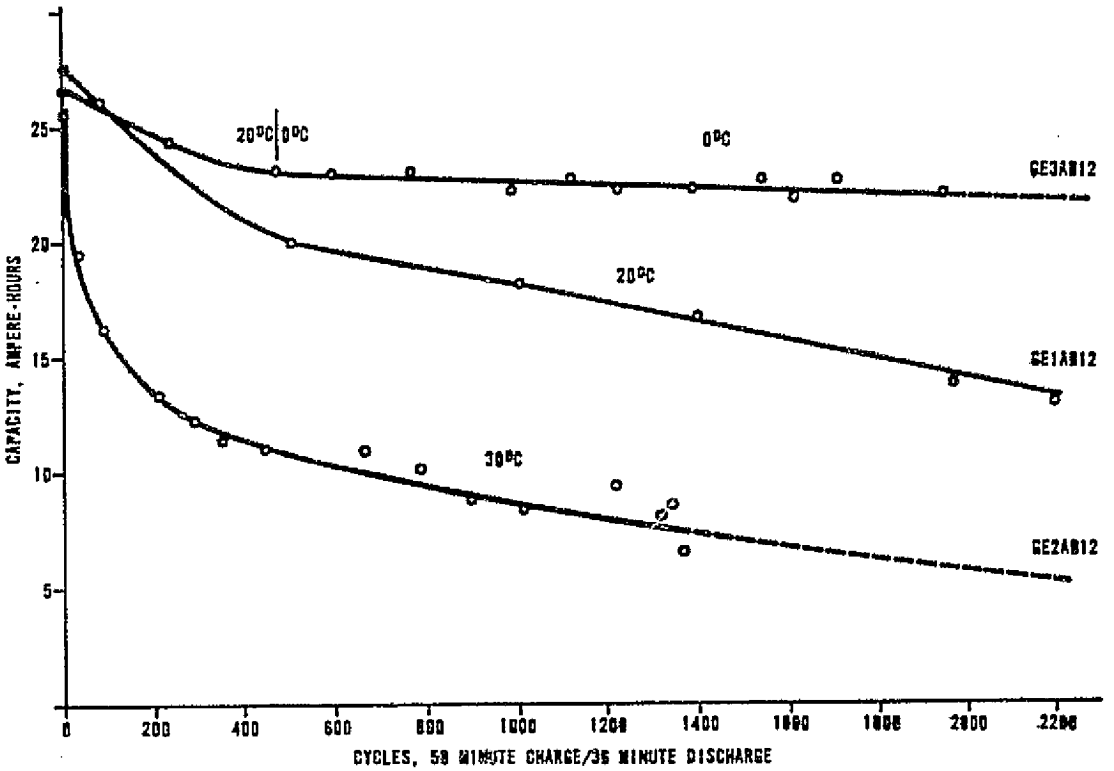

FIGURE 50. TEMPERATURE CHARACTERISTICS - THREE ATM FLIGHT-TYPE BATTERIES

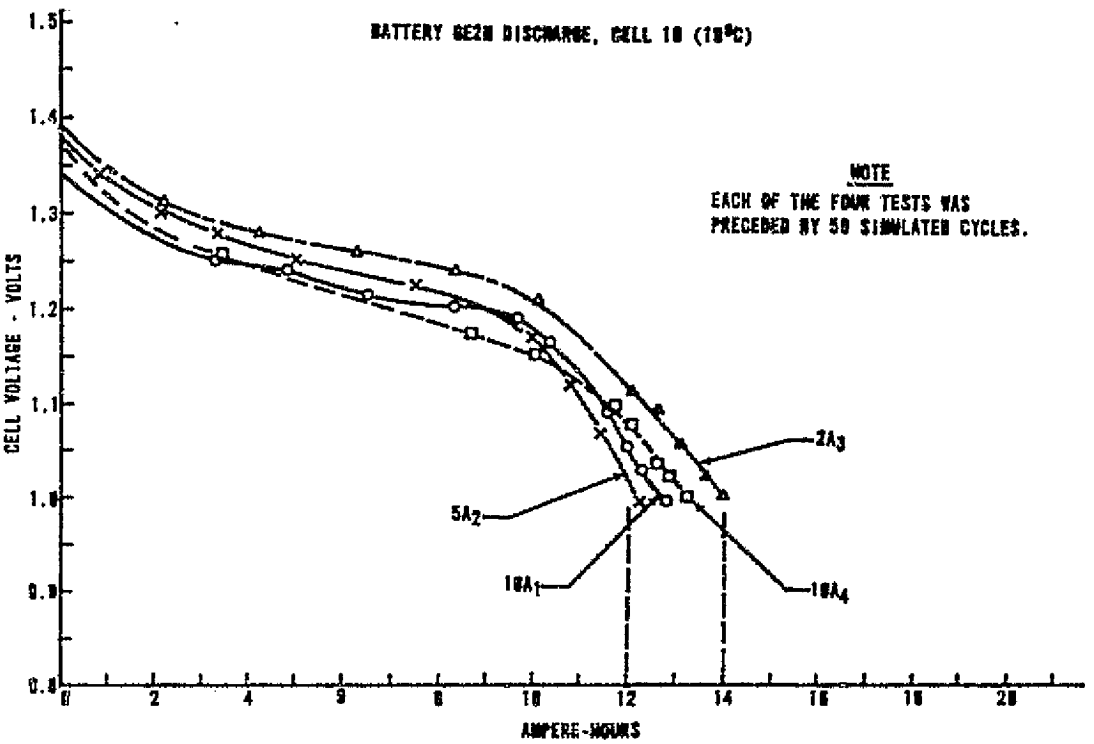

FIGURE 51. BATTERY CAPACITY AS A FUNCTION OF DISCHARGE RATES, AB09 BATTERY

40M 22411

Another technique which can effectively be used to partially recover useful battery capacity is a decrease in operating temperature to 0°C or less. This technique is demonstrated in figure 52 and 53. Figure 52 depicts a partial useful capacity recovery at cycle 1400 and cycle 2550. Figure 53 depicts a partial useful capacity recovery at cycle 4400. In all three situations, recovery was achieved in approximately 400 continuous simulated ATM cycles at 0°C and the amount of recovery was approximately 7 ampere-hours.

A recovery technique which has achieved success is a complete battery discharge such as that shown in figure 54. The indicated strapout for the battery was approximately 2 months. However, a 72-hour strapout is sufficient to achieve a recovery. What the strapout essentially does is to make available capacity which is below usable voltage levels. The limitation of this recovery technique is that individual cell short circuits are required because of cell inequalities. The inequalities would cause a cell voltage reversal and possible cell failure if a battery short circuit were used instead of an individual cell short circuit.

A capacity recovery technique which could be easily applied in space but has limited effectiveness is the trickle charge. Figure 55 shows the test results of two trickle charge tests. The first test was conducted at cycle 1000 at a 2-ampere rate. The second test was performed at cycle 1310 at a 1.5-ampere rate. The first test resulted in thermal runaway and had to be terminated. However, prior to termination at least 10 ampere-hours of trickle charge was delivered to the battery after it had been fully charged. As shown in the figure, the usable capacity did not appreciably increase. The second trickle charge test was composed of two charge rates. A normal simulated ATM charge of approximately 5 ampere-hours was conducted prior to a 22 ampere-hour, 1.5-ampere trickle charge. The trickle charge interrupted the normal cycle routine. The results, as shown in figure 55, increased the total useful battery capacity by approximately 0.6 ampere-hour. This indicates a limited usefulness for an extended trickle charge as a capacity recovery techn[illegible]e.

4.6.3 Post-launch battery characteristics. Tests were conducted on an AB12 type battery to determine the performance characteristics under simulated post-launch preoperational conditions. Prior to this test, this battery had been subjected to 2600 simulated ATM cycles at 20°C.

The simulated post-launch test was conduced in five phases as follows:

(a) Phase I: Following a 72-hour strapout, the battery was charged at 20°C until 30 ampere-hours had been delivered to the battery. A capacity test was then conducted after an 18-hour open-circuit stand to establish a base line value. Following the capacity test, the individual cells were short circuited for 72 hours.

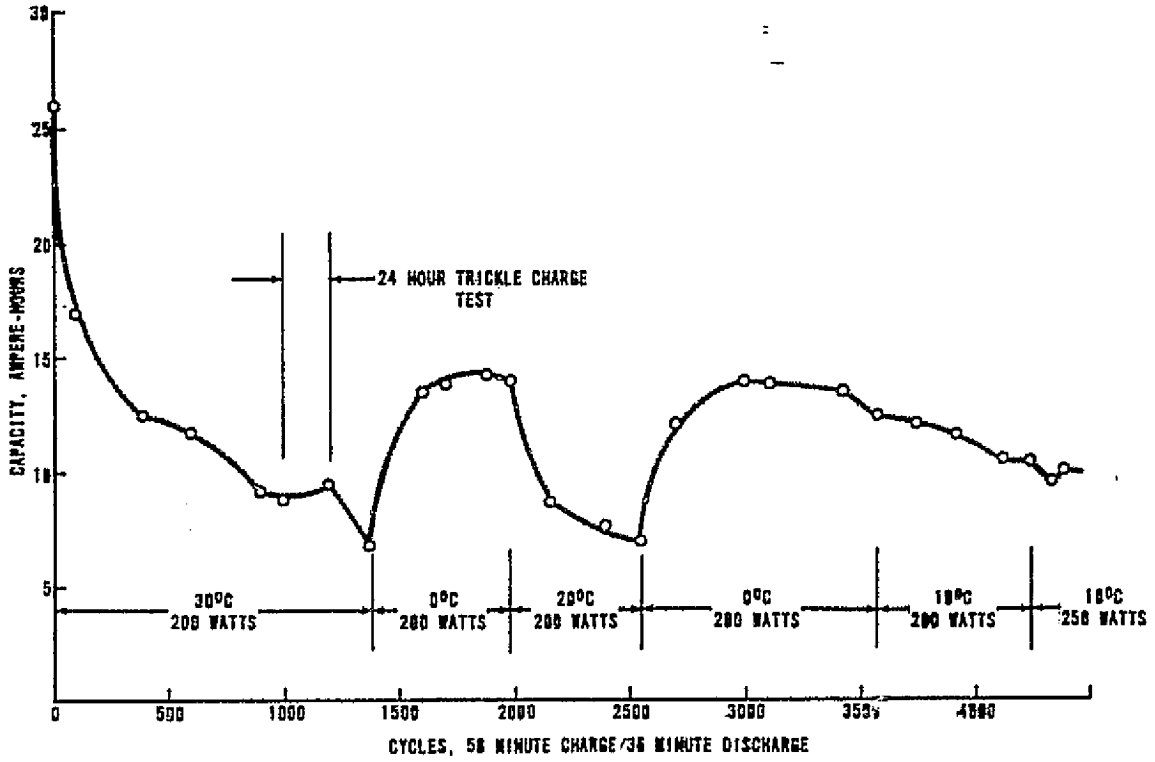

FIGURE 52. BATTERY CAPACITY AS A FUNCTION OF TEMPERATURE, AB12 BATTERY (0, 10, 20, and 30°C)

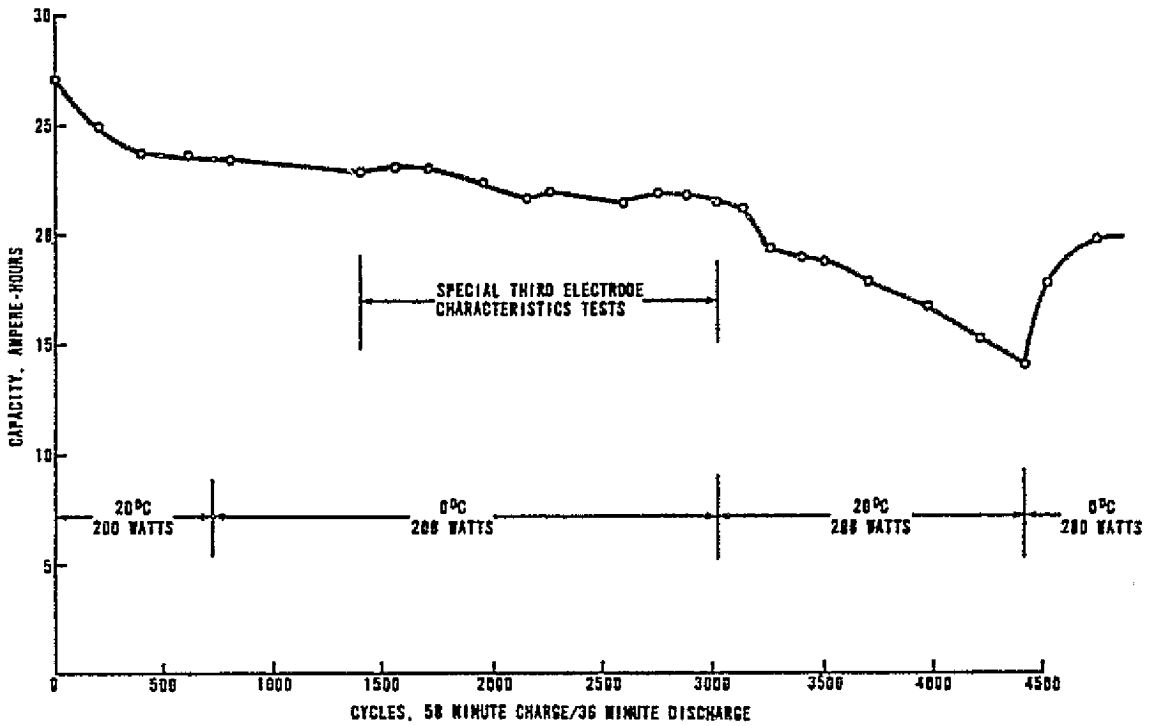

FIGURE 53. BATTERY CAPACITY AS A FUNCTION OF TEMPERATURE, AB12 BATTERY (0 and 20°C)

4014 22411

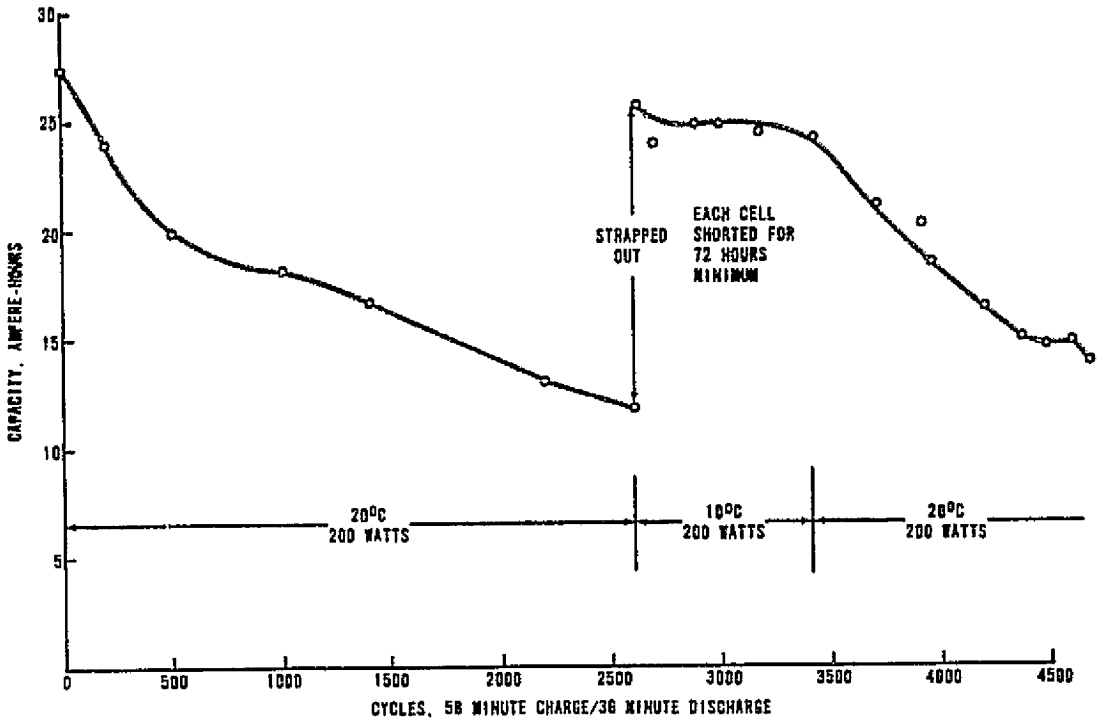

FIGURE 54. BATTERY CAPACITY RECOVERY AS A RESULT OF COMPLETE BATTERY DISCHARGE, AB12 BATTERY

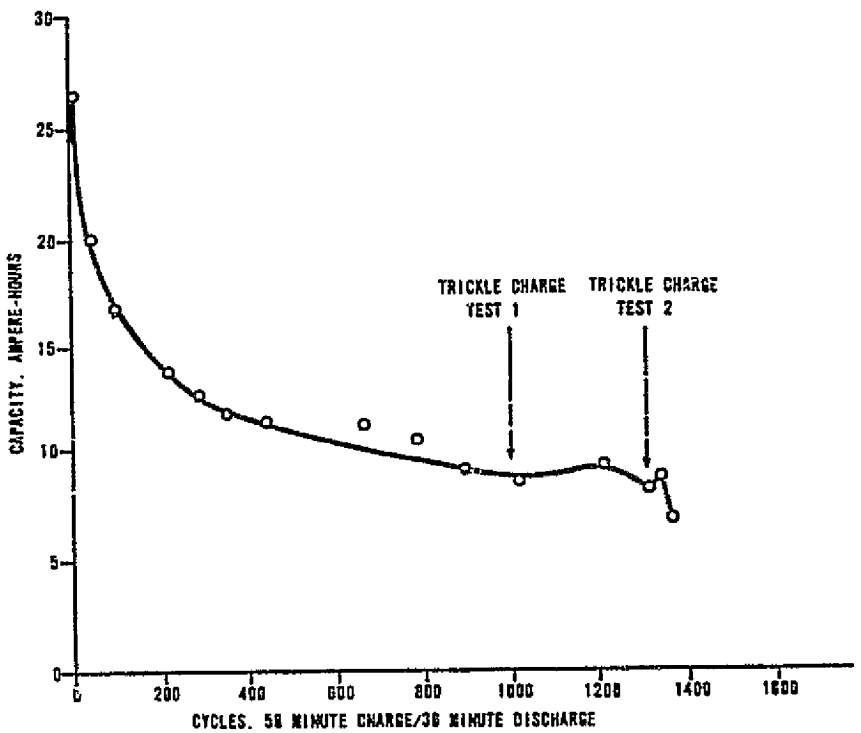

FIGURE 55. BATTERY CAPACITY RECOVERY AS A RESULT OF TRICKLE CHARGE TESTS

(b) Phase II: Following a 30 ampere-hour charge at 20°C, the battery temperature was decreased to minus 14°C. A capacity test was conducted following an 18-hour open-circuit stand. The individual cells were short circuited for 72 hours after the capacity test.

(c) Phase III: Phase III was a repeat of Phase II, except for a lower temperature limit of minus 20° C.

(d) Phase IV and Phase V: A charge of 30 ampere-hours was delivered to the battery at 20°C. After the temperature was decreased to minus 20° C and the battery was open circuited for 18 hours, a 14-hour simulated post-launch discharge was conducted. The post-launch discharge load profile is shown in figure 56. The battery was subjected to simulated ATM cycling for 38 hours immediately following the discharge.

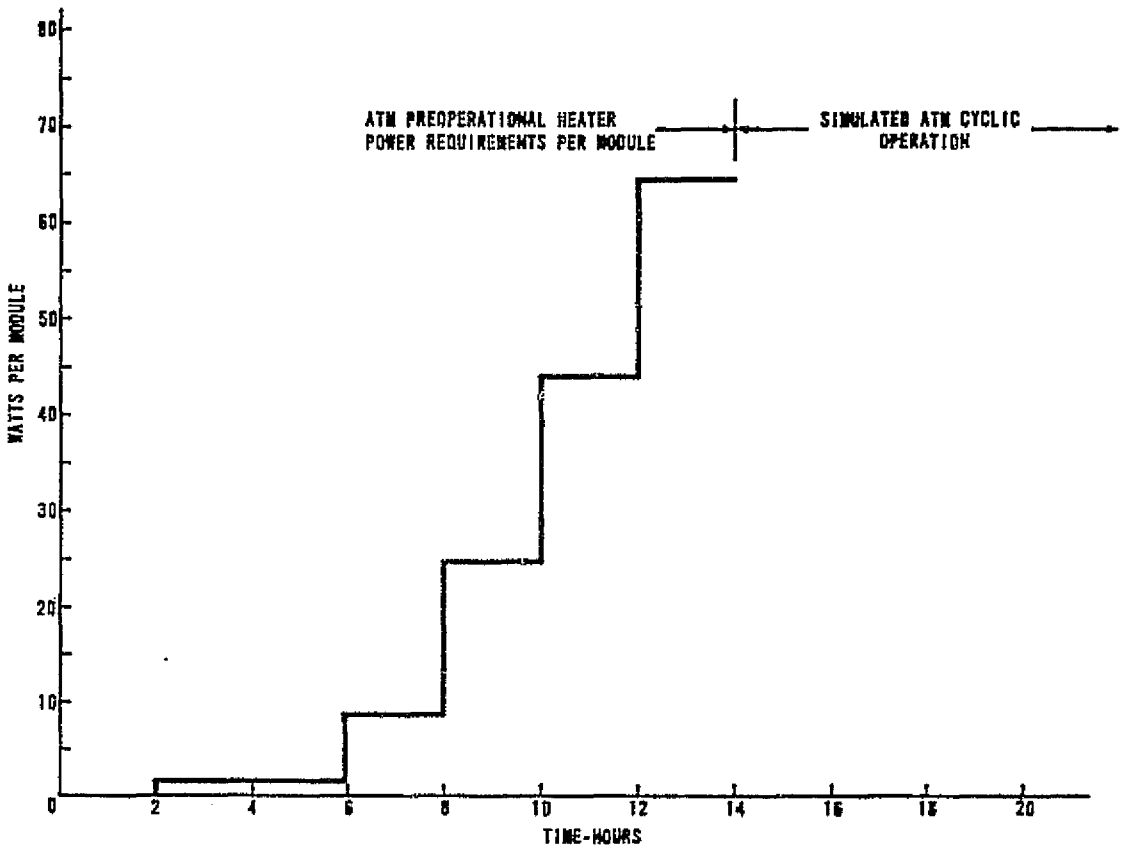

FIGURE 56. SIMULATED POST-LAUNCH DISCHARGE LOAD PROFILE

40M 22411

The results of Phase I through Phase III testing are shown in figure 57. Phase I was conducted twice. On the first run, the battery was subjected to simulated ATM cycling at 20°C following the initial charge, so that all battery parameter adjustments could be made. The base line capacity test was performed on the second run and resulted in 24 ampere-hours capacity at a lower battery voltage limit of 27.2 volts. Two test cycles were also performed during Phase II. Both indicate approximately 19 ampere-hours capacity with a final battery voltage of 27.7 volts. The results of Phase III, as shown in the figure, indicate a capacity of 20 ampere-hours at a final battery voltage of 26.7 volts. Low temperature battery discharges result in a decrease in absolute battery capacity when the charge temperature is above the discharge temperature. The test data indicate a capacity loss of 5 ampere-hours with a 40°C decrease in temperature. There also appears to be no difference in the capacity loss at a 34°C temperature decrease (Phase II) and a 40°C temperature decrease (Phase III).

The results of Phase IV and Phase V are shown in figure 58. It was assumed that at the start of discharge the total battery capacity was 19 ampere-hours. The assumption was based on the results observed in the Phase III test. The total post-launch discharge capacity was 13.4 ampere-hours, which is a 70 percent depth. Battery voltage at the end of the post-launch discharge was 30.08 volts. After the post-launch discharge, the battery was immediately subjected to simulated ATM cyclic

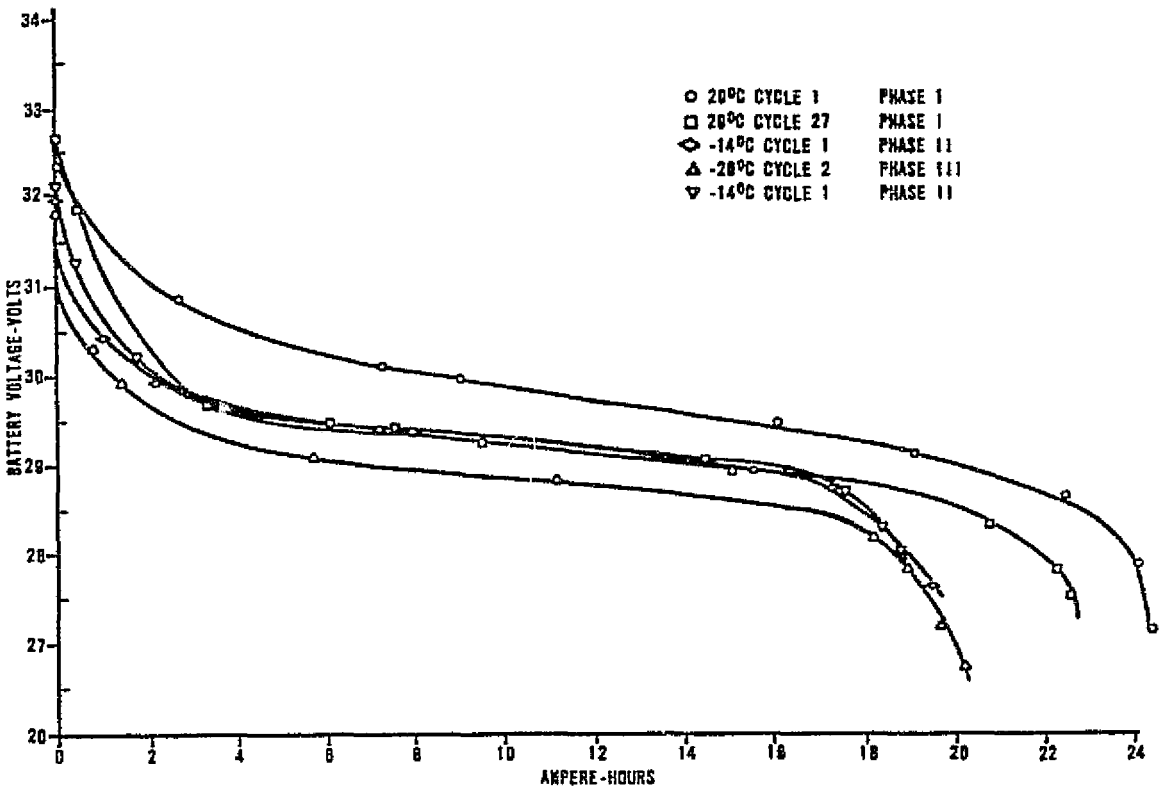

FIGURE 57. POST-LAUNCH PREOPERATIONAL TEST RESULTS-TEST PHASE I THROUGH III, AB12 BATTERY

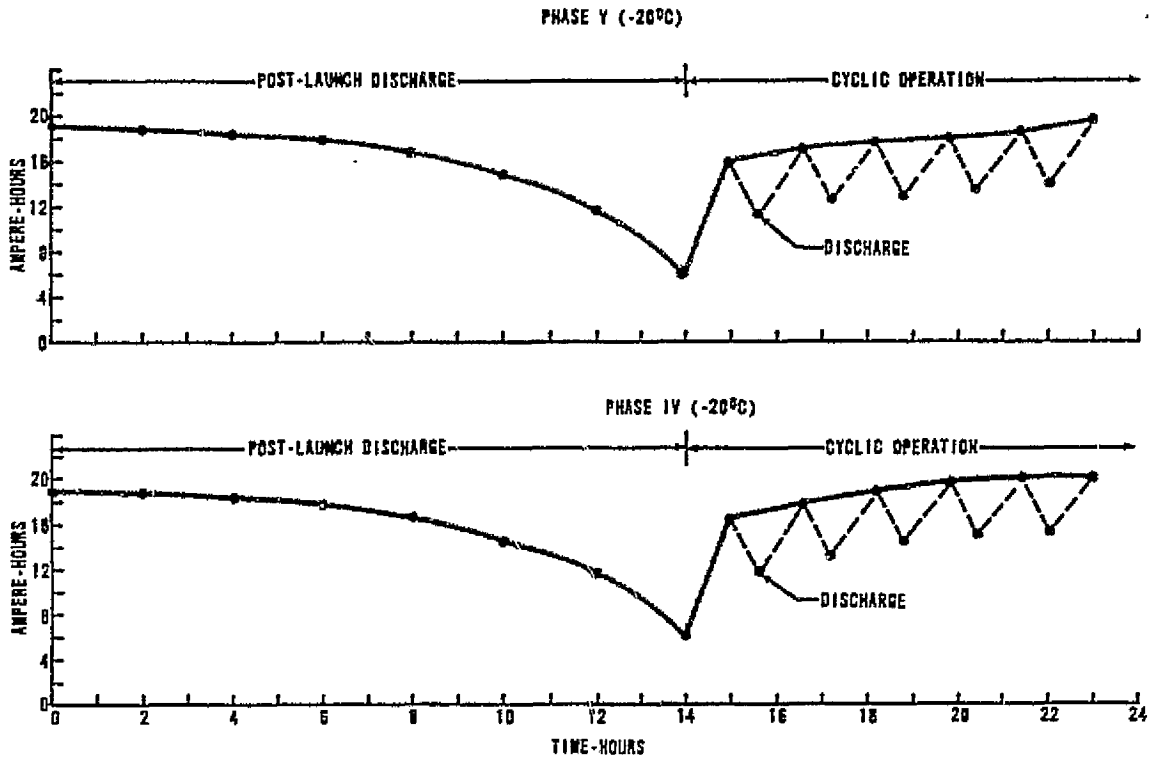

FIGURE 58. POST-LAUNCH PREOPERATIONAL TEST RESULTS, MINUS 20°C, AB12 BATTERY

operation at minus 20°C in which the charge time was 58 minutes and the discharge time was 36 minutes. During discharge, the load was 200 watts for 36 minutes or approximately 4.7 ampere-hours. As shown in figure 58, the available battery capacity was 19 ampere-hours after approximately four simulated ATM cycles.

Following 18 hours of cyclic operation at minus 20°C, the battery temperature was increased to 20°C. After an additional 24 hours of cyclic operation, a capacity test was performed. The results of the final capacity test for Phases IV and V are shown in figure 59. In both tests, the measured capacity was greater than 24 ampere-hours with a final battery voltage above 27.5 volts.

The battery capacity as a result of the post-launch data appears to be a function of the charge and discharge temperature. When the battery was charged at 20° C and discharged at minus 20°C, the capacity was reduced by approximately 5 ampere-hours compared to the 20°C capacity. Likewise, when the battery was charged at minus 20°C and cycled at 20°C, the capacity was again equal to the original 20°C value.

The simulated post-launch preoperational test results indicated all battery characteristics remained within their acceptable operating limits. The battery voltage after the 14-hour discharge was 30.08 volts which is well within the operating limits of the load regulator. Individual cell voltage tracking was within 5 mV during the entire 14-hour discharge. During the subsequent ATM cyclic operation, cell voltages also remained within safe operating limits.

Overall test results indicate excellent battery performance under simulation post-launch preoperational conditions. Although present post-launch conditions require about a 50 percent depth of discharge, the test data indicated successful battery performance at a 70 percent depth of discharge at minus 20° C.

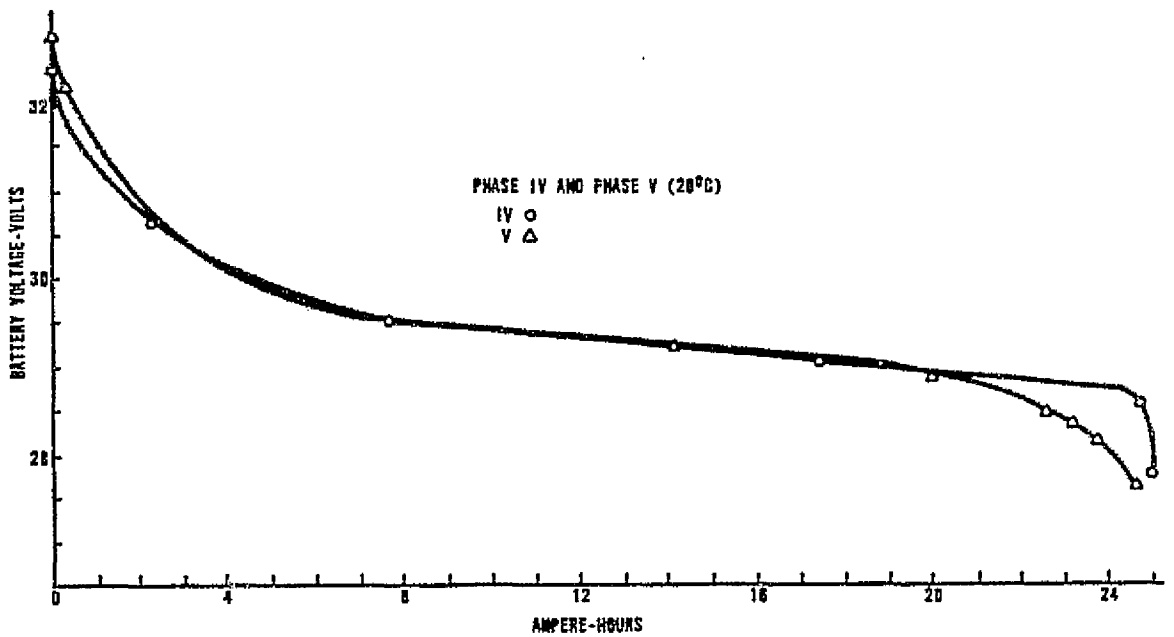

FIGURE 59. POST-LAUNCH PREOPERATIONAL TEST RESULTS, 20°C, AB12 BATTERY

5. CONCLUSIONS AND RECOMMENDATIONS

5.1 Summary of Nickel-Cadmium Battery Tests. Maximum cell voltage of the Ni-Cd batteries is limited by the hydrogen evolution potential which is reported to be 1.47 to 1.55 volts. On a battery basis, the maximum voltage is limited by the cell which contains the minimum capacity because this cell will be the first to reach the individual cell voltage limit. Maximum cell voltage or battery voltage is also temperature dependent. Typical maximum voltage values are 36.8 volts at minus 10°C, 36 volts at 10°C, and 34.6 volts at 30° C. The use of the maximum voltage level as a battery charging limit appears to delay the onset of the memory phenomena.

Charge acceptance in a Ni-Cd cell is most efficient at a 2C charge rate. However, there are temperature limits. During low temperature operation, a high charge rate will cause internal cell hydrogen evolution. Quantitative values on the low temperature operation have yet to be determined. The maximum charge rate of 0.75C has resulted in no observed cell or battery operating anomalies from minus 20°C to 40°C.

The recharge requirements for 20 ampere-hour cells have been empirically determined for loads ranging from 100 to 300 watts, and for temperatures from minus 10°C to 30°C. These recharge values are a considerable improvement in the state-of-the-art. At 20°C with a 200-watt electrical load the battery recharge fraction was decreased from 120 to 107 percent while the battery efficiency was increased from 75 to 80 percent. Under these conditions, the heat generated per cycle has been decreased from approximately 28 watts to 17 watts.

The third electrode signal characteristics resulted in the determination of internal third electrode resistance, temperature response, and nonuniformity of cell response when the cells were subjected to identical cyclic operations. When the internal third electrode signal source is assumed to be a constant, the internal resistance becomes a function of the external load resistance. Maximum internal resistance occurs when the external load is between 150 and 300 ohms. At maximum internal resistance the third electrode signal approaches a constant current source. In the final flight battery assembly the constant current characteristics can be used to facilitate the selection of charge termination control signals.

The usable capacity of a battery is a variable quantity which decreases as a function of battery cyclic history, operating temperature, and charge/discharge control parameters. Capacity degradation, which is considered a memory phenomena can be delayed and under certain conditions reversed. Once memory has developed a significant capacity recovery can be obtained by discharging the battery and shorting each cell for a minimum of 72 hours. Normal battery cycling can be resumed after the strapout. A partial, approximately 7 ampere-hour, battery capacity recovery can be achieved by subjecting the battery to 0°C cyclic operation if the memory was developed during 15°C or higher temperature operation.

40M 22411

5.2 ATM Flight Battery Operating Methods. As previously stated, the purpose of the test program was to establish Ni-Cd cell and battery operating characteristics and control parameters which would maintain battery performance within the ATM mission requirements. The flight battery operating limits and operating specifications have been established. The flight battery will be charged at a rate which is limited by (1) a maximum charge of 15 amperes, (2) available solar array output, (3) maximum allowable battery voltage. When the maximum battery voltage level (figure 19) is reached, the charge is limited to a constant voltage that is maintained 0.8 volt below the maximum allowable battery voltage. Charge termination will be controlled by the highest voltage of three redundant third electrode signals which have been preselected. A typical ATM cycle is shown in figure 44. All the cells contained in a 24-cell battery will be matched on an ampere-hour in-and-out basis. The match criterion will be ± 1 percent. The choice of the third electrode charge termination signal will be determined from preassembly signal data. Redundant signals will be accomplished by proper choice of the third electrode load resistor. The application of this procedure should provide safe operation and maximum useful battery capacity for the duration of the ATM mission.

5.3 Recommendations for Future Nickel-Cadmium Battery Testing. The recording and analysis of test data in most test programs generally uncovers several additional problem areas for each problem resolved. The Ni-Cd battery testing established many of the battery operating characteristics but it also indicated the need for additional specific data in several areas.

Maximum battery voltage is primarily limited by the evolution of hydrogen which occurs somewhere between 1.47 and 1.55 volts. A specific voltage value, as a function of temperature and charge rate, would be very desirable. If, as is likely, the value is a statistical quantity, then statistical limits should be determined and possibly the cell construction variations, which cause the voltage variations from cell to cell.

Charge termination control data provided by the third electrode signal also requires additional quantifying. Specifically, cell pressure and its relation to the signal value as an absolute value or statistical data must be acquired. Statistical data with high signal values would point out the need for improved manufacturing and control techniques. Internal cell pressure values would also provide information and data on cell operating techniques. An important factor, especially if the useful battery cyclic life is extended, is the degradation characteristics of the third electrode signals. Proper battery recharge might not be achievable after extreme cyclic operation if excessible third electrode degradation occurs.

One of the most discernable battery characteristics yet the most difficult to control is the capacity degradation. The solution to the problem must be approached from two sides: manufacturing techniques such as chemical additives or improved

plating, and operating techniques such as improved charging and discharging methods. An additional capacity degradation control technique which requires further investigation and development is cell matching. The approach is particularly applicable to an optimal operating procedure.

Future mission applications of secondary Ni-Cd batteries will be considerably assisted by acquisition of more specific data on operating characteristics of Ni-Cd cells as outlined in the test recommendations. These recommendations would assist power system designers in optimizing secondary battery applications for future missions.

REFERENCES

1. Bauer, Paul: "Batteries for Space Power Systems." NASA SP-172, 1968.

2. Carson, W. N., Jr.: "A Study of Nickel-Cadmium Spacecraft Battery Charge Control Methods." NASA CR-62029, April 1966.